SECURITY MARKING

The classified or limited status of this report applies to each page, unless otherwise marked.
Separate page printouts MUST be marked accordingly.

THIS DOCUMENT CONTAINS INFORMATION AFFECTING THE NATIONAL DEFENSE OF THE UNITED STATES WITHIN THE MEANING OF THE ESPIONAGE LAWS, TITLE 18, U.S.C., SECTIONS 793 AND 794. THE TRANSMISSION OR THE REVELATION OF ITS CONTENTS IN ANY MANNER TO AN UNAUTHORIZED PERSON IS PROHIBITED BY LAW.

NOTICE: When government or other drawings, specifications or other data are used for any purpose other than in connection with a definitely related government procurement operation, the U. S. Government thereby incurs no responsibility, nor any obligation whatsoever; and the fact that the Government may have formulated, furnished, or in any way supplied the said drawings, specifications, or other data is not to be regarded by implication or otherwise as in any manner licensing the holder or any other person or corporation, or conveying any rights or permission to manufacture, use or sell any patented invention that may in any way be related thereto.

POR-3007
(WT-3007)

FERRIS WHEEL SERIES

FLAT TOP EVENT

PROJECT OFFICERS REPORT—PROJECT 1.5b

EJECTA DISTRIBUTION FROM FLAT TOP I EVENT

M. V. Anthony
Project Officer

T. P. Day
C. R. Wauchope

The Boeing Company
Seattle, Washington

Issuance Date: October 18, 1965

POR–3007
(WT–3007)

FERRIS WHEEL SERIES

FLAT TOP EVENT

PROJECT OFFICERS REPORT—PROJECT 1.5b

EJECTA DISTRIBUTION FROM FLAT TOP 1 EVENT

M. V. Anthony, Project Officer
T. P. Day
C. R. Wauchope

The Boeing Company
Seattle, Washington

ABSTRACT

A study was made of the distribution of ejecta from the crater formed by exploding 20 tons of TNT at the surface of a limestone outcrop.

The distributions of both in situ material and material artificially introduced into the medium before the explosion are described. Variations with distance from burst point in ejecta areal density and the size distribution of ejecta are analyzed. Relationships between ejecta distribution and site topography and geology are discussed.

Suggestions are made as to further work directed toward impraving methods of predicting ejecta distribution from large explosions on rock.

PREFACE

A canversatian with H. J. Maare (Branch af Astrogealogy, U. S. Geological Survey) concerning his studies of hypervelacity impacts on rack targets helped determine the farm af analysis used in this study of ejecta size distribution.

Appreciation is also expressed far information received from persannel of ather Flat Tap prajects, especially Projects 1.9 and 9.8, and far the assistance af support groups.

CONTENTS

TABLES

FIGURES

CHAPTER 1

INTRODUCTION

1.1 OBJECTIVES

The objectives of this project were (1) to obtain information on ejecta areal density and thickness as a function of distance from Flat Top I, a 20-ton surface burst of TNT on hard rock; (2) to obtain information on the size distribution of ejecta particles from this explosion; (3) to obtain information on cratering and throwout mechanics from this explosion; and (4) to examine the data obtained from the point of view of previous cratering experiments and theory, in an attempt to establish techniques for predicting ejecta size and areal distribution from militarily significant chemical or nuclear explosions on a hard rock surface.

1.2 BACKGROUND

The spatial distribution of ejecta from cratering explosions received relatively little attention as a factor of military significance in the post-attack environment before the early 1960's. Before this time, virtually all ejecta studies were concerned either with the maximum range at which ejecta, following ballistic trajectories from buried explosions, would constitute a hazard, or with the distribution of the fine particulate portion of the ejecta deposited beyond ballistic range from buried explosions.

Ejecta data published through 1962 is summarized in Reference 1 in the form of plots showing areal density as a function of distance from surface zero. This reference also describes an empiricol method for predicting ejecta areal density versus distance as a function of apparent crater depth and radius, and chorge weight.

With increasing emphasis on buried installations designed to survive overpressures close to the edge of craters from megaton surface bursts, it became necessary to predict ejecta thickness at these close-in ranges. Reliable information on close-in ejecta thickness would then allow measures to be taken to insure that the installations would not be made inoperative because ejecta covered exits, communication and control fixtures, etc., even though the structures themselves hod survived the shock effects of the attack.

Ejecta studies reported in References 2 and 3, employing a technique described in Reference 4, were made on three Plowshare events in the desert alluvium of the Nevada Test Site (NTS). These studies, although made for peaceful applications, report data on ejecta areal density throughout the range of military significance.

In these studies of buried explosions it was noted that the ejecta mass is deposited relatively nearer the crater edge as the scaled depth of burial is increased, and that a greater proportion of the mass represented by the apparent crater

volume is accounted for by ejecta from chemical explosions than from nuclear explosions. These studies also established an empirical relationship between the mass of fine particulate and apparent crater volume and examined relationships between various mass quantities as a function of yield and depth of burial for underground explosions in NTS alluvium.

In References 2 and 3 an assumption implicit in calculations of areal density for the ballistically deposited portion of the ejecta is that drag effects are unimportant. It is assumed that the trajectories of small cylindrical pellets with a specific gravity of about 6.5 simulate the trajectories of large clods of dirt, which have a specific gravity of only 1.6 and which tend to gyrate and disaggregate in flight. When disagreement is observed between computed areal densities and areal densities actually measured at the same distance, the difference is attributed to inadequacies in the techniques used to physically sample areal density.

Reference 5 describes a method of scaling ejecta mass as a function of distance from surface zero that evades problems concerning the dependence of crater parameters on charge weight, yield, depth of burial, and properties of the medium. This method, which was used to analyze the Sedan event, uses the apparent crater radius instead of functions of charge weight and depth of burial as a scaling parameter.

Two dimensionless ratios are related: (1) the incremental mass of ejecta summed to the distance of interest divided by the total mass of ejecta,

and (2) the distance of interest divided by the apparent crater radius. In Reference 5 and subsequent related reports, plots showing th'. relationship are termed mass distribution curves.

Mass distribution curves are useful for studying the relative distance of which different proportions of the total mass of ejecta are deposited when a single parameter such as charge weight or depth of burial is varied. However, to use these curves for predicting areal density as a function of distance from surface zero, it is still necessary to predict crater dimensions and total ejecta mass as a function of charge weight, depth of burial, and properties of the medium.

Reference 6 reports the results of applying the mass distribution method to the analysis of five large high-explosive (HE) and three nuclear cratering events. One of these shots was fired in the clayey silt of the Suffield Experimental Station, Alberta, Canada; this shot was a 100-ton hemisphere of stacked TNT with its center of gravity above ground and its diametral plane on the ground surface. Other events treated in this report were detonations at various depths in NTS alluvium.

A relationship between total ejecta mass and the mass represented by the apparent crater was derived for shots in this type soil. it was found that chemical explosions gave an average ratio of 0.73 for total throwout mass/ apparent crater mass, whereas nuclear explosions gave an average ratio of

only 0.56. This confirmed earlier observations reported in References 2 and 3.

It was also reported that near-surface bursts tend to deposit ejecta relatively farther from the crater edge than do more deeply buried shots. This also confirmed earlier observations reported in References 2 and 3.

It was found that the mass distribution curves for Sedan, a 100-kiloton nuclear explosion, and for Scooter, a 500-ton HE shot at the same scaled depth of burial, were practically identical. This suggested that shots at the same scaled depth give similar mass distribution curves over a wide range of yields. There were too few shots analyzed to give other comparisons in which only one parameter was varied.

It was pointed out that the statistical distribution of areal density at a given range from surface zero, due to ejecta being deposited in a ray pattern, is distinctly nongaussian; however, the exact form of the distribution was not determined.

Achieving mass balances by comparing known volumes is particularly simple for dry NTS alluvium, since the unit weights of the undisturbed material, fallback, and ejecta are all approximately the same, as was assumed in References 2, 3, 5, and 6.

Reference 2 reports density tests of undisturbed alluvium and alluvium taken from crater lips that show negligible differences in dry unit weight. A

comparison between the undisturbed density determinations and the results of modified AASHO compaction tests given in this report shows volume changes of less than 10 percent for dry NTS alluvium. Both the dry unit weight of undisturbed material and its compaction under this effort are lower than usual for soils with a grain size distribution like the NTS alluvium.

It has been found from shaft-sinking experience in this unusual material that bucket loads of blasted muck show an increase in volume only about 8 to 12 percent above that occupied by the material in situ (Reference 7). Since the muck is handled while still damp from the drilling cycle and some swell can be attributed to the moisture content, it is obvious that little account need be taken of swelling in ejecta and fallback when obtaining mass balances for craters in dry NTS alluvium.

Reference 8 reports the results obtained by reducing ejecta data and plotting mass distribution curves for the Air Vent series of HE shots in Frenchman playa silt. Considerable difficulty was encountered in obtaining mass balances to establish relationships between crater and ejecta parameters for these bursts. This difficulty was due to lack of sufficient data on the unit weights of undisturbed material, material in the region of distortion and uplift around the crater, fallback, and ejecta. Despite insufficient sampling, important differences were found in the unit weights of the material from these different regions for any given burst.

This study verified earlier statements that the relative positions of ejecta from shots of the same charge weight in the same material vary with

depth of burst. The shape of mass distribution curves for surface bursts in playa silt was also found to vary as a function of charge weight. This would seem to contradict the suggestion made in Reference 6 that different charge weights at the same scaled depth of burial give similar mass distribution curves.

Reference 9 reports the results obtained by preparing mass distribution curves of all cratering events for which sufficient published data were available through 1964. In addition to the cratering events discussed previously in this section, Danny Boy (a buried nuclear burst in basalt) and Flat Top II and III (HE surface bursts in playa silt) were also studied. Preliminary data on Flat Top I were also incorporated in this report.

The mass distribution curves shown in this report for Danny Boy and Flat Top I are inconclusive as to whether significant differences exist between the mass distribution of ejecta from craters in rock and those in soil. The Danny Boy curve is different from curves for soil, but the Flat Top I curve is not.

Other investigations of the throwout mechanics from cratering shots have been made by placing objects at known positions within the anticipated crater region and noting their postshot locations (References 10 through 14).

References 10 and 11 report studies made to determine the hazard from missiles due to rocks in the medium or to concrete pavements and walls near the epicenter of shallow underground shots in soil.

Reference 11 summarizes these studies with the following statement: "It is concluded that on large shallow underground explosions damage by the mechanism of air blast will extend further than damage by the mechanism of missiles. This conclusion is sufficiently firm that no further missile experiments appear necessary."

Reference 12 reports the results of a throwout study conducted on Danny Boy. Objects were emplaced at various regions within the anticipated crater area, both at the ground surface and below. Although data were obtained from surface objects, the recovery of the buried objects was too poor to draw conclusions about throwout mechanics.

Two other coded ejecta experiments are known to have been made, but their results are not yet published. The experiments referred to were conducted by burying objects at known positions within the anticipated crater region from shots in soil. One experiment (Reference 13) was conducted at the Suffield Experimental Station and the other (Reference 14) on Frenchman playa at NTS.

It is expected that these experiments will provide valuable information on the applicability of this method in determining true areal density-distance relationships for surface-burst-cratering explosions on soil. Additional information on the initial velocity field in the crater region, and on the compression and distortion in the region surrounding craters from explosions in soil, is also expected from these studies.

As has been indicated in this summary, the most significant explosive-burst geometry for present military planning is the surface burst. However, prior to the Air Vent/Flat Top test series, useful data on ejecta distribution from surface bursts on soil were scarce and no such useful data from a surface burst on rock had been obtained.

CHAPTER 2

EXPERIMENTAL PROCEDURE

2.1 EXPERIMENTAL PLAN

Because analysis of the data obtained from this project would be based on statistical inferences from samples, the data requirements were simply to obtain the maximum possible information on comminution and areal distribution of ejecta that available time and funds would permit. The proposal for this study was made before the site had been visited, and some changes in the original plan were necessary because of unusual site conditions. The proposed study plan was as follows (Reference 15):

Total ejecta were to be sampled as a function of range and azimuth from the burst point. The volume of a portion of the ejecta between 1 and 3 crater radii would be determined, after which these ejecta would be screened and weighed. Other portions of the ejecta deposited farther from the crater edge would be weighed and, if time permitted, screened.

A sector around the burst point was to be thoroughly searched for portions of the ejecta originally coded and emplaced at known locations within the anticipated crater. This coded material was to be composed of material with properties matching the properties of the Flat Top I medium; its postshot areal distribution would be recorded to give information on cratering and throwout mechanics.

Data on true and apparent crater parameters, lip upthrust, and in situ properties of the medium were required from Project 1.9 personnel.

2.2 SITE TOPOGRAPHY AND GEOLOGY

Factors of the Flat Top I topography and geology were expected to influence cratering and throwout mechanics, and these were taken into account in preparing the ejecta sampling array. Elements of site topography also influenced the choice of sectors used for the throwout study and far-out missile survey.

Figure 2.1 shows the general topography of the Flat Top I site. Figure 2.2 is a geologic sketch of the immediate vicinity surrounding ground zero (GZ), prepared from information in Reference 16.

The Flat Top I site is on a limestone outcrop near the southeast end of Banded Mountain in Area 9 of NTS. From GZ the slope of the outcrop is down about 4 degrees to the west and south. To the east it rises more gently. To the north it rises about 4 degrees for the first 150 feet where a small limestone knoll, an outlier of Banded Mountain, rises abruptly.

The site is in the middle subunit of the Banded Mountain Member of the Bonanza King Formation. This subunit is composed of thick to very thin beds of light-gray to yellowish-gray, fine-grained limestone. Chemical analyses of three samples from the site showed nearly pure calcium carbonate. A fourth sample was somewhat magnesian.

Alluvium composed of limestone detritus with a small component of tuff overlaps the outcrop to the west, south, and east; it also fills declivities caused by differential weathering along the strike of the outcrop.

The strike of the beds is approximately N 27° W near GZ, and the dip is about 55 degrees to the southwest.

A frequency distribution study of 378 fractures within about 50 feet of GZ showed an average of about 4 fractures, predominantly vertical, per 100 square feet of ground surface. Over half of these fractures had a strike between N 60° E and N 80° E. This study was made before the alluvium had been stripped from a circular area with a radius of 50 feet centered on GZ. It was apparent, after the area had been stripped, that the number of fractures had been considerably underestimated. Figure 2.3 is a photograph taken from about 25 feet east of GZ (marked by the steel pipe) looking approximately down dip.

Core from drill holes showed from one to four fractures per vertical foot, some of which were due to vibrations from drilling.

It was estimated that calcite or clay filled about 90 percent of the fractures, sealing them more or less tightly. The other 10 percent of the fractures were open.

Figure 2.4 is another view of the site taken a few feet northeast of GZ looking south.

Table 2.1 is a summary of the results of physical property determinations made on rock samples collected from the ground surface to a depth of 15 feet at the Flat Top I site. Determinations were made by U. S. Geological Survey and Waterways Experiment Station (WES) personnel (Reference 17).

2.3 EXPERIMENTAL ARRAY

In order to get an estimate of crater and ejecta parameters to use in planning the ejecta sampling array and screening plant capacity, data from previous surface bursts on hard rock were scaled to the Flat Top I charge weight. Data were available from only two sources. Two surface shots of 200 pounds of TNT had been detonated in basalt during the ICS series in Panama and two surface shots of 64 pounds of TNT had been detonated by Boeing in argillite.

Depending on the choice of data and scaling exponent, this analysis gave an apparent crater radius ranging from 23 to 36 feet and an apparent depth from 8 to 13 feet for Flat Top I. For planning purposes the average apparent radius was assumed to be 30 (±3) feet and the apparent depth 10 (±1) feet.

It was expected that ejecta would completely cover the ground surface to a distance of about 3 crater radii from GZ, and that virtually all the ejecta mass would be deposited within 10 crater radii from GZ; therefore, most of the ejecta sampling stations were placed between 3 crater radii from

GZ, the distance ta which the ejecta wauld be completely excavated in a selected sectar, and 9 crater radii, the distance beyand which ejecta wauld be sparsely distributed.

The ejecta sampling stations used within this region were 3-by-3-foot by 4-inch-thick concrete pads. It was thought that these pads wauld survive the airblast and wauld satisfactorily simulate the surface of the limestone autcrop.

It was alsc expected that the configuration af the crater and ejecta would be strongly influenced by the gealogic and topographic features af the site discussed in Section 2.2.

To check the influence of bedding dip and fracture pattern on the ejecta distribution, ejecta sampling stations were placed ta a maximum distance of 520 feet on three radials approximately alang the strike of the beds to the southeast and on three radials appraximately alang the strike of the major fracture pattern (i.e. along the dip of the beds) to the sauthwest.

Because the ground surface in the region af these extended radials was alluvium, and because no prablems of survival due ta airblast were expected, 3-foot 8-inch-square canvas tarpaulins were used for sampling stations. It was thought that the collection surface pravided by the tarps would satisfactarily simulate the resiliency and frictional characteristics af the alluvium.

The array of ejecta collectian stations is shown in Figure 2.5. Slight adjustments in the regular pattern of the array were necessary to avoid the

airblast experimental array to the southeast. Some tarpaulins were offset a few feet to avoid obstructions or poor locations. Three stations were eliminated to the northeast because of unsatisfactory topography. A total of 111 ejecta collection stations were used.

To reduce the number of geologic variables influencing the coded throwout experiment it was necessary to emplace the coded grout on a radial from GZ that would be either parallel or perpendicular to the strike of the beds and major fracture pattern. Radials parallel to the strike of the beds were ruled out because of the steep topography to the northwest and probable interference with airblast and ground-shock experiments to the southeast.

Since the topography was more open and level down dip than up, it was decided to emplace the coded grout on the radial extending down dip. As noted previously, the direction of dip at GZ had been determined to be S 63° W. This direction was also considered to be satisfactorily parallel to the strike of the major fracture pattern so that the azimuth of trajectories of the coded grout would not be influenced by inhomogeneities of the medium.

Four vertical 6-inch holes were drilled on this radial at distances of 6, 12, 18, and 24 feet from GZ. Cylinders of coded grout 3 inches in diameter and 1 foot long were lowered into these holes and grouted in place, thus forming continuous cylinders of grout extending from a depth about 16 feet below the elevation of the charge center to the ground surface.

The coding employed to denote initial horizontal position was to make all the cylinders in a given hole from grout dyed one color. Vertical position was coded by introducing about 1/2 pound of glass beads into the grout composing each 1-foot cylinder. A given color of bead indicated a predetermined 1-foot vertical interval. The vertical positions of the tops of the cylinders were recorded to the nearest 0.1 foot. Figures 2.6 and 2.7 show grout cylinders being emplaced. The irregularity of the outcrop surface is well illustrated in Figure 2.6.

A 3-foot-wide by 40-foot-long grout pad was emplaced with its centerline on the S 63° W radial. This pad was cast in four 10-foot sections, each section of a different color. The pad extended from the edge of the TNT sphere to about 45.5 feet from GZ.

The grout used for the coded cylinders and pad was designed by WES personnel to match the density of the medium. Only four easily distinguished colors could be furnished and requirements for a grout matching strength properties of the rock could not be met.

The limited number of colors available, the low strength of the grout, and the difficulty of emplacing a pad of uniform thickness over the irregular ground surface restricted the usefulness of the coded pad in the throwout mechanics study. It had been planned to use data on areal distribution and comminution of fragments from the pad to (1) gain insight into the change from

compressive to tensile failure of rock at the ground surface as a function of distance from the burst point, and (2) study differences in throwout trajectories of fragments from zones in and near the crater having these different failure modes. Figure 2.5 shows the array of the coded grout experiment. Figure 2.8 shows the coded grout pad in place. The tops of the uppermost coded grout cylinders are also visible in this photograph.

Since it was necessary to recover fragments of coded grout that would be buried in the ejecta lip, it was decided to excavate a 30-degree sector centered on the S 63° W radial, from the crater edge to a distance 3 crater radii from GZ after the shot. The material excavated would be used as the close-in ejecta samples for determinations of fragment size and bulk density as a function of distance from GZ. Figure 2.9 is a view of the site made from the knoll north of GZ after the charge was stacked.

2.4 DATA RECOVERY

The Flat Top I event took place at 0930 on 22 June 1964. The surface wind was blowing from N 30° E at 12 knots. At about 500 feet above ground the wind was from N 36° E at 18 knots; at about 1,000 feet above ground, the wind direction was N 30° E, and the velocity was 14 knots.

Figures 2.10 and 2.11 are views of the crater and ejecta. Figure 2.10 is a view into the crater from the north lip. Figure 2.11 looks north from

about 65 feet south of GZ.

Collection of ejecta samples from the stations farthest from GZ was begun by H + 30 minutes. Collection of ejecta from all sampling stations was completed on D + 1.

The ejecta samples beyond about 125 feet from GZ were badly contaminated by alluvium and organic material blown onto the collection stations by the airblast. Loss of fine particulate due to wind or collection procedure was negligible.

In the case of large fragments found partly on and partly off a collection station, the portion on the station was marked in the recovery procedure. In determining fragment size distribution later, the weight of the portion on the station was recorded with the equivalent diameter of the whole fragment.

The sample from Station J-18 was lost due to destruction of the tarpaulin by the airblast. Other stations were damaged, but samples from all other collection stations, a total of 110, were recovered.

Figures 2. 12 through 2. 19 show the ejecta samples at various collection stations. Appendix A gives a brief description of the postshot condition of each collection station.

At some close-in stations, a pileup of debris on the side of the 4-inch-thick pad facing GZ was noted. Figures 2. 13 and 2. 14 show pronounced examples of this. The qualitative effect of this condition on the

ejecta sample is noted in Appendix A for all occurrences. This same effect was noted at positions not occupied by collection stations because of irregularities in the surface of the rock outcrop.

While the samples were being collected, it was realized that the collector array was inadequate to provide an accurate estimate of areal density as a function of distance. The reason was that beyond a few crater radii most of the ejecta mass at a given radial distance from GZ was concentrated in relatively few large fragments, and these fragments were too sparsely distributed to be adequately represented in the small area sampled. Figures 2.15 and 2.17 illustrate this problem.

It was proposed to handpick the ejecta in four 29-foot annular strips across the 30-degree sector from about 175 to 800 feet from GZ; this would have allowed comparison between the large annular samples and the samples collected on the three extended radials. The comparison would have given an indication of the reliability of sampling ejecta from shots in rock by small collector stations.

The extra effort involved could not be accomplished within the scope of the contract and, since it was decided not to enlarge the contract scope, the comparison could not be made.

The samples were bagged, identified, and stored for shipment to the Nevada Testing Laboratory (NTL) in Las Vegas.

At NTL the samples were weighed and screened. The methods used and the data obtained from each collection station are described in Appendix B.

The remaining field work involving data collection for other portions of the project was accomplished as manpower and equipment became available. All field work was completed by 22 July 1964.

A survey crew provided by Holmes and Narver (H and N) determined the elevation of the ejecta and fallback surface at 5-foot intervals along radials from GZ to a distance of 90 feet. This leveling was done on 15 radials at 3-degree intervals from S 42° W to S 84° W in order to cover completely the 30-degree sector centered on S 63° W and any adjoining area that might slump while ejecta were being removed from the 30-degree sector. Elevations were determined to the nearest 0.1 foot.

The ejecta in this sector were then removed in two increments by hand labor. The increment from 2 to 3 crater radii formed one sample and that from 1 to 2 crater radii another. Early results of Project 1.9 indicated an apparent crater radius of 29 feet; therefore, the samples were collected from 29 to 58 feet and from 58 to 87 feet from GZ.

After the lip ejecta had been removed, the H and N survey crew determined elevations over the excavated surface at the same distances and azimuths that had been covered in the pre-excavation survey. Again the elevations were determined to the nearest 0.1 foot. Because there had been

no slump in the ejecta adjoining the excavated 30-degree sector, the post-excavation survey covered only the 11 radials 3 degrees apart from S 48° W to S 78° W.

Appendix C gives the pre- and post-excavation profiles made over the crater lip in this sector. Figure 2.20 shows the 30-degree sector after excavation of the outermost sample was almost complete. Figure 2.21 is a post-excavation view of the area in which the innermost sample was taken.

The personnel shown in Figure 2.21 are standing 29 feet from GZ along the limiting radials of the 30-degree sector.

Figure 2.22 is a closeup of the uplifted surface of the sector after excavation. This view looks almost north from the southernmost limit of the excavated sector. The camera bag is about 45 feet from GZ along the S 63° W radial.

In the close-in region the uplifted surface was covered with rock dust from the explosion. This dust and the extreme fracturing of the uplifted rock near the crater edge made it difficult to distinguish between ejecta and the uplifted surface. It is doubtful that this distinction could have been made if the original rock surface had not been painted before the event.

Fragments with an equivalent diameter greater than 2 feet were separated at the site and weighed individually. The proportion inside the sector was estimated for large fragments on the sector border and the weight of the proportion inside the sector recorded with the total fragment size. The

ejecta from the excavated sector less than 2 feet in equivalent diameter were taken to a screening plant located about a mile south of GZ where they were classified by size into four intervals. The sized ejecta were then transported by truck to Mercury, Nevada, where they were weighed.

Figures 2.23 through 2.25 show the screening plant. Truckloads of the material recovered were dumped over an 8-1/2-inch-square grizzly. The undersize material passed into a chute and up a conveyor belt onto a 3-inch vibrating screen. The oversize material passed into a truck, and the undersize material passed onto a 1-inch vibrating screen. From the 1-inch screen the oversize material passed into a truck, and the undersize material passed into a Jones riffle where it was quartered. Fragments smaller than 1 inch were coned and quartered again and further sizing was done on these samples at NTL.

Loss of fine particulate was unavoidable in screening these large samples. The total loss of fines from the two samples is estimated to be of the order of 100 pounds. Reduction in size of the ejecta due to handling was considered to be a second-order effect. Appendix D presents the data obtained from the two close-in samples.

The search for close-in fragments of coded grout was made concurrently with excavation of the 30-degree sector of the lip and with excavation of fallback along the S 63° W radial by Project 1.9 personnel. In the close-in region the location of coded fragments was determined by plane tabling or by taping distances to fixed points.

Excavation of the fallback was done with a crane-mounted clamshell (Figure 2.26); a thorough search for grout fragments within the apparent crater was precluded by the speed with which the material was excavated.

Thorough recovery of grout fragments within the crater was further complicated by the covering of rock dust over surfaces of limestone blocks containing the grout. A typical close-in fragment of grout with the dust removed is shown in Figure 2.27.

Beyond 3 crater radii from GZ, the 30-degree sector was divided into 25-foot radial increments to a distance of 1,000 feet from GZ. The limits of each annular increment were outlined with lath. Each increment was then thoroughly searched for grout fragments by from three to five men. Figure 2.28 shows a large fragment of a coded cylinder found about 200 feet from GZ. A few fragments as small as the ultimate identifiable particle, containing only a single bead, were found.

The location of fragments of coded cylinders was marked on a plane table map by the H and N survey crew, after which the fragments were identified and bagged. The location of fragments was plotted to an accuracy closer than 5 feet.

On each sweep of a 25-foot annular area, the location of the first and last fragment of each color of the coded pad found was also plotted on the plane table map.

Because all detailed reports of the distribution of coded ejecta from cratering explosions indicate that deviations from radial trajectories are common, angular dispersion of the grout fragments was expected. However, because of the care taken to align the coded material along a radial where the effect of geologic inhomogeneities on trajectory azimuths would be minimized, it was expected that virtually all of the fragments would be found within 15 degrees of S 63° W.

Actually the trajectories of most of the fragments were deflected considerably to the south, and the sector searched beyond 3 crater radii was extended another 25 degrees to the south. The procedure used to search the extended sector was the same as that used in searching the original 30-degree sector.

A cursory search for fragments of the coded pad was made beyond 1,000 feet from GZ to determine the maximum range for fragments of each grout color. Another cursory search was made south of the extended sector, where a few fragments of the coded ejecta were found. Available time was insufficient to extend farther the sector in which a thorough search for fragments could be made.

It is considered likely that extending the thorough search to the south would have resulted in discovery of a significant number of fragments of the two colored segments of the coded pad nearest GZ. It is unlikely, however,

that this extended search would have resulted in discovery of enough fragments of the other two segments of the coded pad, or of the coded cylinders, to cause significant changes in the conclusions drawn in the following chapter.

Appendix E gives the range from GZ and azimuth of the recovered fragments of coded cylinders. The distribution of fragments of the coded pad is presented graphically in the following chapter.

There was general interest as to the distribution of ejecta at distances beyond about 2,500 feet from GZ. Safety criteria for the hazard from flyrock had been based on data that indicated that there would be essentially no ejecta thrown beyond 2,550 feet from GZ; however, this range was obviously exceeded by a great number of fragments from the Flat Top I event, some of which passed over manned stations.

The Scientific Director suggested that some effort be devoted to determining the distribution of ejecta beyond a range of 2,550 feet; therefore, a helicopter flight was arranged to enable the Project Officer to assess roughly the distribution of the far-out missiles.

It was found that the greatest concentration of missiles and maximum ranges from GZ occurred in a poorly defined lobe to the northwest of the site. Fewer missiles at somewhat less range from GZ were found in a rough lobe to the southeast, and somewhat fewer yet to the northeast and southwest. Impressions of the roughly lobate character of the far-out missile distribution

were formed entirely on the basis of observations during the flight. Time and funds were not available to substantiate these observations by detailed work.

In the lobe to the southwest, missiles were seen on the west slope of Balloon Hill. Missiles in the northwest and northeast lobes were seen far up on the steep limestone outcrops of Banded Mountain and on the ridge between Banded Mountain and Jangle Ridge (see Figure 2.1). The orientation of these lobes, assuming that they are real, was roughly along the strike of the beds and parallel to the dip.

The Project Officer directed the H and N survey crew to establish control points and begin triangulation of impact points of missiles thrown beyond 2,500 feet to the southeast of GZ. This work was done intermittently, as other survey work on the project permitted, until 17 July 1964. On this date permission was obtained from the Test Group Director to survey the sector from S 12° E to S 72° E for far-out missiles.

The decision to concentrate on this area was made for the following reasons: First, the terrain was most open and accessible to the surveyors in the southeast quadrant and a minimum of triangulation stations were necessary to locate points in this area. By the time the far-out missile search had been officially approved, about half of the 60-degree sector had already been searched. Second, the ground surface to the southeast is alluvium, and impact points were more easily determined on soil than on rock. A heavy rain on

10 July 1964 had obliterated many impact marks made by missiles striking rock. Third, it was thought that the missile concentration in this area was fairly representative of the average distribution of missiles in the lobes beyond 2,500 feet from GZ. Finally, motion pictures had been made of the Flat Top I event from stations southeast and southwest of GZ (Figure 2.1). Thus it would be possible to check initial velocities and angles of missiles thrown to the southeast from pictures made southwest of GZ. Pictures made from the southwest would provide information on the number of missiles thrown in this direction and the proportion falling a distance less than the camera distance from GZ.

Location of impact points of the far-out missiles was done without increasing the scope of the contract. The work was accomplished by H and N survey crews with a minimum of supervision by project personnel.

Appendix F presents the results of the far-out missile survey.

TABLE 2.1 SUMMARY OF ROCK SAMPLE DATA

	Dry Unit Weight	Grain Density	Porosity	Compressional Wave Velocity	Dynamic Young's Modulus
	g/cc	g/cc	percent	ft/sec x 10^{-3}	psi x 10^{-6}
Mean	2.71	2.71	0.6	19.9	11.5
Range	2.67 to 2.74	2.71 to 2.72	0.2 to 0.8	19.0 to 20.8	10.5 to 12.5
Determinations	10[a]	3[a]	3[a]	7[a]	11[a, b]

	Dynamic Poisson's Ratio	Tensile Splitting Strength	Compressive[c] Strength
		psi	psi x 10^{-3}
Mean	0.31	640	15.1
Range	0.27 to 0.36	513 to 797	12.2 to 16.7
Determinations	11[a, b]	5	5

[a]Data for one weathered specimen from ground surface are excluded.

[b]Data from only seven specimens; determinations made by two methods on four of these specimens.

[c]Data are for confining pressures ranging from 100 to 300 psi. Data are insufficient to construct a Mohr envelope.

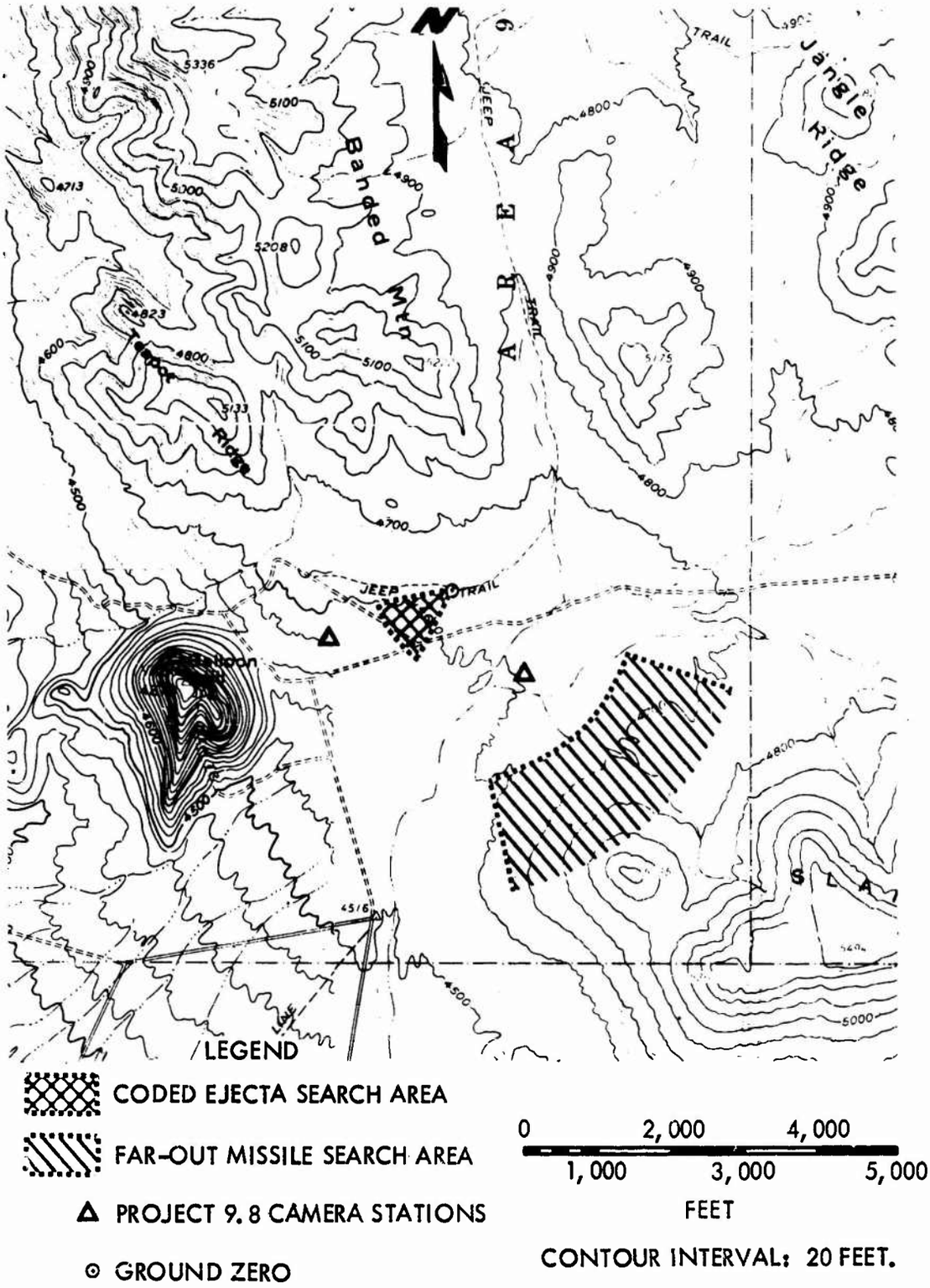

Figure 2.1 Flat Top 1 site, Area 9, Nevada Test Si..

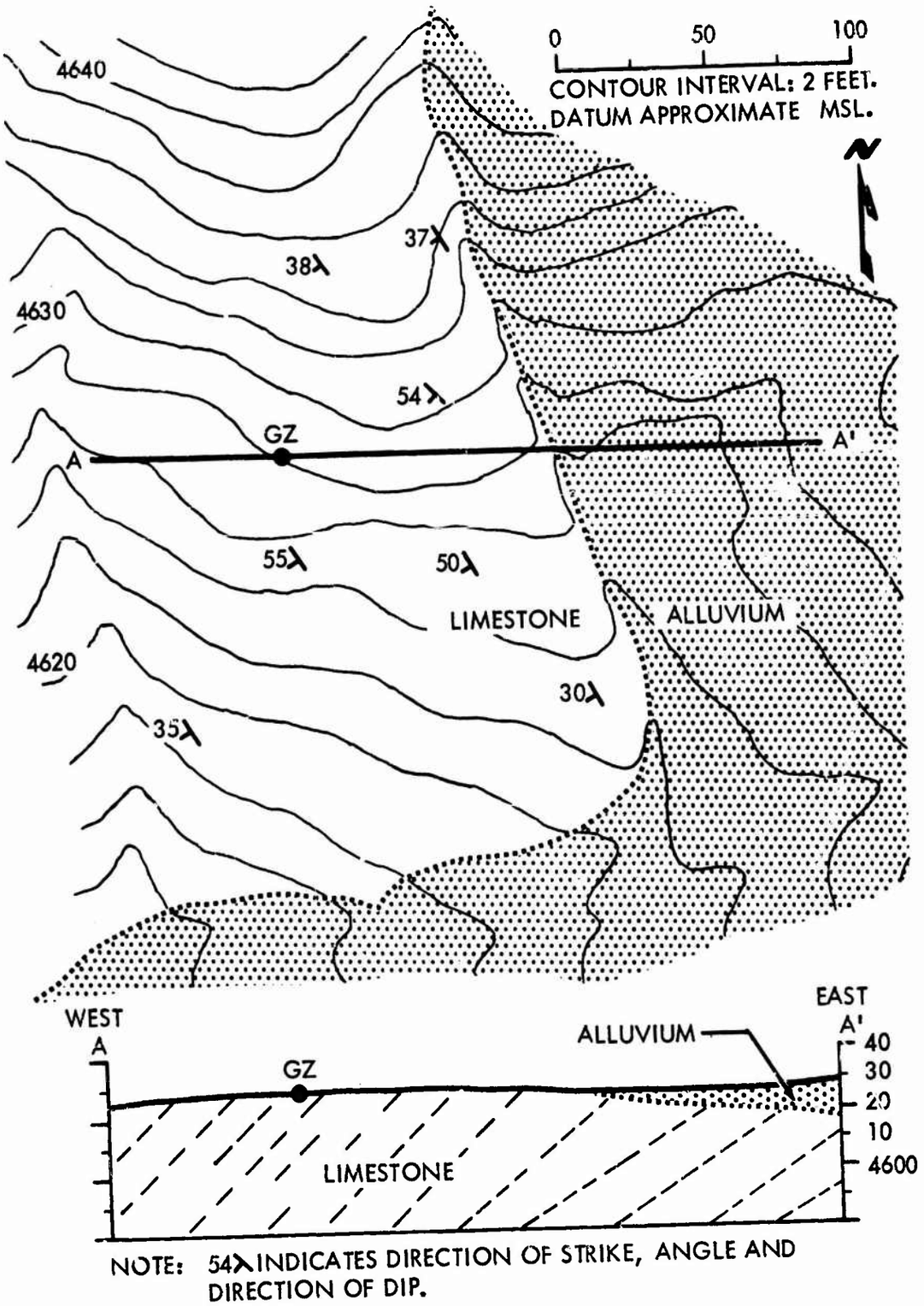

Figure 2.2 Geologic sketch of Flat Top 1 site.

Figure 2.3 Flat Top 1 ground zero after stripping alluvium (looking southwest). (DASA 39-01-NTS-64)

Figure 2.4 Flat Top 1 ground zero after stripping alluvium (looking south). (DASA 43-09-NTS-64)

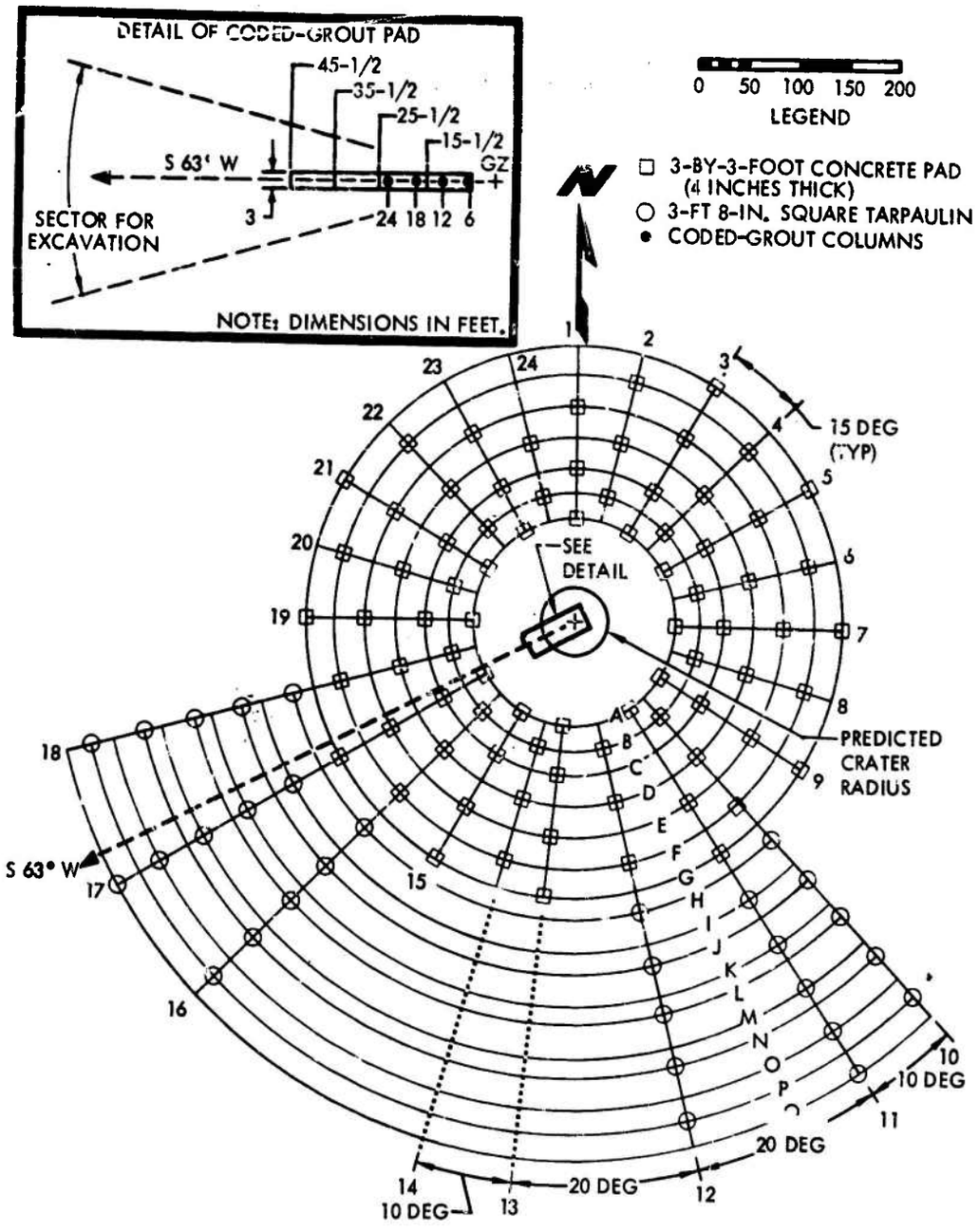

Figure 2.5 Experimental array.

Figure 2.6 Emplacement of coded grout cylinders. (DASA 58-02-NTS-64)

Figure 2.7 Detail of coded cylinder emplacement. (DASA 58-01-NTS-64)

Figure 2.8 Coded grout pad in place. (DASA 58-04-NTS-64)

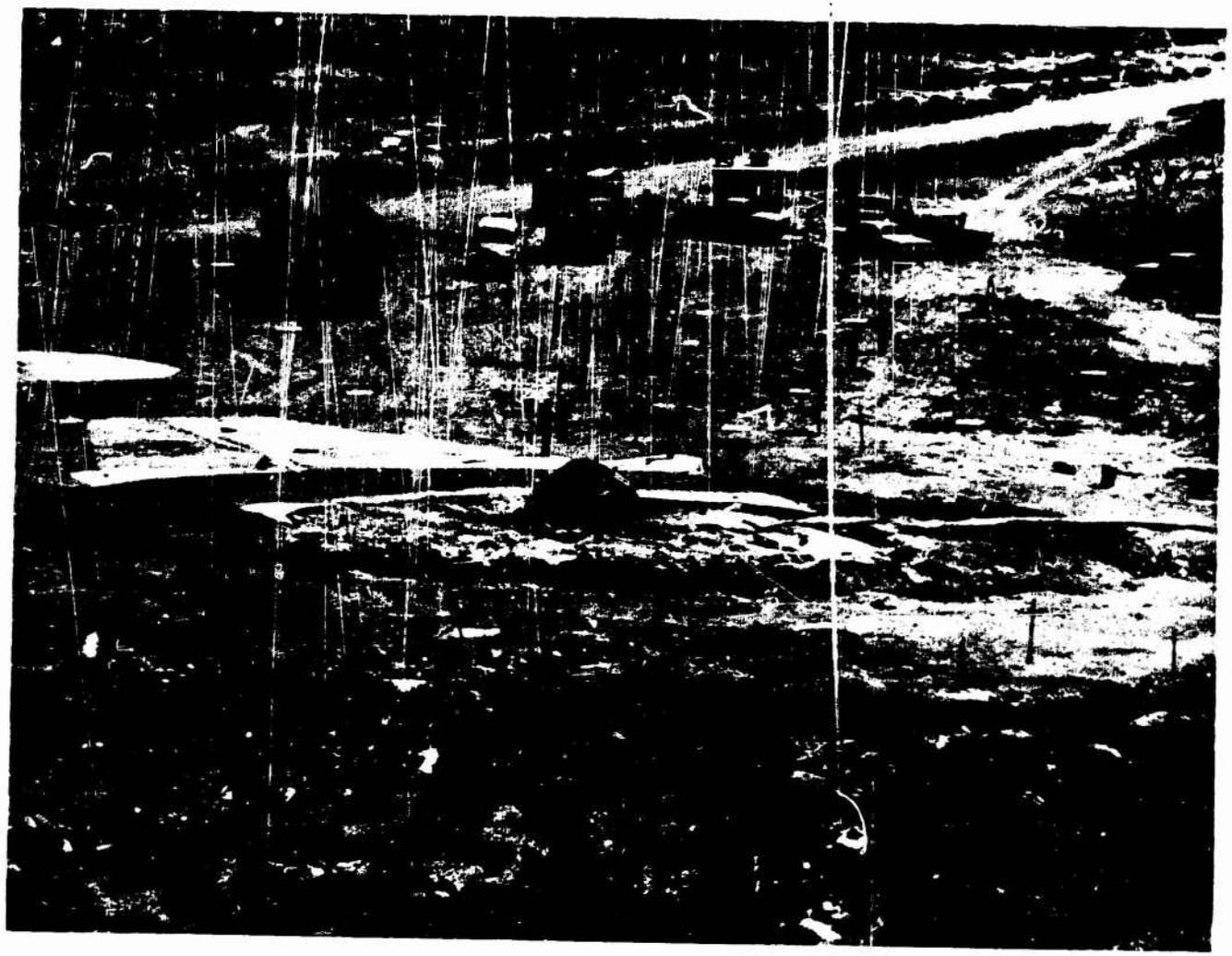

Figure 2.9 View of Flat Top 1 site with charge emplaced. (DASA 63-20-NTS-64)

Figure 2.10 View of Flat Top 1 crater from north lip. (DASA 64-33-NTS-64)

Figure 2.11 Crater lip from south of ground zero. (DASA 73-01-NTS-64)

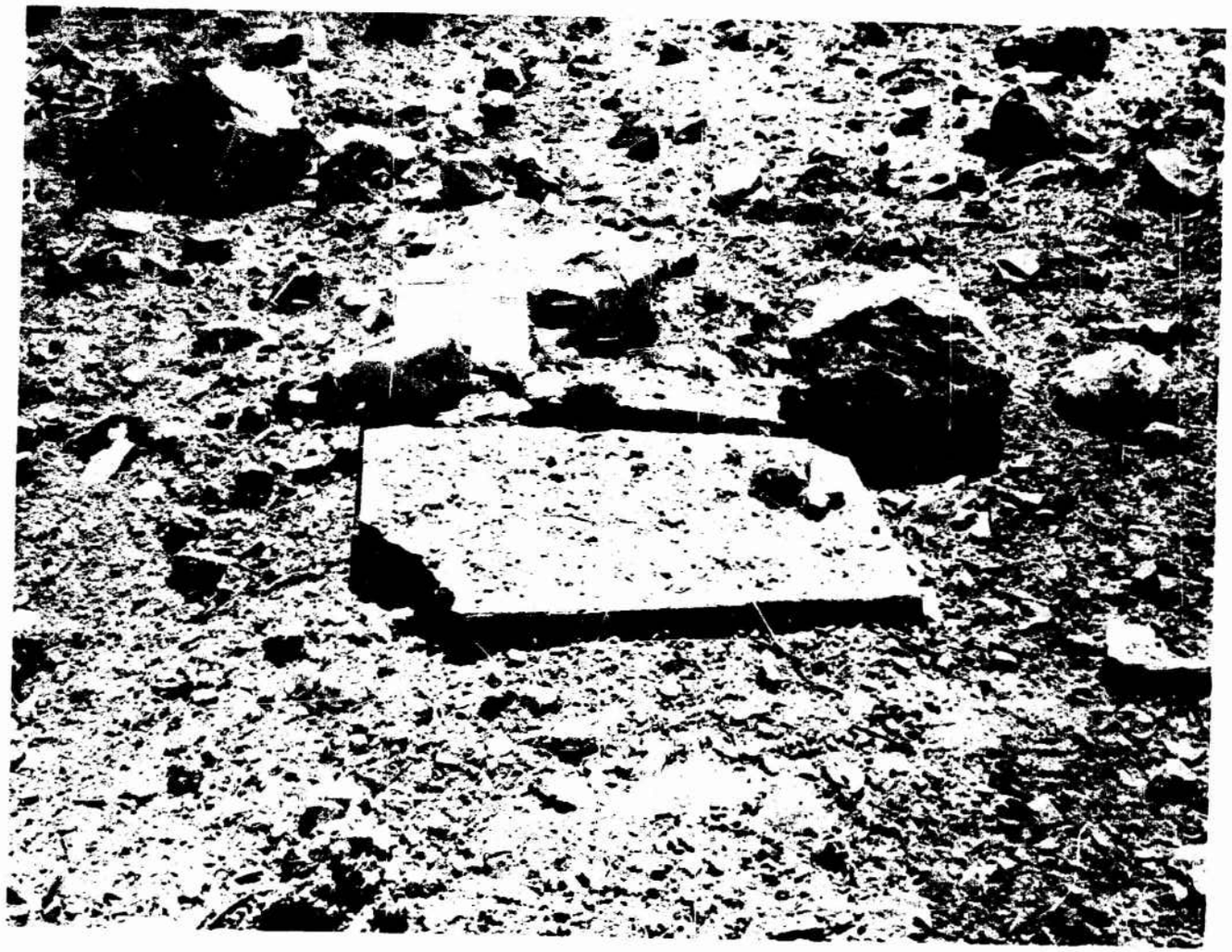

Figure 2.12 Station A-5. (DASA 67-17-NTS-64)

Figure 2.13 Station A-11. (DASA 67-10-NTS-64)

Figure 2.14 Station A-17. (DASA 67-03-NTS-64)

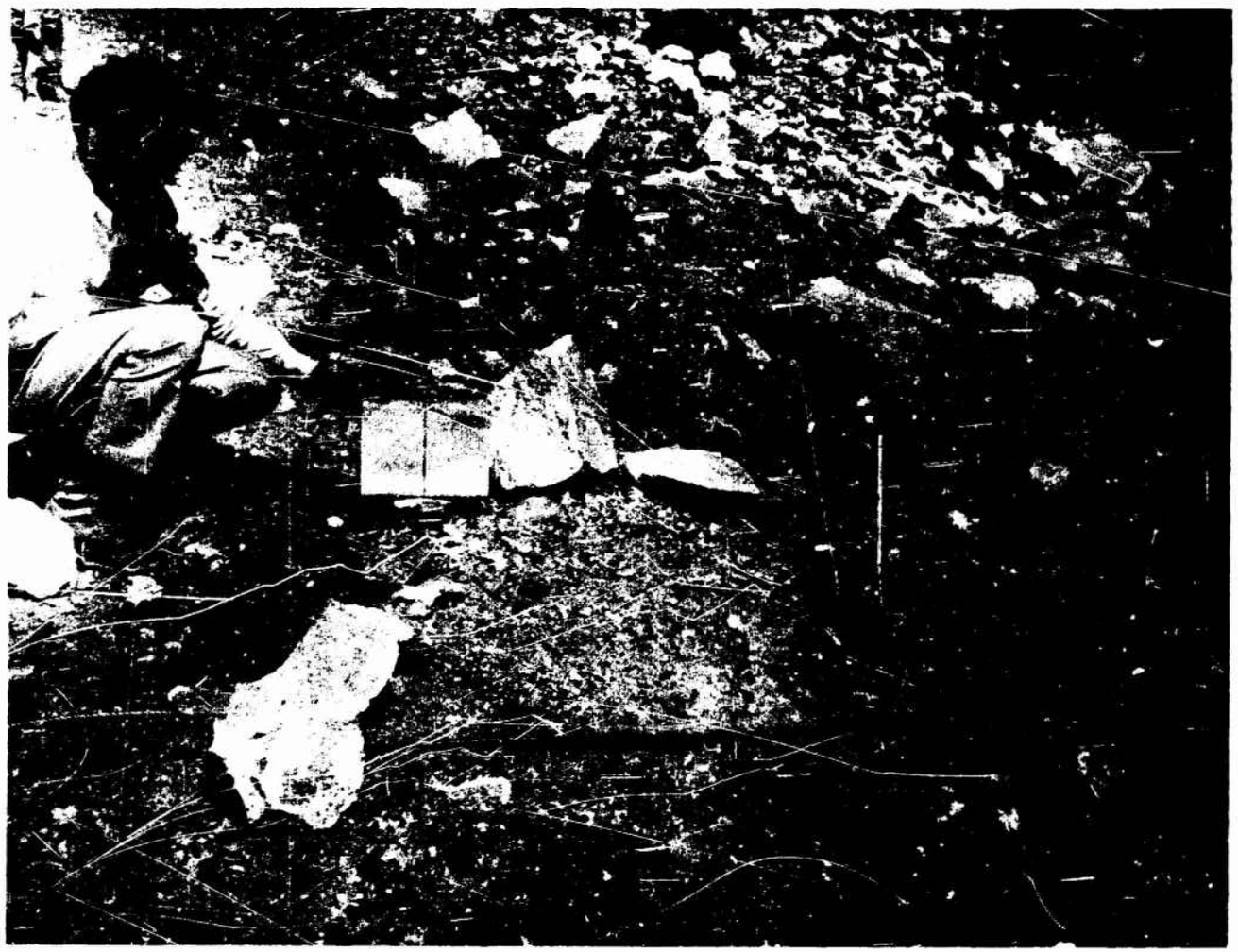

Figure 2.15 Station A-19. (DASA 67-04-NTS-64)

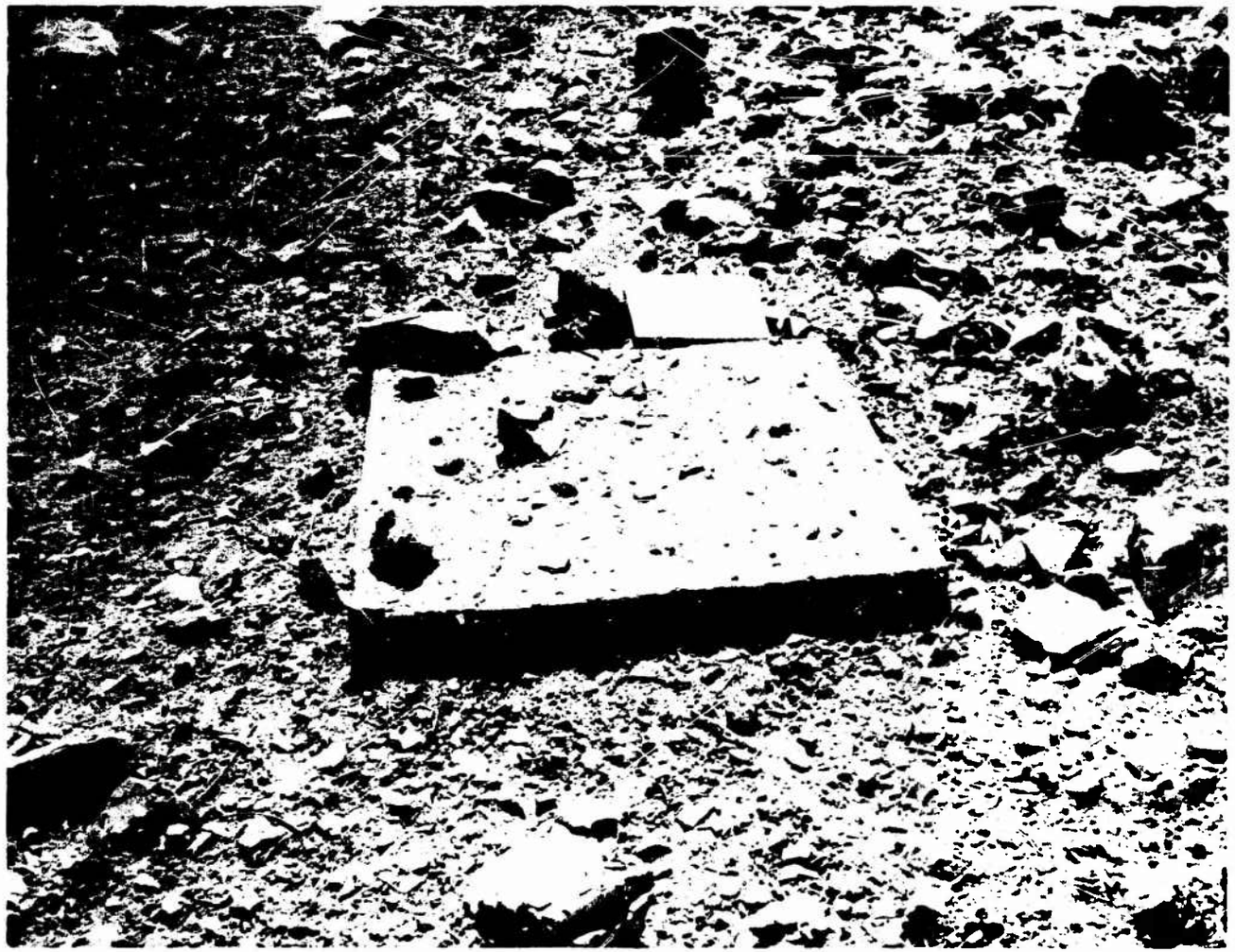

Figure 2.16 Station B-6. (DASA 67-15-NTS-64)

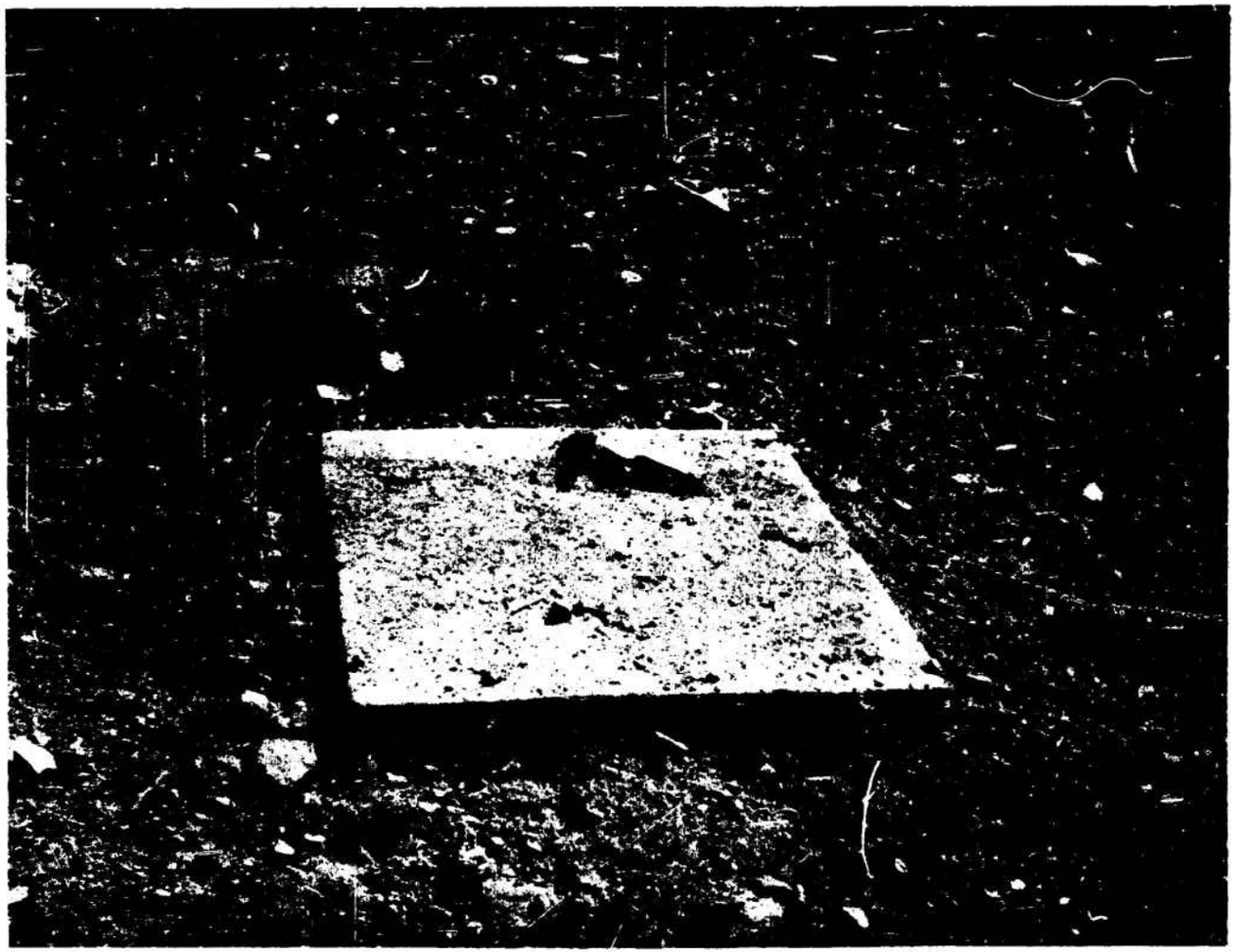

Figure 2.17 Station D-10. (DASA 67-09-NTS-64)

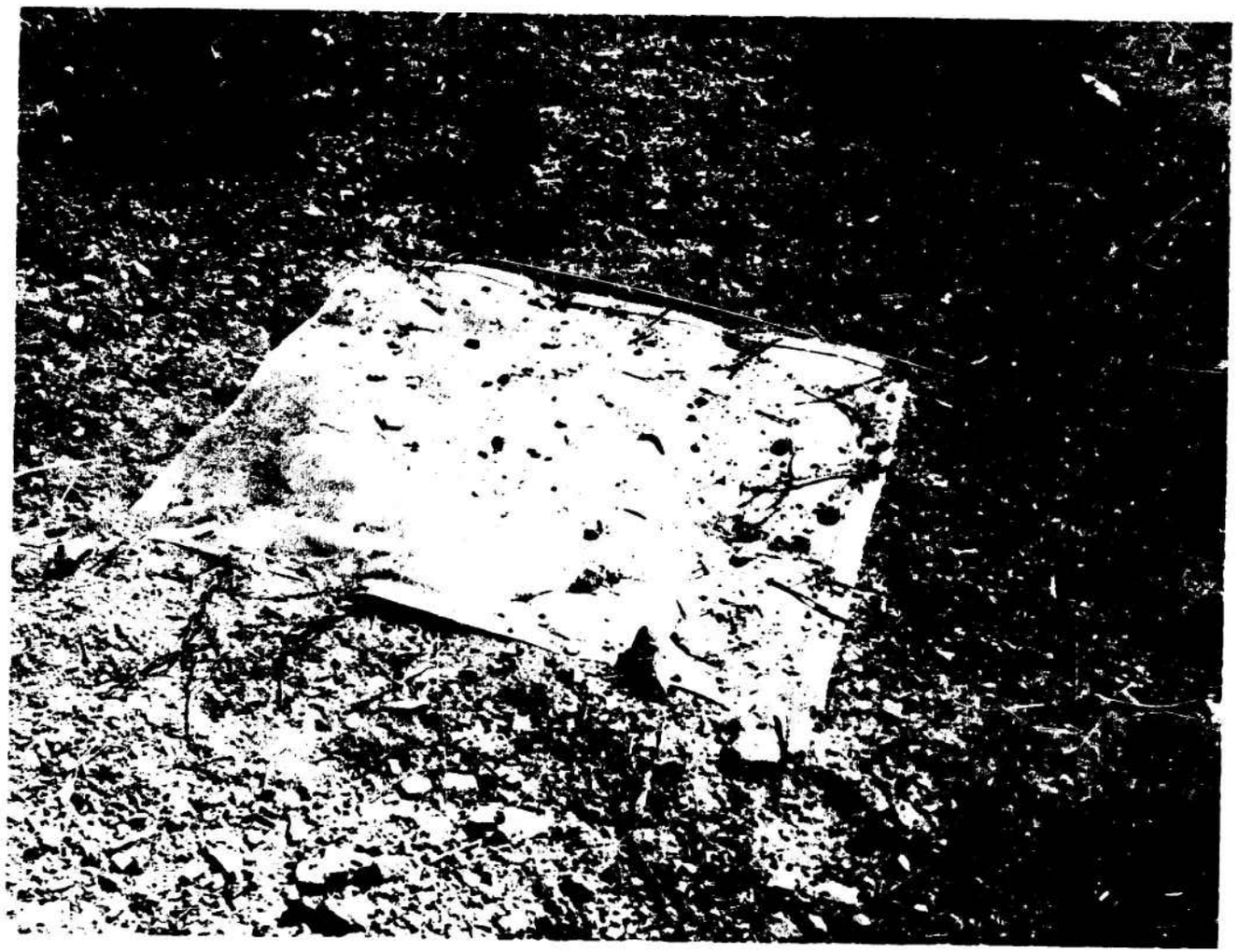

Figure 2.18 Station O-17. (DASA 64-30-NTS-64)

Figure 2.19 Station Q-17. (DASA 64-25-NTS-64)

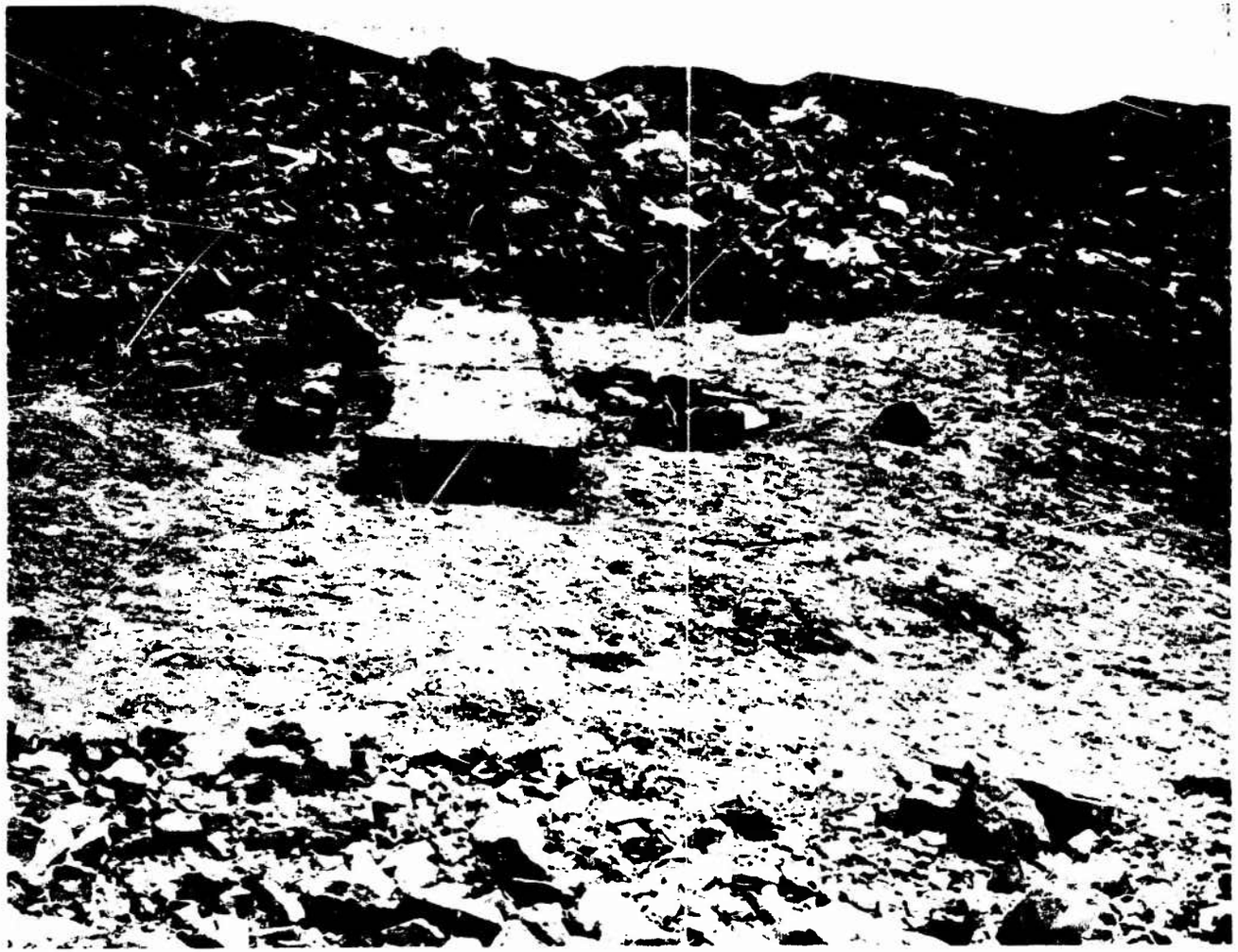

Figure 2.20 Excavated sector of lip, 58- to 87-foot sample area. (DASA 71-07-NTS-64)

Figure 2.21 Excavated sector of lip, 29- to 56-foot sample area. (DASA 7 -20-NTS-64)

Figure 2.22 Uplifted surface of excavated area. (DASA 73-11-NTS-64)

Figure 2.23 Truck dumping over grizzly at screening plant. (DASA 70-11-NTS-64)

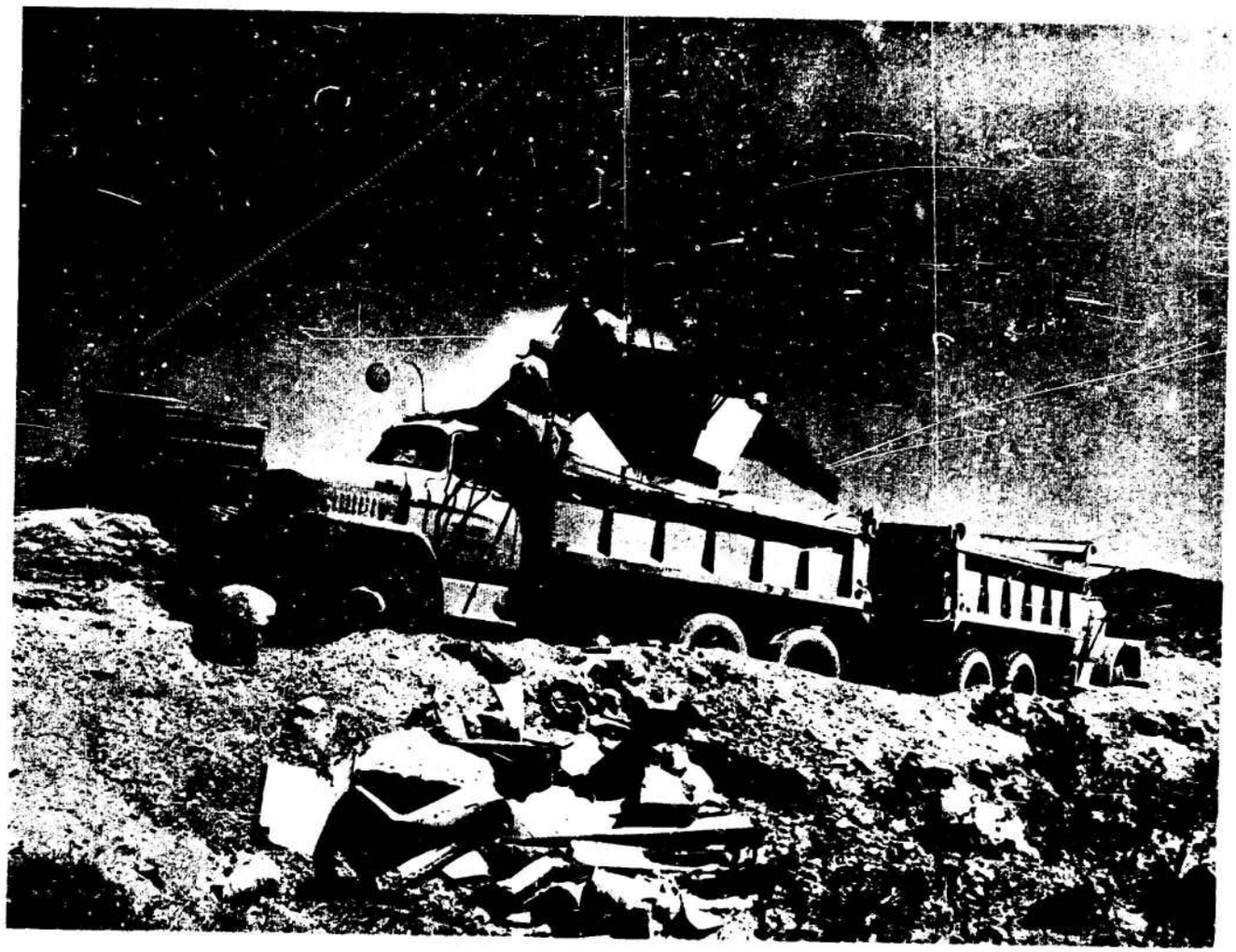

Figure 2.24 Loading of 1- and 3-inch screen sizes. (DASA 70-13-NTS-64)

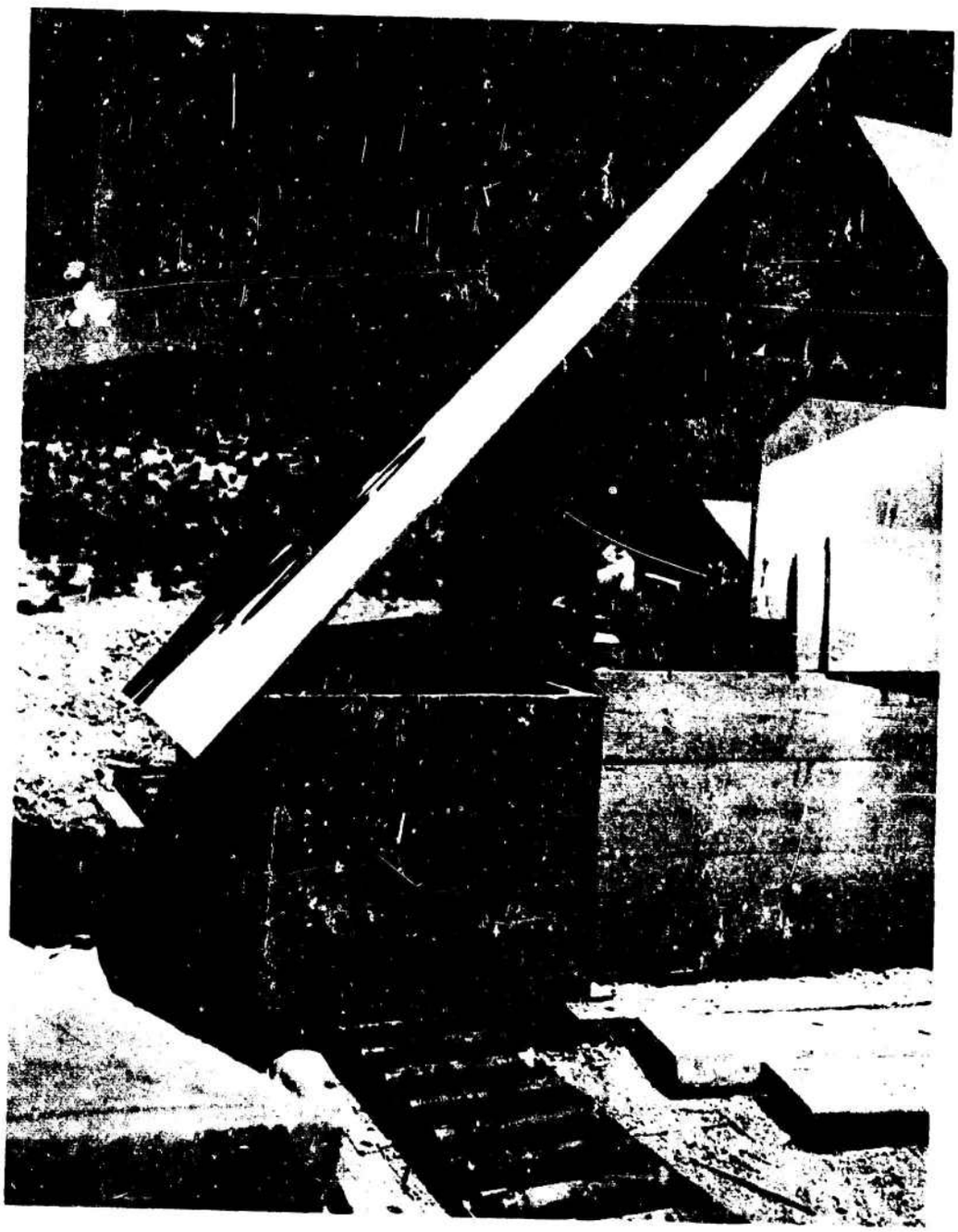

Figure 2.25 Jones riffle used at screening plant. (DASA 70-14-NTS-64)

Figure 2.26 Excavation of fallback material. (DASA 72-09-NTS-64)

Figure 2.27 Coded grout in rock fragment. (DASA 70-19-NTS-64)

Figure 2.28 Cylinder of coded grout broken loose from enclosing rock. (DASA 65-18-NTS-64)

CHAPTER 3

DATA ANALYSIS

3.1 EJECTA MASS DISTRIBUTION

As had been anticipated, the crater configuration and ejecta distribution were strongly influenced by the site geology. The apparent crater was roughly elliptical with its major axis parallel to the strike and its minor axis perpendicular to the strike.

The close-in ejecta were deposited in a rayed pattern. Six distinct rays were formed. The four most prominent rays were nearly parallel with the strike and perpendicular to it, although the northwesterly ray was displaced somewhat west of the strike. The most pronounced ray was down dip, covering the 30-degree sector centered on the S 63° W radial. The two other prominent rays were deposited due north and about N 40° E of GZ. These rays correlate fairly well with secondary highs in joint frequency. It is possible that they were caused by these secondary joint patterns. If so, their symmetrical occurrence in the southern quadrant may have been prevented by the large concrete pad emplaced there for Project 1.2 (see Figure 2.9). The rayed ejecta pattern is clearly visible on aerial photographs of the crater, but a suitable copy of such a photograph was not available for enclosure in the report.

The lip about due west of GZ (i.e. just north of the excavated sector)

was almost completely bare of ejecta (see Figures 2.22 and 3.1). Ejecta were only sparsely deposited in a sector centered on the radial about S 55° E from GZ. This sector was sheltered by the uplift of a large block of the Project 1.2 concrete pad (see Figures 3.2 and 3.3).

Figure 3.4 is a plot of elevation differences between pre- and postshot topographic maps of the crater area by American Aerial Surveys, Inc. The contours showing changes in elevation include the effect of uplift as well as ejecta thickness. The rayed pattern of ejecta distribution can be seen in this illustration.

Figure 3.5 is an isopachous plot of ejecta thickness in the 30-degree sector centered on the S 63° W radial. This plot was made from the H and N surveys over the pre- and post-excavation surfaces. Although it was not part of Project 1.5 to obtain uplift information, the uplift profile along the S 63° W radial was obtained as a byproduct of Project 1.5 data and is presented in Figure 3.5.

The volume of ejecta in the 30-degree sector 29 to 87 feet from GZ was determined by three methods: (1) The centroids of the thickness profiles from the H and N survey were revolved through appropriate arcs and the resulting volumes summed. (2) The isopachs of Figure 3.5, from the H and N surveys, were planimetered and the volume computed. (3) The contours of equal pre- and postshot differences in elevation of Figure 3.4, from the aerial surveys, were planimetered and the volume computed. From this the

volume of the uplifted lip, obtained by revolving the S 63° W uplift profile through 30 degrees, was subtracted. Contour intervals from the aerial surveys were not detailed enough to give reliable results in the region from 58 to 87 feet.

The results of these computotions are given in Toble 3.1. The bulk density of the ejecta from the two samples was computed by dividing the weight of the samples by the average volumes found by methods No. 1 and No. 2. The bulk density of the sample 29 to 58 feet from GZ averaged 100 pcf, and the sample from 58 to 87 feet averoged 142 pcf.

The difference in bulk density as a function of distance is ottributed to differences in ejecto thickness. In the sector sampled, ejecto thickness ranged from about 0.5 to 6.5 feet at radial distances of 29 to 58 feet from GZ; hence, bulking of fragments was significant in this region (see Figure 3.6). Ejecta thickness ranged from 0 to about 1.5 feet at radial distances from 58 to 87 feet. Over much of this areo the ejecta distribution was nearly a monolayer of particles.

Six truckloads of the fallback removed by Project 1.9 personnel had an average bulk density of about 100 pcf in the as-loaded condition (Reference 17). Truckloads of the screened material also averaged about 100 pcf.

Areal density as a function of distance from GZ was computed from

determinations of ejecta thickness in the lip area. Ejecta thickness was found along the 24 sample radials from Figure 3.4, after which corrections were made for uplift. The uplift corrections were made by assuming that the two uplift profiles along the strike and the two perpendicular to the strike were representative of their respective 90-degree sectors. Uplift profiles used, except along the S 63° W radial, were furnished by Project 1.9 personnel (Reference 17).

Ejecta bulk density was assumed to be 100 pcf where the elevation differences of Figure 3.4 were greater than 2 feet. In the region between 100 and 520 feet from GZ, ejecta areal densities were determined by taking the mean of the samples collected at a given radial distance. Figure 3.7 is a plot of mean ejecta areal density as a function of distance from GZ.

Ejecta mass through 100 feet from GZ was found by planimeter to be 2.63×10^6 pounds. This number includes a small adjustment for the uplift of the Project 1.2 pad as well as adjustment for the four uplift profiles. Integration of the area under the areal density versus distance curve of Figure 3.7 gave an ejecta mass of 2.26×10^6 pounds through 100 feet from GZ. This was a machine integration from point to point assuming a power law fit between points.

Two methods were used to integrate the areal density-distance curve to obtain the ejecta mass between 100 and 520 feet: One method assumed

areol density varied as the two line segments shown in Figure 3.7. These segments represent best fit mean values of the slope through 270 feet, extended to 520 feet. Computed ejecta mass from 100 to 520 feet was 0.26×10^6 pounds by this method. The other method used was the point-to-point machine integration. This colculotion gove an ejecta moss of 0.34×10^6 pounds from 100 to 520 feet. Thus, calculotions of ejecta mass through 520 feet give values ranging from about 2.52 to 2.97×10^6 pounds, depending on the procedure used.

With the ejecto sampling data that are available, it is not possible to compute total ejecta mass with the accuracy hoped for when the project was planned. An approximate lower bound of 2.52×10^6 pounds is obtoined by accepting the minimum colculation based on sample data through 520 feet and assuming that the ejecta deposited beyond this distance are negligible. This is not a particularly good assumption, as discussion of the far-out missile survey (Section 3.3) will demonstrate.

An attempt was made to draw an upper bound for total ejecta mass by the following calculation: The toil of the areal density curve is usually approximated by a power law fit that is terminated at some arbitrary distance. Using this assumption, the areal density-distance curve was extrapolated to 4,000 feet, the approximote distance of the farthest recorded missile, by extending the power law best fit of data points between 125 and 520 feet.

Integration of this curve gave a completely unreasonable value of 1.44×10^7 pounds for total ejecta mass.

Data from Project 1.9 indicate an apparent crater volume of about 370 yd^3 and a true crater volume of about 900(±100) yd^3 (Reference 17). If it is assumed that total ejecta mass is equal to the preshot mass of the true crater volume less the mass of fallback material, computed at 100 pcf, total ejecta mass ranges between about 2.44 and 2.82×10^6 pounds. The effect on true crater volume of density changes in the medium around the crater due to shattering of the rock cannot be evaluated.

Because of differences in definition of crater parameters to be discussed in Section 3.4, the Project 1.9 data are not comparable with those used in this analysis; therefore, close agreement between results of ejecta mass calculations using the two sets of data is not to be expected.

The ratio of the range of areal density to mean areal density at a given radial distance is shown in Figure 3.7. This ratio, rather than the standard deviation, is given to emphasize that the distribution of areal density as a function of azimuth is unknown. The ratio of range to mean is seen to increase almost exponentially with distance from GZ through 270 feet, where the number of sampling stations per ring was decreased.

The increase of sample scatter with distance is attributed to two factors: One factor is the increasing concentration with distance of ejecta

mass in a relatively few large fragments. The likelihood of obtaining representative ejecta samples with a few small collector surfaces under these conditions is remote. An example illustrating this point was seen at the 270-foot sampling ring where over 80 percent of the mass collected from 10 pads was in a single fragment. The second factor concerns concentration of the ejecta mass in rays. Intuition suggests that for a rayed deposition pattern the true probability density function for areal density at a given distance is at least bimodal. For a distribution of this type, the mean is not necessarily a good estimate of central tendency; something must be known about the relative probabilities of being on a ray or between rays.

For the Flat Top I event the sample array was inadequate to define differences in ejecta distribution as a function of azimuth. There was a complete hiatus in sampling of noncoded ejecta between 520 and 2,500 feet. A qualitative description of ejecta distribution beyond 2,500 feet is given in Section 3.3.

3.2 EJECTA SIZE DISTRIBUTION

The site geology caused differences in the size of lip ejecta up dip and down dip from GZ. Up dip, large blocks of limestone parted along bedding planes, sliding up and away from GZ. Figure 3.8 shows the best example of this. The largest portion of the block shown had dimensions of about 5-by-3-1/2-by-2 feet. It is a question of definition as to whether

these upthrust blocks are ejecta or uplift; for this analysis they were assumed to be ejecta.

In Figure 3.9, also taken on the eastern portion of the lip, the large fragment behind the camera bag has been overturned, with little horizontal displacement. The smooth upper surface to the right is a bedding plane. The painted surface originally at ground level is lying face down.

No fragments as large as the upthrust block shown in Figure 3.8 were included in the ejecta along the western side of the crater. The beds dipped away from GZ in this direction, and large blocks separating along bedding planes tended to be displaced upward more or less as a unit. These blocks were defined as the uplift surface. Figure 3.10 illustrates this phenomenon. The view is of the bare surface, just north of the excavated sector, looking east toward the crater. In the excavated sector this intense fracturing of the uplifted surface extended about 35 feet from GZ (see Figure 2.22).

The largest ejecta fragment in the sector between 29 and 58 feet from GZ measured 4 by 2-1/4 by 2 feet, and weighed 1,190 pounds; the largest ejecta fragment between 58 and 87 feet from GZ measured 3 by 2 by 1 feet, and weighed 722 pounds.

Figure 3.11 shows plots of cumulative percentage of ejecta finer than a given size and incremental percentage of ejecta in given size intervals, as a function of fragment size. These plots are for the samples of ejecta

taken in the 30-degree sector and in the sampling rings at 100 ond 125 feet from GZ. For reasons discussed previously, the sampling array was inadequate to provide representative data on ejecta size distribution beyond 125 feet. (It was originally planned to size a sample of the fallback material excavated by Project 1.9, but this was precluded by lack of time.)

The plots in Figure 3.11 show that, within the range of distances for which valid data were obtained, the size of the largest ejecta fragment decreases, and the proportion by weight of fragments in given size intervals increases with decreasing size, as the distance from GZ becomes greater. The results are not unexpected, but as far as is known, these relationships have not previously been investigated in a quantitative manner.

Figure 3.12 shows the results of combining all the ejecta size data after weighting with respect to ejecta mass represented by each sample. The machine computation of ejecta mass using the areal density data plotted in Figure 3.7 was used in the weighting procedure. The hump in the size interval from 3 to 8-1/2 inches may be related to the spacing of fractures and bedding planes. From field observations it seems likely that the hump would be more pronounced if the class intervals had been so chosen that one interval was intermediate between the 3-to-8-1/2-inch and the 8-1/2-to-24 inch intervals.

The relative proportions of intervals of fines were not accurately determined, but this has little effect on the proportions determined for the intervals of coarser material. Limitations on the accuracy in determining the proportion of fine material are discussed in Appendix B and Section 3.3. The cumulative effect of all limitations of the size analysis results in an understatement of the true amount of comminution caused by the explosion. (The data were not sufficient to analyze variations in ejecta size distribution as a function of azimuth.)

3.3 FAR-OUT MISSILE SEARCH

As noted previously, no effort was made to collect data on noncoded ejecta distribution between 520 and 2,500 feet from GZ. A particularly large splash crater was seen in the sector searched for coded grout fragments about 1,250 feet from GZ. This crater was formed by the impact of a large limestone fragment on alluvium. The crater diameter was about 5 feet and its depth about 1.5 feet. Secondary particles of the limestone fragment were found as far as 75 feet beyond the impact point.

Virtually all the ejecta found beyond 2,500 feet from GZ were in the form of shock comminuted but coherent masses of dust-size limestone particles. The massive fragments had considerable cohesive strength but were friable and could be powdered between the fingers. They were white and showed grooves or slickensides on surfaces not broken by the impact

of landing (see Figure 3.13). These ejecta are referred to as shatter canes.

Figure 3.14 shows a thin section from the normal, unshattered ejecta fragment shown in Figure 3.13. The photograph was made with polarized light at a magnification af 160 diameters. The individual calcite grains are unbroken. This figure may be compared with Figure 3.15, u thin section from a shatter cane photographed at the same magnification. The shatter cone thin section shows innumerable close-spaced fractures cutting individual grains with no apparent control by grain boundaries.

Obviously, the size analysis of Sectian 3.2, based on screening ejecta that included large shatter cone fragments, does not show the true extent of comminution caused by the explosion.

Limestone and other carbonate rocks are knawn to possess some ductility, and they exhibit a pseudoplastic behavior. The shatter cones are fragments of limestone stressed beyond the yield point inta the region of pseudoplastic behavior. (Reference 18 summarizes the behavior of limestone under slow application of large stresses.)

A precursor has been abserved traveling at approximately sonic velocity and at a stress level af about 5.5 kilobars in samples af Banded Mountain limestone shocked at 110 kilabars (Reference 19). Allowing for the strain-rate effects known to exist in limestane (see, far example, Reference 20),

5.5 kilobars is close enough to the confined static yield strength of 3.4 ta 5 kilobars reported for a similar dense, fine-grained limestone (References 18 and 21) to be taken as the dynamic yield strength of the Flat Top I medium. The compressive strength of about 1 kilobar reported in Table 2.1 does not represent the yield strength as the term is used here.

Preliminary reports of close-in stress measurements made on the Flat Top I event indicate a transition to elastic-wave behavior at a peak stress of about 6 kilobars. This transition occurred abaut 10 feet from the center of the charge. Assuming that all the shatter cone fragments came from the pseudoplastic zone within 10 feet of the charge center, a rough upper limit or the weight of ejecta deposited beyond 2,500 feet can be calculated.

The limestone in the pseudoplastic zone within 10 feet of the charge center weighed about 3.1×10^5 pounds. Since virtually all of the ejecta beyond 2,500 feet were in the form of shatter cones and the ejecta beyond 2,500 feet comprised only part of the shatter cone material, no more than 3.1×10^5 pounds of ejecta could have been deposited beyond 2,500 feet.

Figures 3.16 through 3.19 show early and late stages of the Flat Top I event from the two camera stations of Project 9.8 designated on Figure 2.1. The trajectories of the shatter canes are clearly defined by trails of white limestone dust. Since the camera stations from which these pictures were taken were only 1,451 and 1,778 feet from GZ, it is obvious

that much of the shatter cone moteriol wos deposited closer to GZ than 2,500 feet.

It is clear from the eorly photograph mode southeast of GZ that the initial trajectory ongle of shatter cone ejecta was offected by the dip of the beds. The early photograph mode southwest of GZ shows thot shatter cone ejecta were more abundant and hod o higher initial trojectory ongle to the northwest. This evidence tends to confirm the visual observotions of for-out ejecto distribution mode during the helicopter reconnaissance. The higher initiol ongle to the northwest moy be related to the topographic slope. The late photographs mode from both stations show thot deposition of shotter cone ejecto relotively close to GZ wos more obundant in the southeost sector thon elsewhere.

Figure 3.20 shows the impact point of o shatter cone about 3,300 feet from GZ on the east slope of Balloon Hill; this missile disaggregoted to powder upon impacting ogoinst rock.

Impoct points of some high-angle shatter cone fragments deposited near GZ ore shown in Figures 3.21 through 3.23. Figure 3.21 wos mode obout 75 feet, Figure 3.22 about 180 feet, and Figure 3.23 about 270 feet from GZ. In Figure 3.23 the smoll disaggregoted shatter cone impacted on o coded grout ejecto fragment olready at rest. This piece of grout was originally emploced at the surface 24 feet from GZ.

Figure 3.24 shows the distribution of missile impact points mapped by the H and N survey crews beyond 2,500 feet in the sector from S 12° E to S 72° E. When these data had been plotted, it was thought unusual that the distribution of missiles should be so uniform over the range of distances from GZ covered by the survey; therefore, four areas, each covering about 2 acres, were selected for investigation. Two areas were chosen where impact points were relatively scarce and two where impact points were relatively concentrated. These areas are outlined on Figure 3.24.

On a trip to NTS during the middle of September 1964, the Project Officer checked these areas by walking them on 25-foot centers. Because the alluvium and shatter-cone dust had been washed by several heavy rains, some impact points were difficult to identify. Craters thought to be impact points but which were not absolutely identified as such are termed probable.

No unmapped impact points were found in the two areas of low missile concentration; however, in both areas of high concentration, unmapped impact craters were found.

In one area, where six impact points had been mapped, three definite and two probable unmapped impact craters were found. In the other area, where seven craters had been mapped, three definite and one probable unmapped craters were found.

From these data it appears that only about 50 to 75 percent of the impact points in areas of greatest concentration were mapped, whereas almost all of them were mapped in areas of low concentration.

When the mapped frequency of impact points is corrected on the basis of these observations, a maximum concentration of three to four impact points per 10,000 square feet is obtained for the sector from S 12° E to S 72° E beyond 2,500 feet from GZ.

Little data could be collected on the size of impacting missiles in the far-out region because of the tendency for missiles to shatter on impact. The most spectacular shatter cone impact point seen was to the northwest of GZ at an estimated distance of about 2,700 feet. This shatter cone fell on a limestone outcrop and splashed over an irregular, elongated area paced off as about 125 feet long by about 35 feet wide. The long axis of the splash paralleled the radial from GZ through the impact point. The impacting missile is estimated to have weighed at least a few hundred pounds.

To the southeast, where impact points were mostly on alluvium, a few shatter cones were found more or less intact in their impact craters. Measured dimensions of these missiles in the area checked by the Project Officer ranged from about 3 by 2 by 2 inches to 10 by 10 by 5 inches. Their weights ranged from about 1 to 50 pounds. The most distant missile found in the southeast sector was about 4,060 feet horizontally from and 325 feet vertically above GZ. The largest fragment of this missile measured about 18 by 12 by 9 inches. The combined weight of all its fragments was estimated to be about 250 pounds.

The shatter cone to the left in Figure 3.13 is listed as Missile 71 in Appendix F. It is the smallest missile, which had not disaggregated appreciably on impact, that was found during the Project Officer's check.

3.4 DISTRIBUTION OF CODED EJECTA

The coded grout pad was intended to provide information on the distribution of ejecta originally at the ground surface near the burst point. However, because of the low strength and uneven thickness of the pad, the postshot distribution of its fragments could not be expected to simulate the medium ejecta distribution; therefore, no effort was spent in analyzing the distribution of pad fragments beyond outlining their limits.

The compressive strength of the pad grout was not determined, but it is estimated to have been between one and two orders of magnitude less than that of the limestone. The grout pad was completely stripped from the uplifted surface.

An extension of the grout pad from 45.5 to 75 feet had been made of concrete to provide a collection surface for the ejecta fines. The concrete extension remained in place over its entire length, although it was broken into segments ranging from about 1 to 4 feet in length (see Figures 2.20 and 2.21).

The compressive strength of the concrete can be assumed to be of the order of 1,500 to 2,000 psi and that of the grout considerably less.

These strengths are markedly lower than the value of about 15,000 psi determined for the compressive strength of the limestone.

Frogments from the red portion of the coded pad, which extended from the edge of the TNT sphere to 15.5 feet from GZ, were very obviously smaller than fragments of other pad colors emplaced further from GZ. However, because grout fragment size could not be reloted to limestone ejecta size, no quantitative assessment of grout fragment size distribution was attempted.

Figure 3.25 shows the limits of the areal distribution of fragments from the coded pad. The southern ond westernmost limits of fragments from the red ond yellow pad segments, which were nearest GZ, are only approximate becouse of the cursory search conducted in these regions. The areo searched thoroughly for coded ejecta is outlined.

Fragments from the individual 1-foot cylinders of coded grout appear to have been moved from their original positions in the medium in two modes. (The emplacement position of the tops of individual cylinders is given in Appendix G.) In the upper portion of the true crater region, the mode was evidently by ejection along high-angle/high-velocity trajectories similar to those shown in Figures 3.16 through 3.19.

In the lower portion of the true crater region, the mode was evidently a pushing of the broken fragments away from GZ by forces with a downward

component from the charge center. The uppermost fragments moved in this mode were pushed up over the true crater surface and deposited in the ejecta lip, where they were defined as ejecta. The lower fragments moved in this mode remained in the true crater, where they were defined as fallback.

Figure 3.26 is a section through the crater along the S 63° W radial showing the zones in which the ejecta fragments are thought to have been moved in the modes described. For this illustration the ejecta lip is defined to extend between 27 and 81 feet from GZ. This is 2 mean apparent crater radii from the mean apparent crater edge. Along the S 63° W radial this area was covered with ejecta.

The vertical transition between ballistically ejected fragments and those pushed into the ejecta lip was abrupt, as if the transition between the modes had taken place across a shear plane. The horizontal distance between the uppermost-pushed fragment and lowest ballistically ejected fragment recovered from individual grout columns was 586 feet for the column at 6 feet from GZ, 90 feet for the column at 12 feet, 200 feet for the column at 18 feet, and 51 feet for the column at 24 feet.

The line in Figure 3.26 showing the transition between pushed ejecta and pushed fallback is essentially a matter of definition. For this analysis the crater nomenclature used is that recommended by Hansen et al in Reference 22. It is obvious from this illustration that much of the broken

material within the true crater, as defined by Project 1.9 personnel, is defined as ejecta for this analysis.

The uppermost fragment of fallback from the grout column at 12 feet was found 3 feet nearer GZ than the lowest fragment of lip ejecta. For the column at 18 feet this separation was 12 feet. There were no fragments found in the ejecta lip from the column at 6 feet, and there were no fragments found within the true crater, as defined for this analysis, from the column at 24 feet.

A total of 350 fragments from the coded cylinders was recovered and their locations mapped. Sections of whole cross sections of cylinders longer than 1 inch were measured, and small fragments were combined and weighed to determine percentage recovery of the coded material emplaced.

Of the coded material emplaced within the limits of the true crater, 42 percent was recovered. Recovery was very unevenly distributed among the columns as shown in Figure 3.26, where the percent of recovery of ballistically ejected and pushed fragments is given for each coded grout column.

Of the ballistically ejected coded material, 41 percent was recovered. The low recovery of pushed coded material from the columns at 12 and 18 feet from GZ was probably due to the impossibility of thoroughly examining fallback being excavated with the crane-mounted clamshell.

Because the low strength of the grout made it impossible to relate coded and in situ material fragment sizes, no detailed analysis of the size distribution of coded cylinder fragments was made. It was noted, however, that fragments were generally larger from cylinders placed successively deeper below the ground surface and horizontally more distant from GZ.

Essentially all of the coded fragments found in the fallback and ejecta lip were whole cross sections of cylinders longer than 1 inch. No whole cross sections longer than 1 inch were found among recovered fragments of the ballistically ejected material from the columns at 6 and 12 feet from GZ. Of the ballistically ejected material, 24 percent recovered from the column at 18 feet was in whole cross sections longer than 1 inch. About 95 percent of the ejected material was recovered in this form from the column at 24 feet.

Fragments from individual 1-foot cylinders of ballistically ejected coded grout were deposited over a range of distances from GZ usually in excess of their mean distance. Figures 3. 27 and 3. 28 are plots showing typical distributions of ejecta from individual cylinders. The intersecting bars indicate the mean and standard deviation of the distributions.

The cumulative frequencies of these ejecta as a function of distance were found to be approximated by Gaussian distributions. Figure 3. 29 shows probability plots of the cumulative frequency of the ejecta distributions shown in Figures 3. 27 and 3. 28. Comparison with the straight lines

representing Gaussian distributions having the sample means and standard distributions illustrates the goodness of fit. The upper distribution is one of the better fits found, and the lower, one of the poorer fits.

Both cylinders from which these distributions of ejecta were found were emplaced 12 feet horizontally from the charge center. The upper distribution of fragments came from a cylinder emplaced with its center a vertical distance about 3 feet lower than the charge center; the lower distribution came from a cylinder with its center about 5 feet lower than the charge center.

The general trend of ejecta distribution from individual cylinders was toward decreasing mean distance from GZ with increasing depth of emplacement at a given horizontal distance. Distributions from cylinders emplaced at the same depth generally tended to be located further from GZ as their horizontal emplacement distance from the charge center decreased.

Figure 3.30 shows the mean distance of fragments from GZ for all cylinders from which fragments were found beyond 27 feet, the average apparent crater radius. Median distances are about the same, as would be expected for Gaussian distributions.

The contours of Figure 3.31 show equal mean horizontal displacement of coded fragments from the point of emplacement of their respective cylinders. These isodistance contours were obtained by assuming that the midpoint

of each cylinder represented the mean horizontal distance of its fragments from GZ, less the horizantal emplacement distance of the cylinder from GZ. When the ballistic-push transition occurred within the length of a cylinder, the mean fragment distances were calculated separately. The correctian due to angular deflection of the fragments was ignored.

The mean distance of fragments from the uppermost cylinders af the grout calumns at 12 and 18 feet from GZ was less than the mean distance af fragments from the second highest cylinders. This is attributed to the uppermost cylinder in each calumn having been emplaced in the coded grout pad. The velocity of the density-matching graut was undaubtedly lower than that of the limestone. The distributian of fragments from the cylinder emplaced between 4 and 5 feet below the charge center, 6 feet from GZ, does not fit into the general pattern af the other distributians.

The mean azimuth of fragment distributions fram many of the cylinders was deflected counterclackwise from the prajected radius originating at GZ and passing through the point of emplacement of the cylinders. (This is well illustrated in Figures 3.27 and 3.28.)

Figure 3.32 is a plot showing cantaurs of mean equal caunterclackwise deflection far ballistically ejected fragments from individual cylinders. For this plot it was assumed that the mid-paint af each cylinder represented the mean af its fragment angular displacements measured by angles ariginating

at GZ. For the distances and angles considered, there would be little change in the contours if angular deflections originating at the vertical centerlines of each grout column had been used.

The northeasterly surface wind at shot time could have caused a small part of the observed deflection of particles but could not possibly account for all of it.

There is a tendency for fragments from cylinders within the region that would have been most affected by strong shock reflections off the large block of in situ rock directly beneath the charge to be those most deflected.

Figure 3.33 is a view from inside the crater looking southeast. The lath is vertically below original GZ, and the rock mentioned above is to its right. Measurements on this rock surface showed a dip ranging from about 25 to 35 degrees in the direction S 45° W. This direction is 18 degrees counterclockwise from the radial along which the grout cylinders were emplaced. Measurements of the strike of beds immediately west of the crater gave N 27° W within the limit of accuracy of surveying by Brunton compass. It is suggested that the reflection surface provided by this rock face was largely responsible for the deflections observed in the fragment distributions.

Although this shear surface may have been caused by the rock failing along a natural plane of weakness, it is noted that the direction of the

instrumentation tunnel, which passed under the crater, was practically the same as the strike of the shear surface. On the other hand, the strike af the bedding planes, that of the most likely failure surface, was oriented 18 degrees clockwise from the strike of the shear plane. It is also noted that the dip of the bedding planes was some 20 to 30 degrees greater than the dip of the shear plane.

That the presence of the instrumentation tunnel influenced ejecta distribution cannot be proved on the basis of these observations, but the possibility shauld not be ruled out.

Elevations taken on the top of coded grout calumns in place at the true crater surface showed na vertical movement due ta the explosion at 6 and 12 feet from GZ. The top of the exposed cylinder 18 feet from GZ had moved up about 0.7 foot. The cylinder exposed at the true crater surface 24 feet from GZ was broken off within one of the 1-foot coded intervals, and all that could be determined was that the cylinder had moved up more than 0.1 foot but less than 1.1 feet.

TABLE 3.1 EJECTA VOLUME IN S 63° W SECTOR

Method	Sample 1 (29 to 58 Feet)	Sample 2 (58 to 87 Feet)
	$ft^3 \times 10^{-3}$	$ft^3 \times 10^{-2}$
No. 1	1.63	2.76
No. 2	1.78	2.84
No. 3	1.83	--

Figure 3.1 Bare lip north of excavated sector. (DASA 70-15-NTS-64)

Figure 3.2 Uplift of Project 1.2 pad (looking southwest). (DASA 73-12-NTS-64)

Figure 3.3 Uplift of Project 2.1 pad (looking northwest). (DASA 73-15-NTS-64)

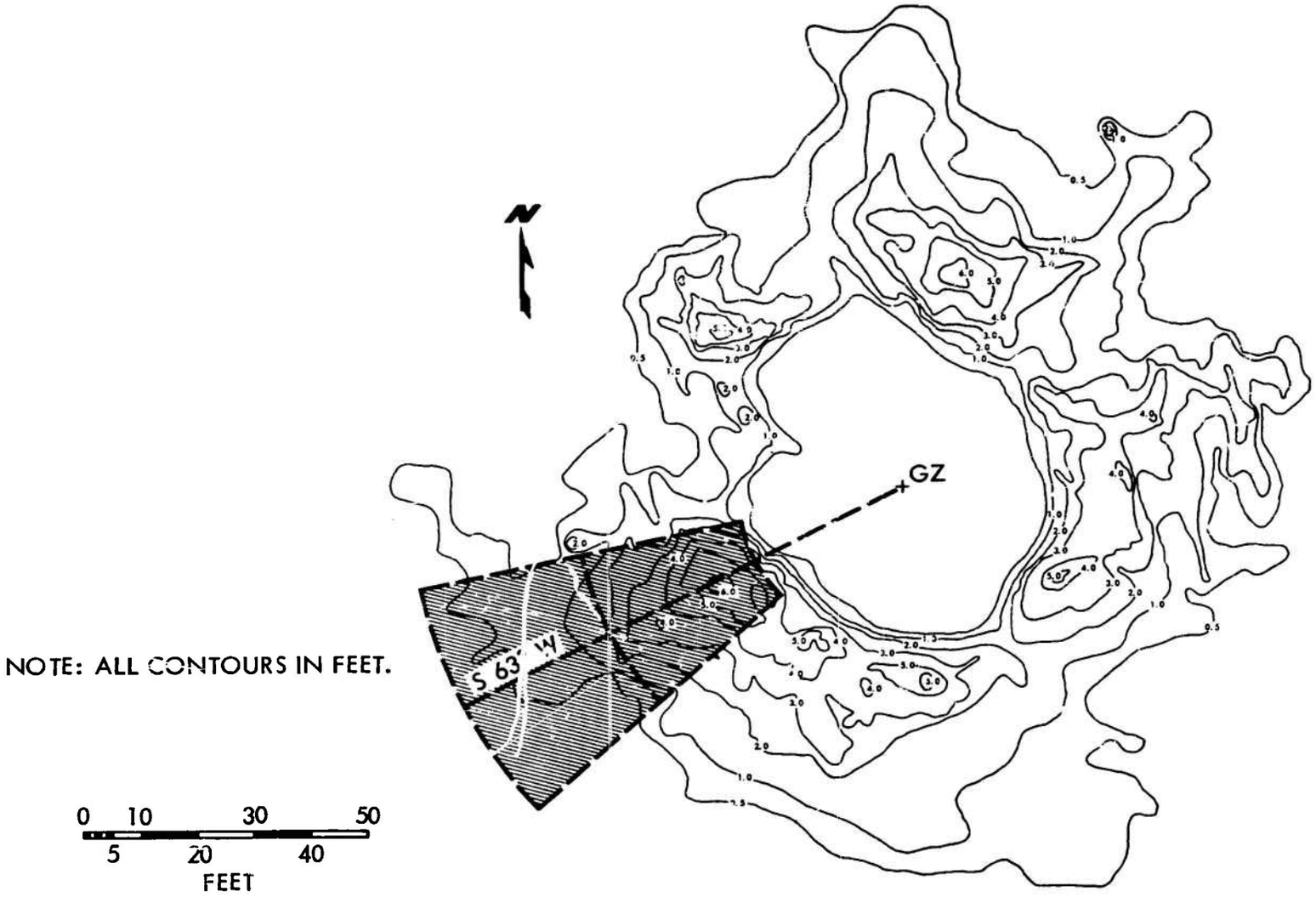

Figure 3.4 Differences in elevation between pre- and postshot aerial surveys.

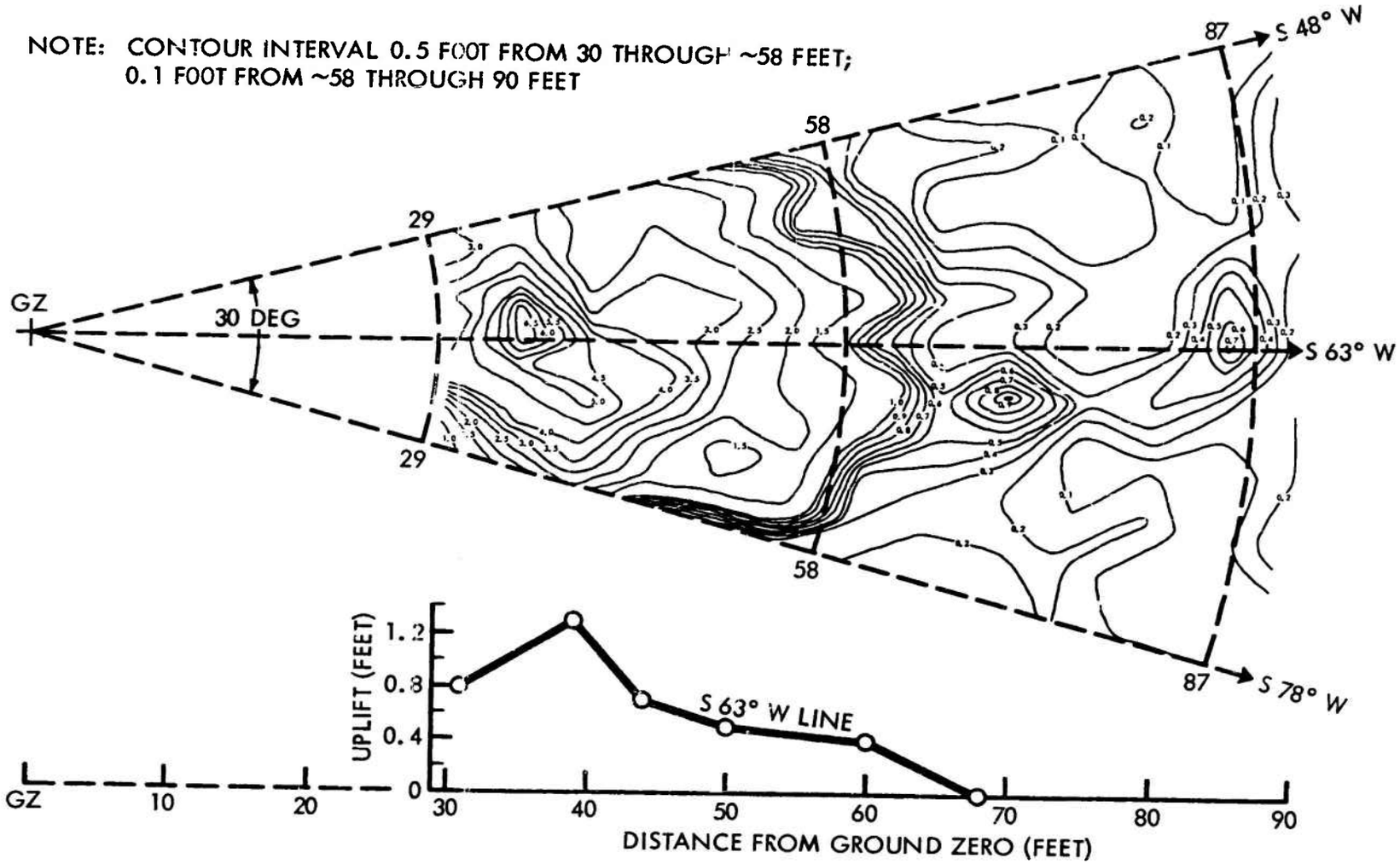

Figure 3.5 Ejecta thickness and uplift in excavated sector.

Figure 3.6 Close-in sample area during excavation (looking south). (DASA 70-21-NTS-64)

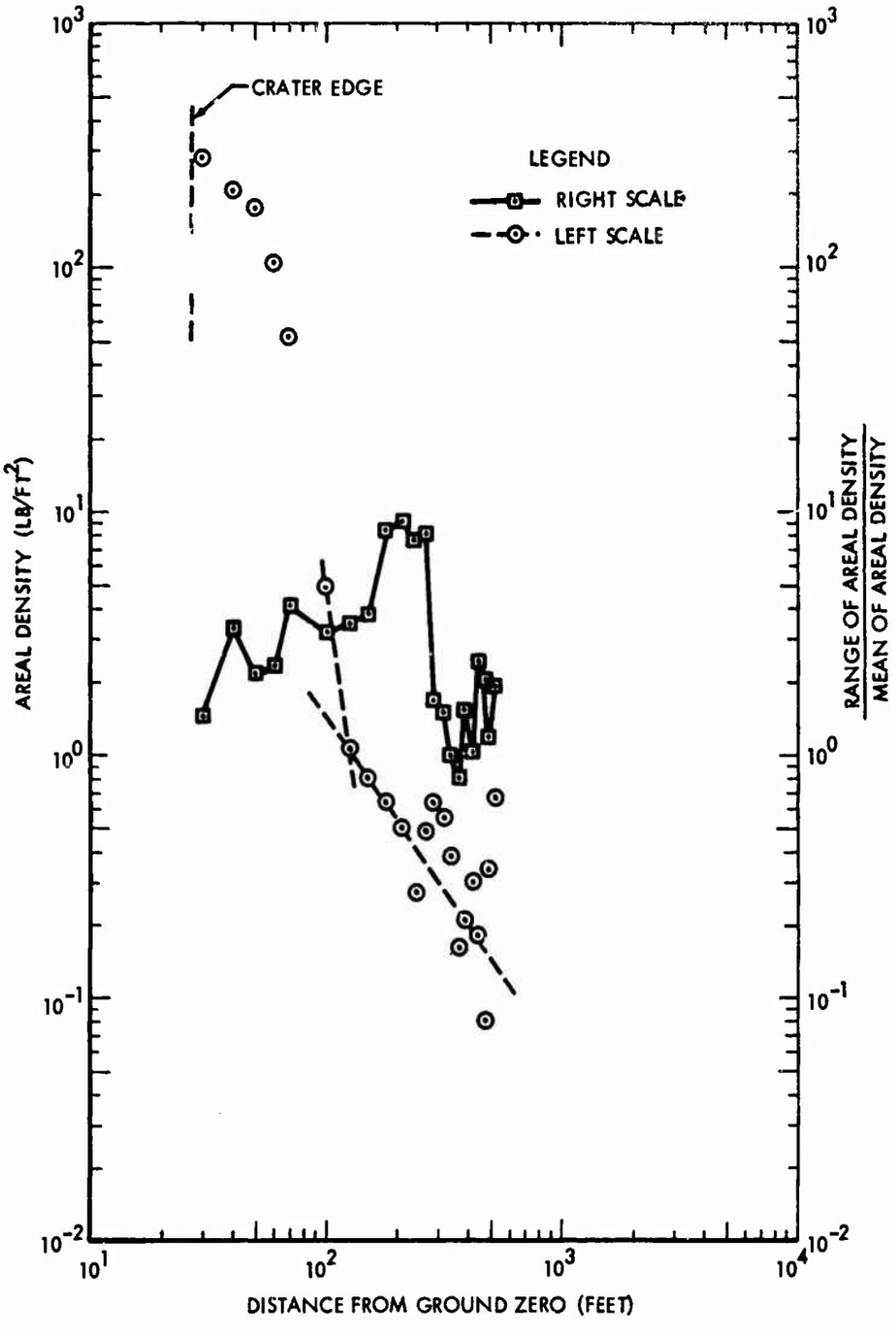

Figure 3.7 Ejecta areal density as a function of distance for Flat Top 1.

Figure 3.8 Upthrust along bedding planes. (DASA 73-14-NTS-64)

Figure 3.9 Overturned block. (DASA 73-04-NTS-64)

Figure 3.10 Uplifted surface. (DASA 71-04-NTS-64)

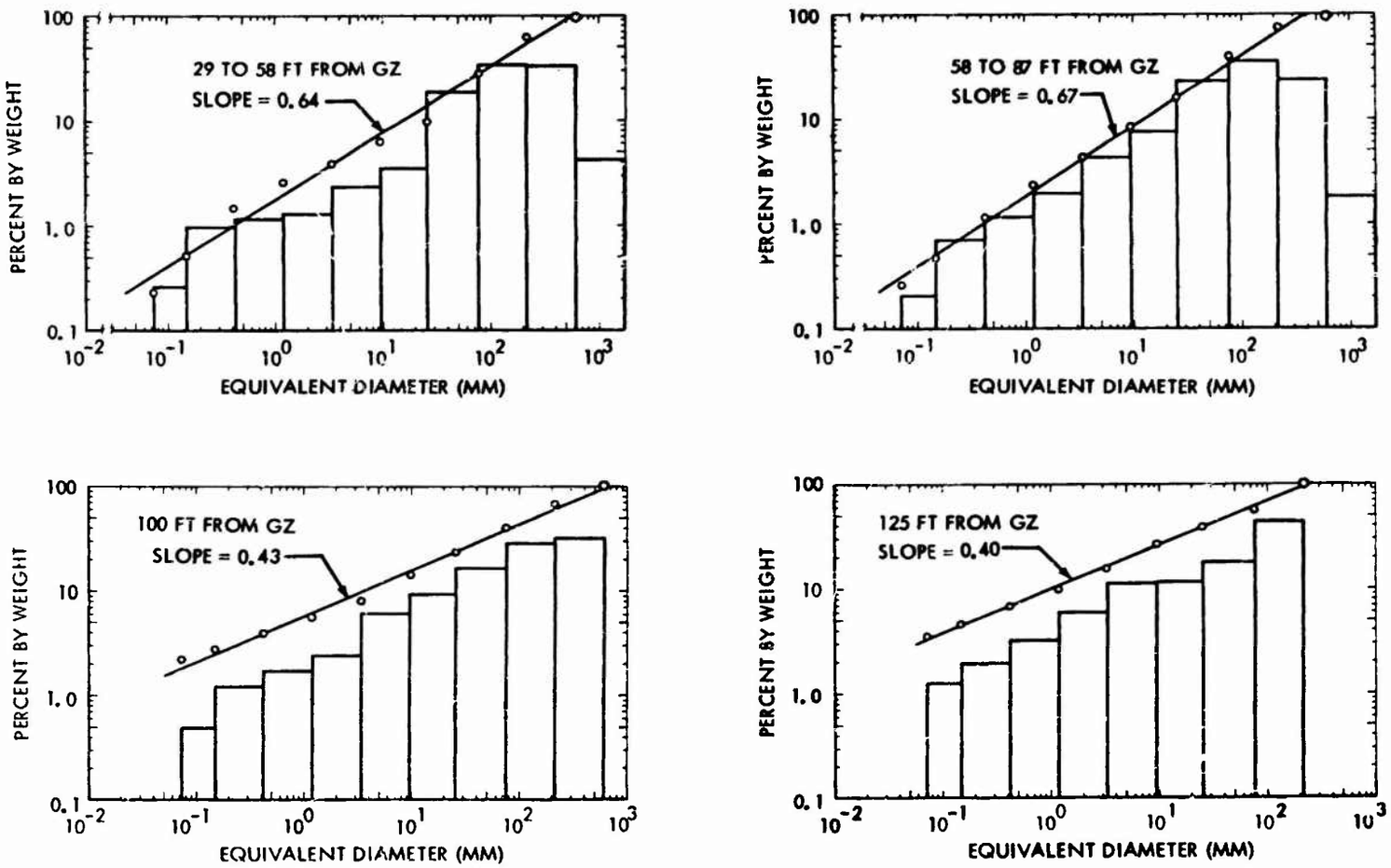

Figure 3.11 Size distributions of ejecta as a function of distance.

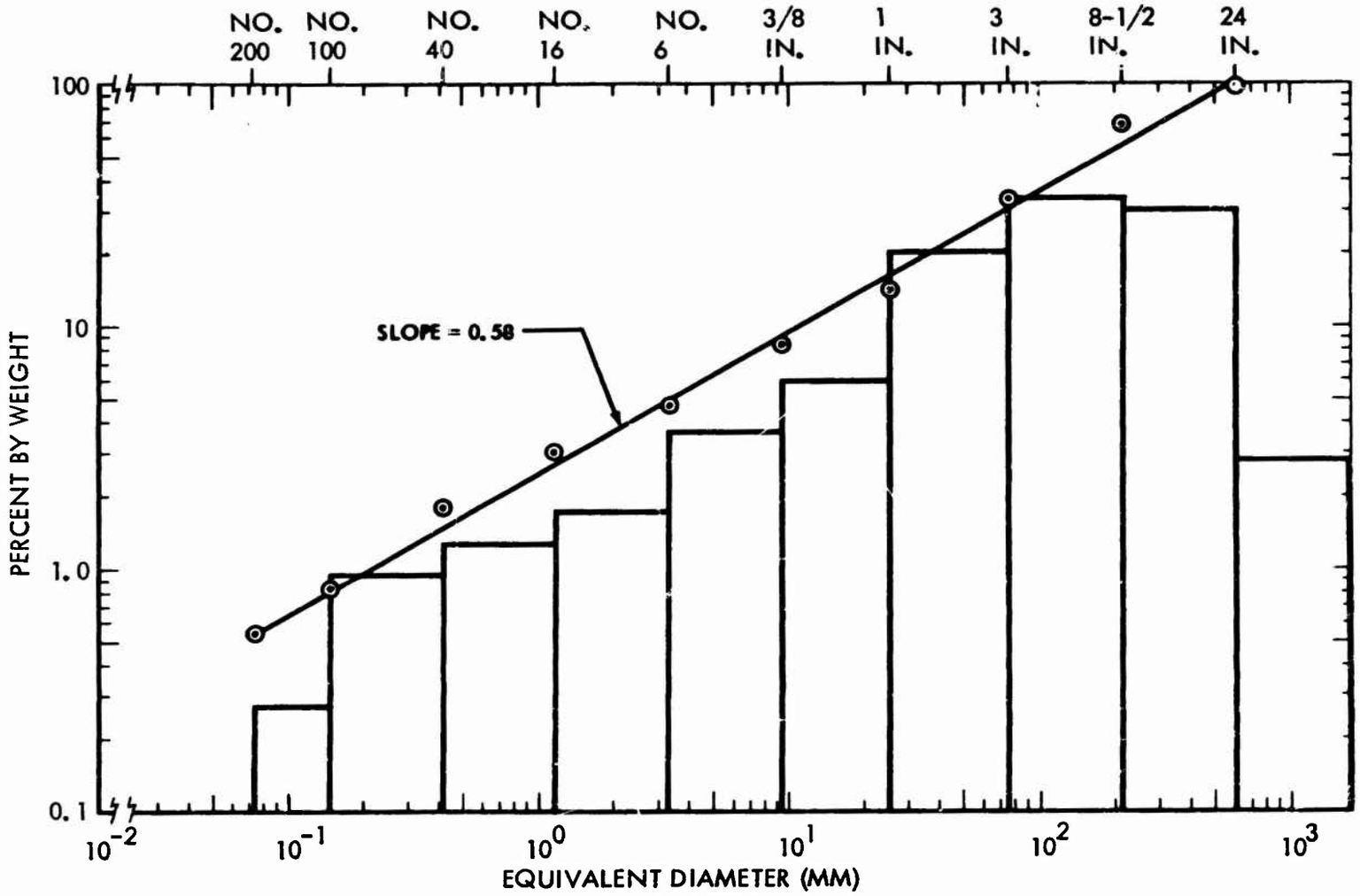

Figure 3.12 Size distribution of total ejecta through 520 feet.

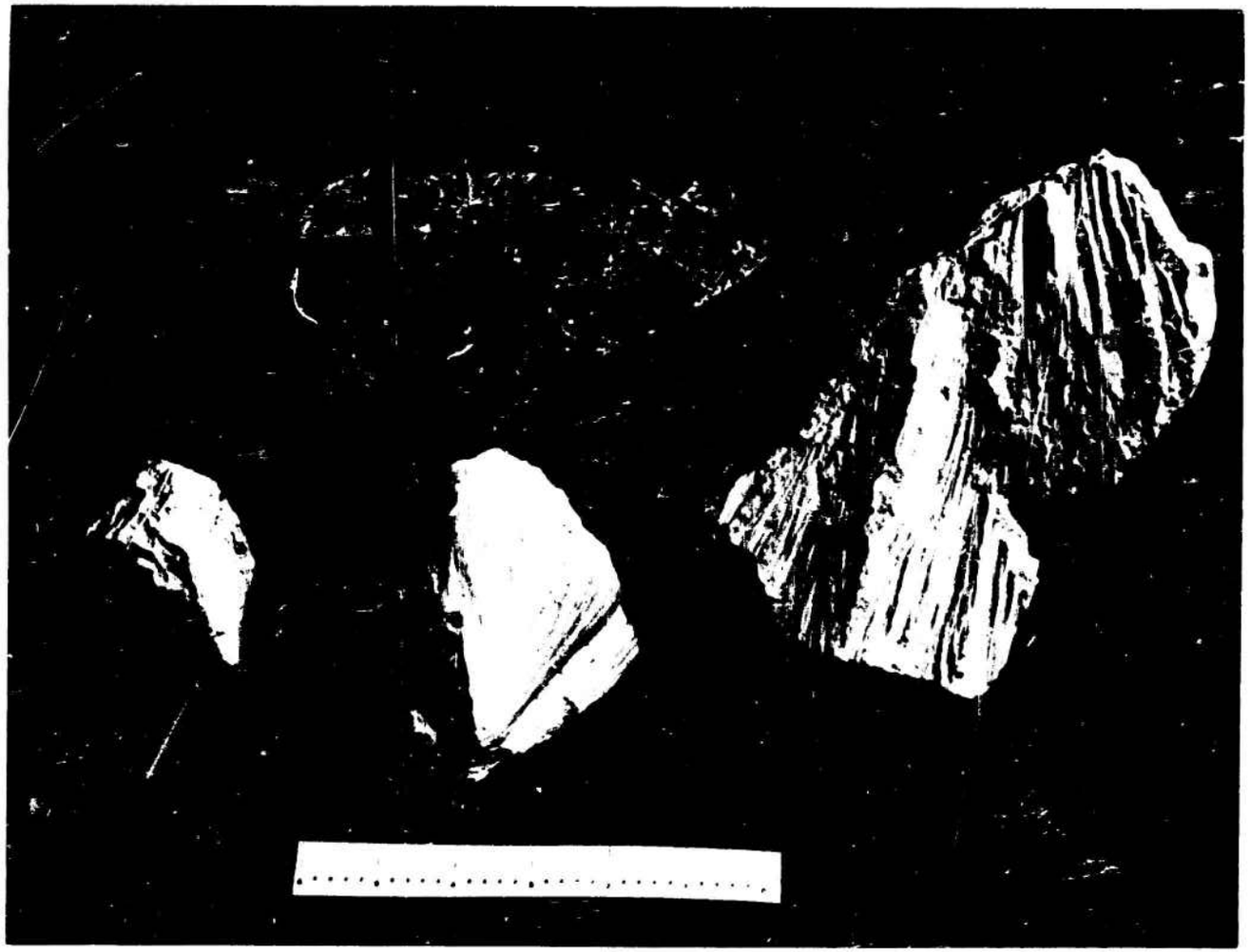

Figure 3.13 Shatter cones and normal ejecta fragment. (Boeing Neg. 2A196561)

Figure 3.14 Thin section from normal ejecta fragment. (Boeing Neg. 2A188269)

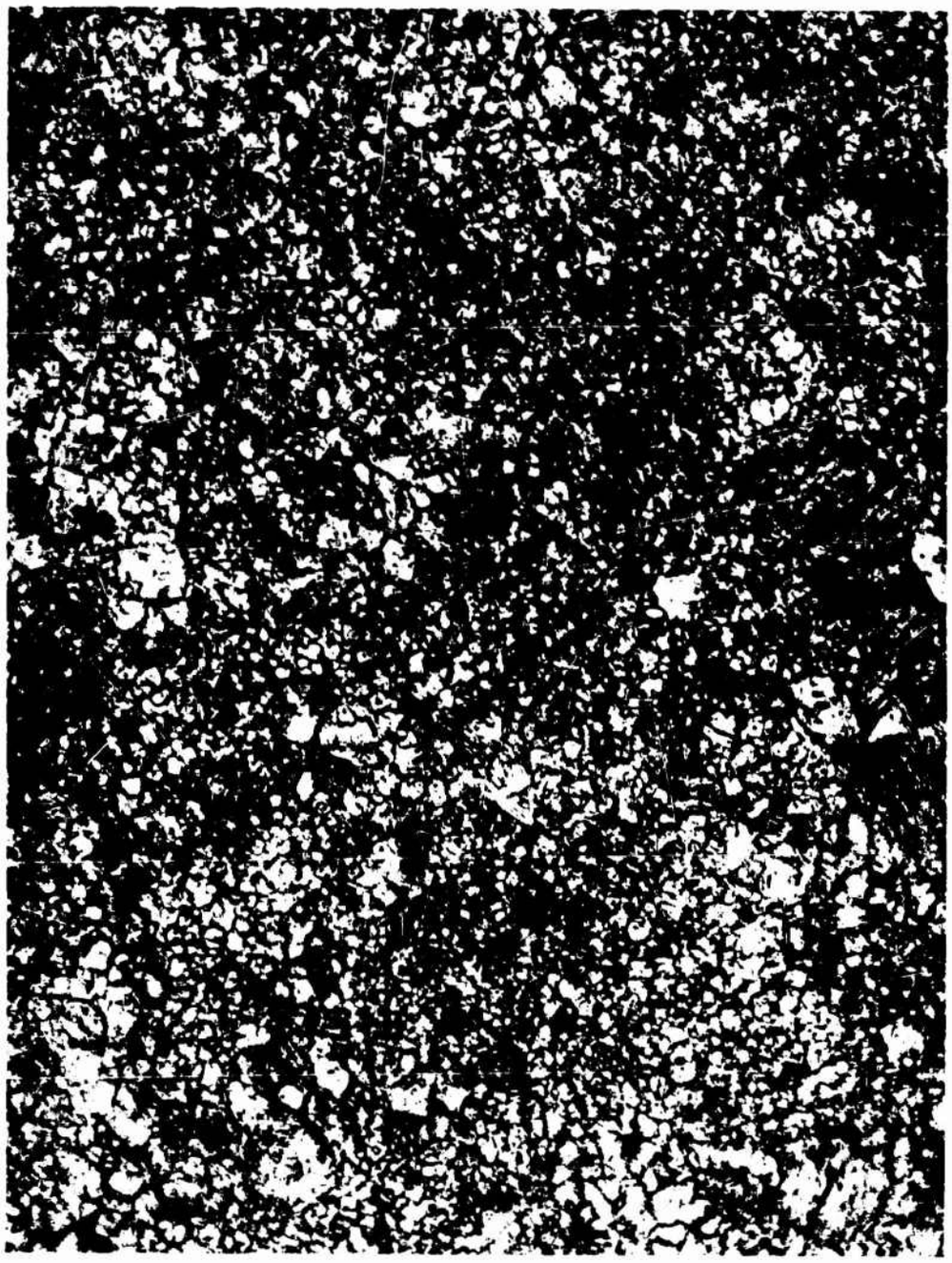

Figure 3.15 Thin section from shatter cone. (Boeing Neg. 2A188271)

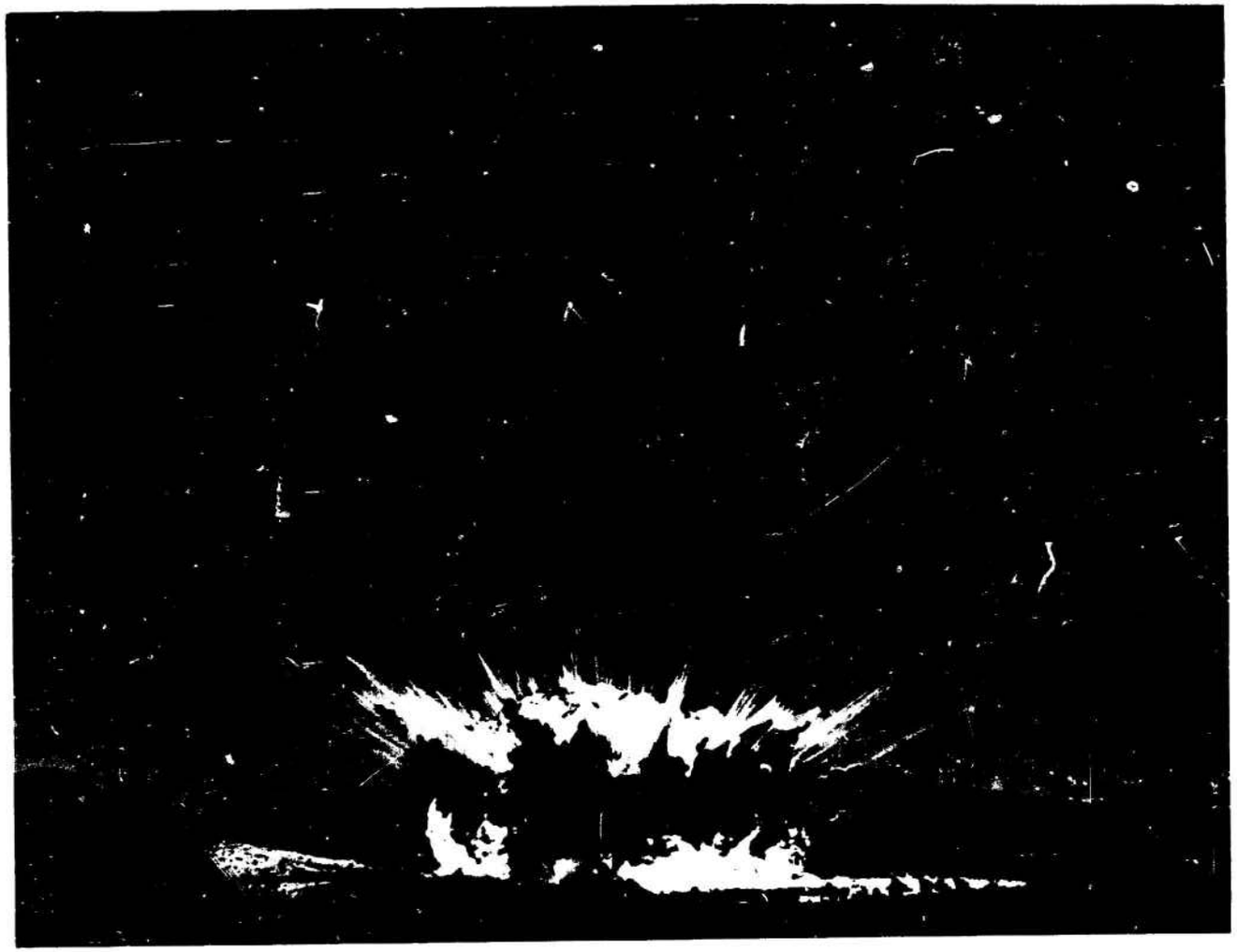

Figure 3.16 Flat Top 1 + 250 msec (from southwest of ground zero). (Boeing photo)

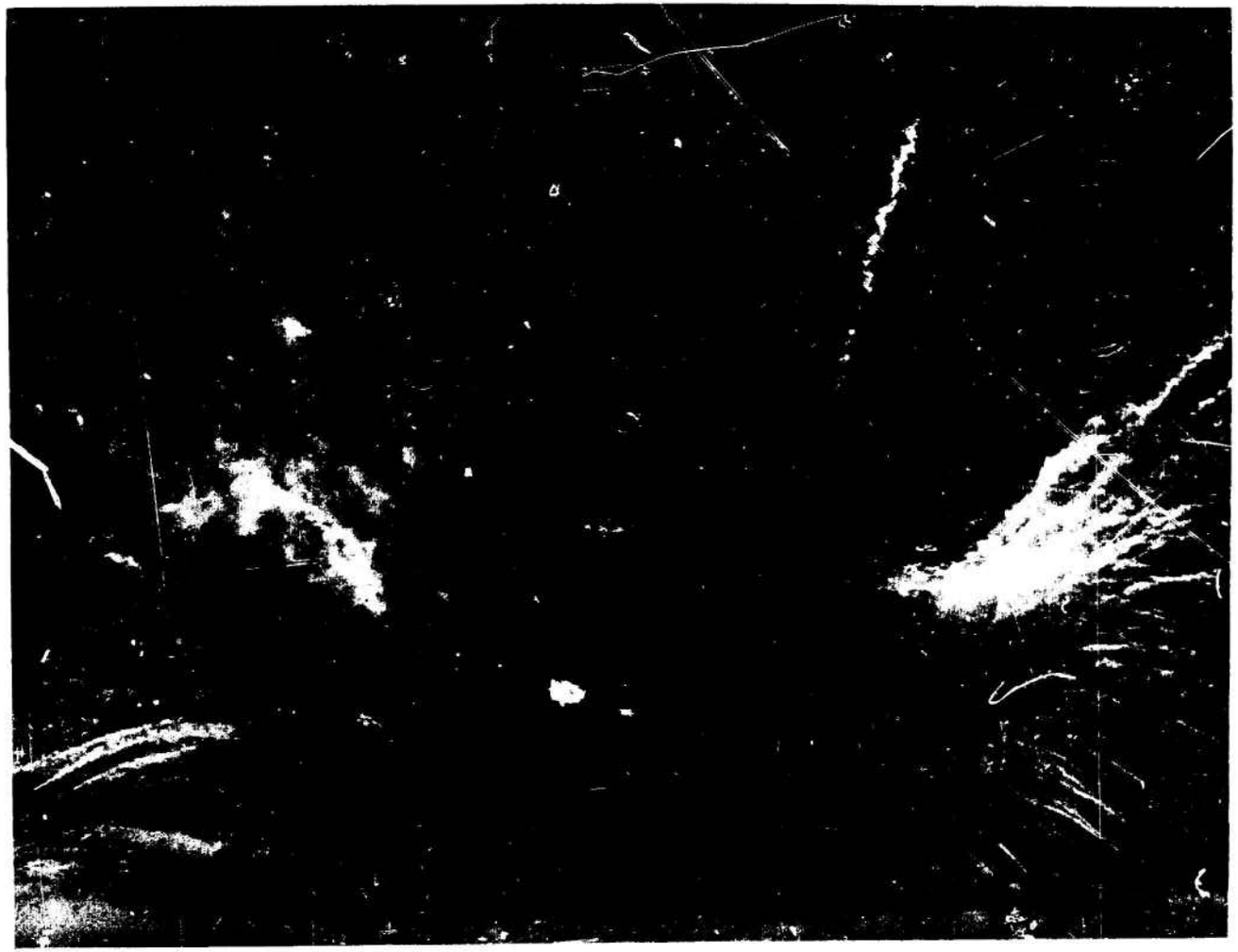

Figure 3.17 Flat Top 1+4,570 msec (from southwest of ground zero). (Boeing photo)

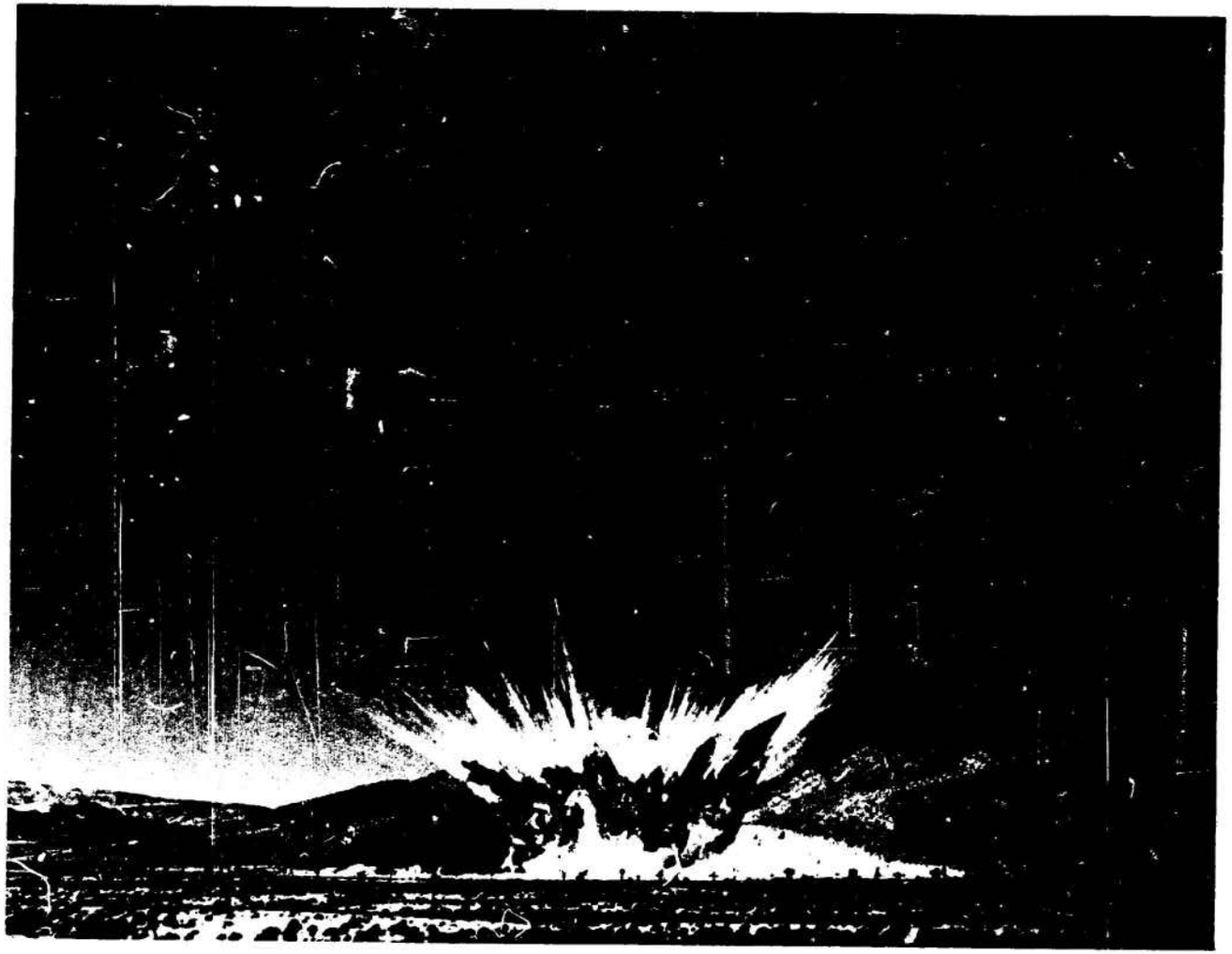

Figure 3.18 Flat Top 1 + 417 msec (from southeast of ground zero). (Boeing photo)

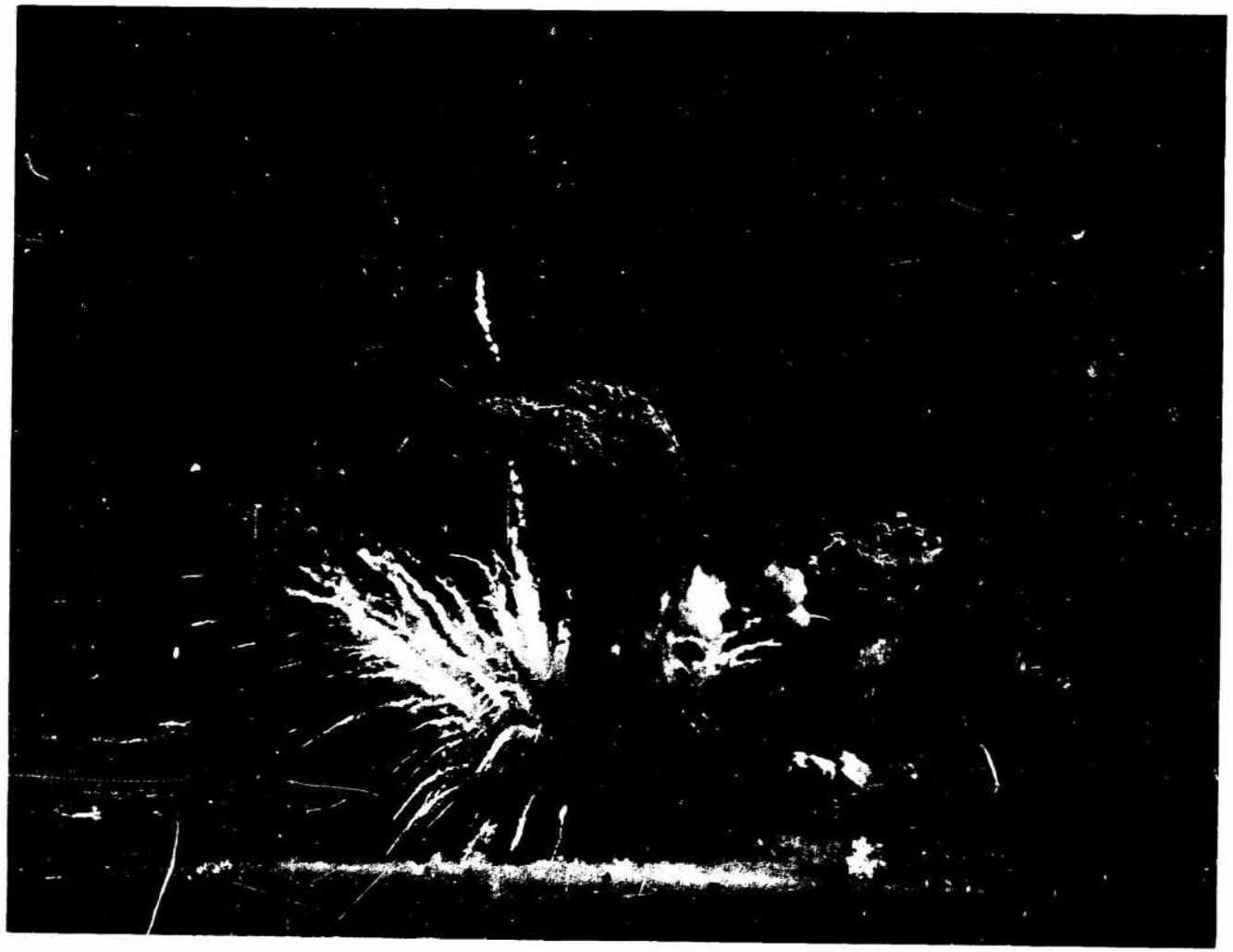

Figure 3.19 Flat Top 1 + 4,570 msec (from southeast of ground zero). (Boeing photo)

Figure 3.20 Shatter-cone impact point on Balloon Hill. (DASA 69-10-NTS-64)

Figure 3.21 Shatter cones near ground zero. (DASA 69-09-NTS-64)

Figure 3.22 Partly disaggregated shatter cone. (DASA 69-05-NTS-64)

Figure 3.23 Intact shatter cone (right of pipe) and disaggregated shatter cone (above pipe). (DASA 69-12-NTS-64)

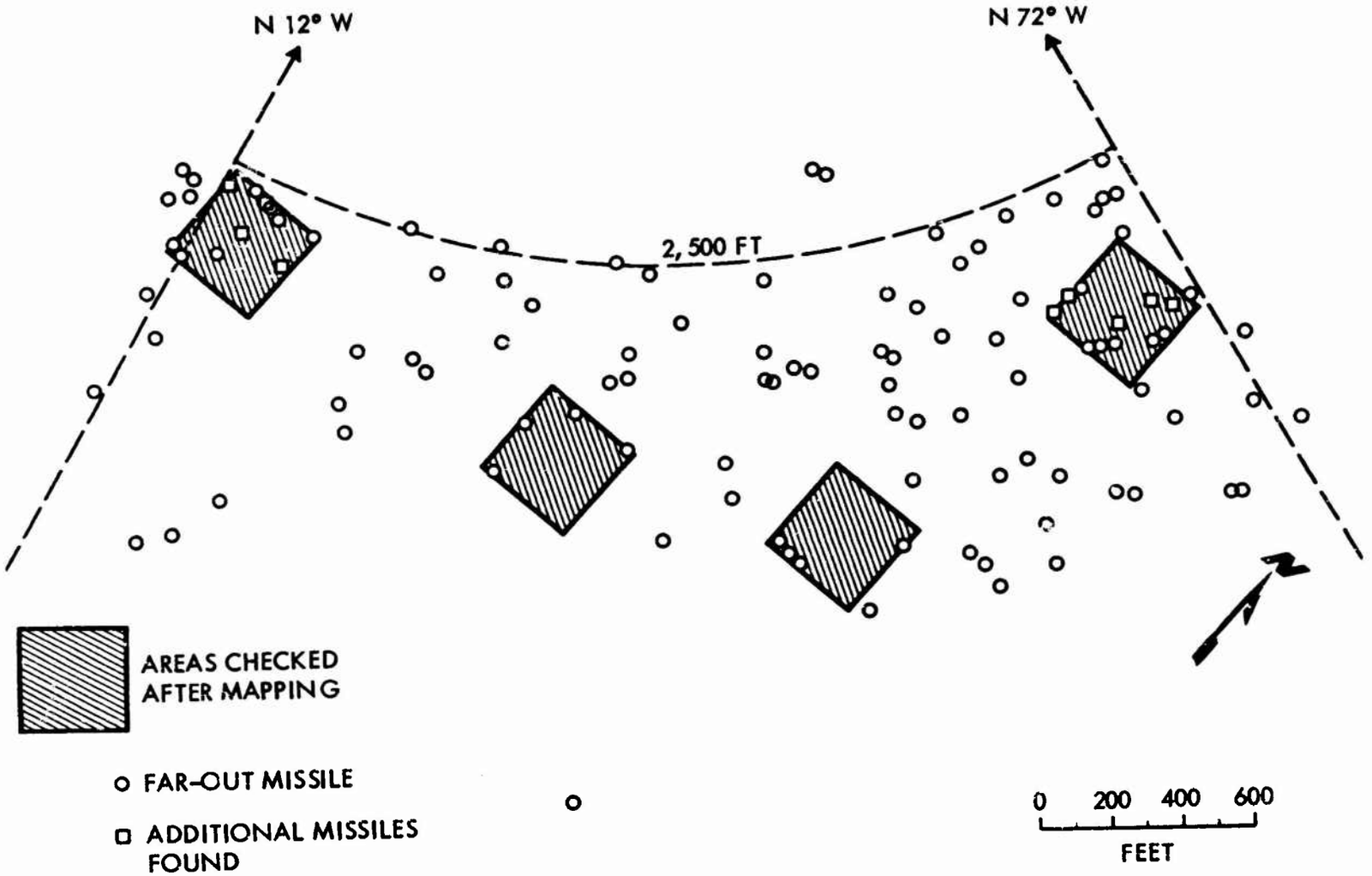

Figure 3.24 Distribution of far-out missiles, Flat Top 1.

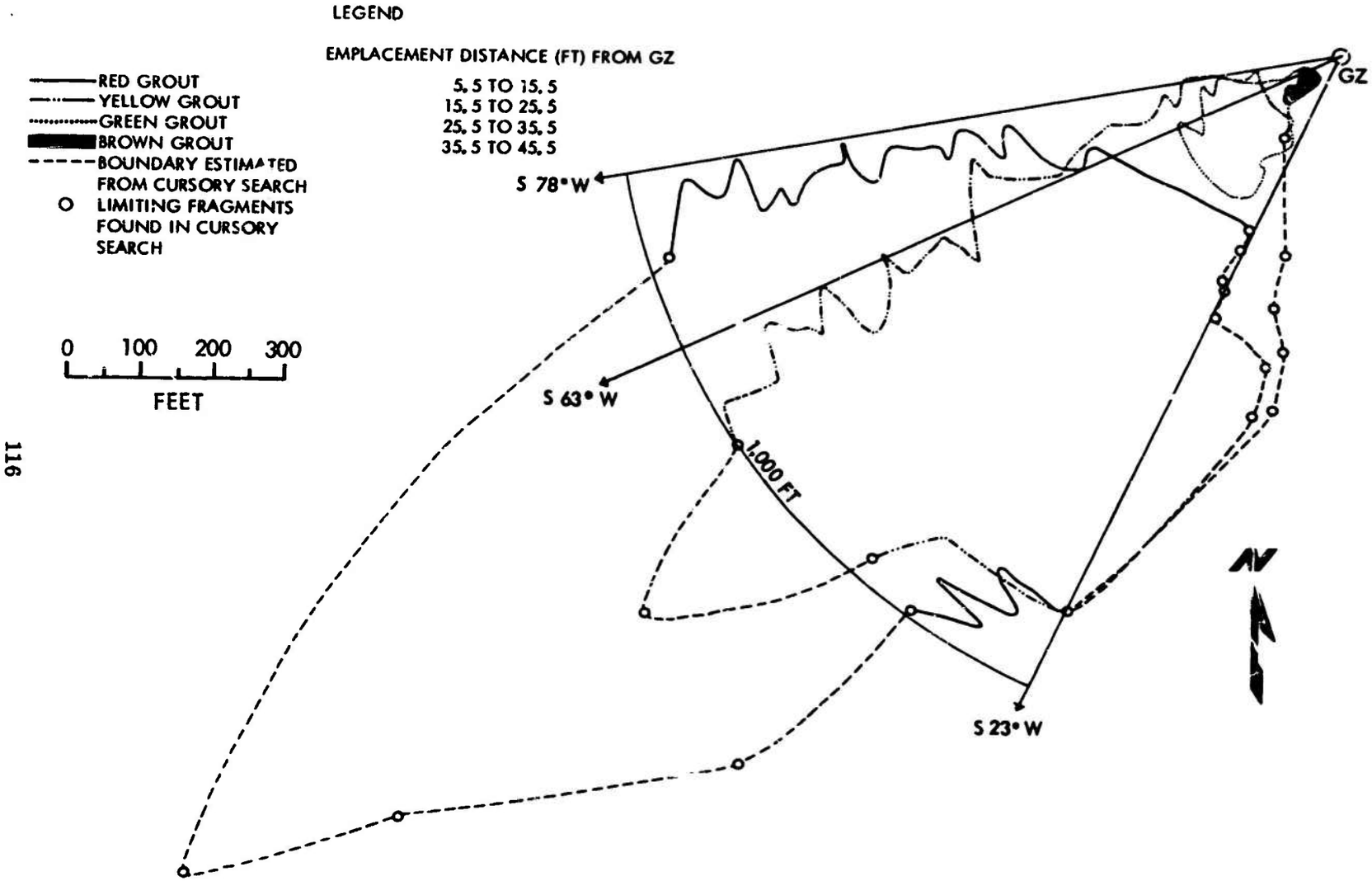

Figure 3.25 Limits of areal distribution of coded pad fragments.

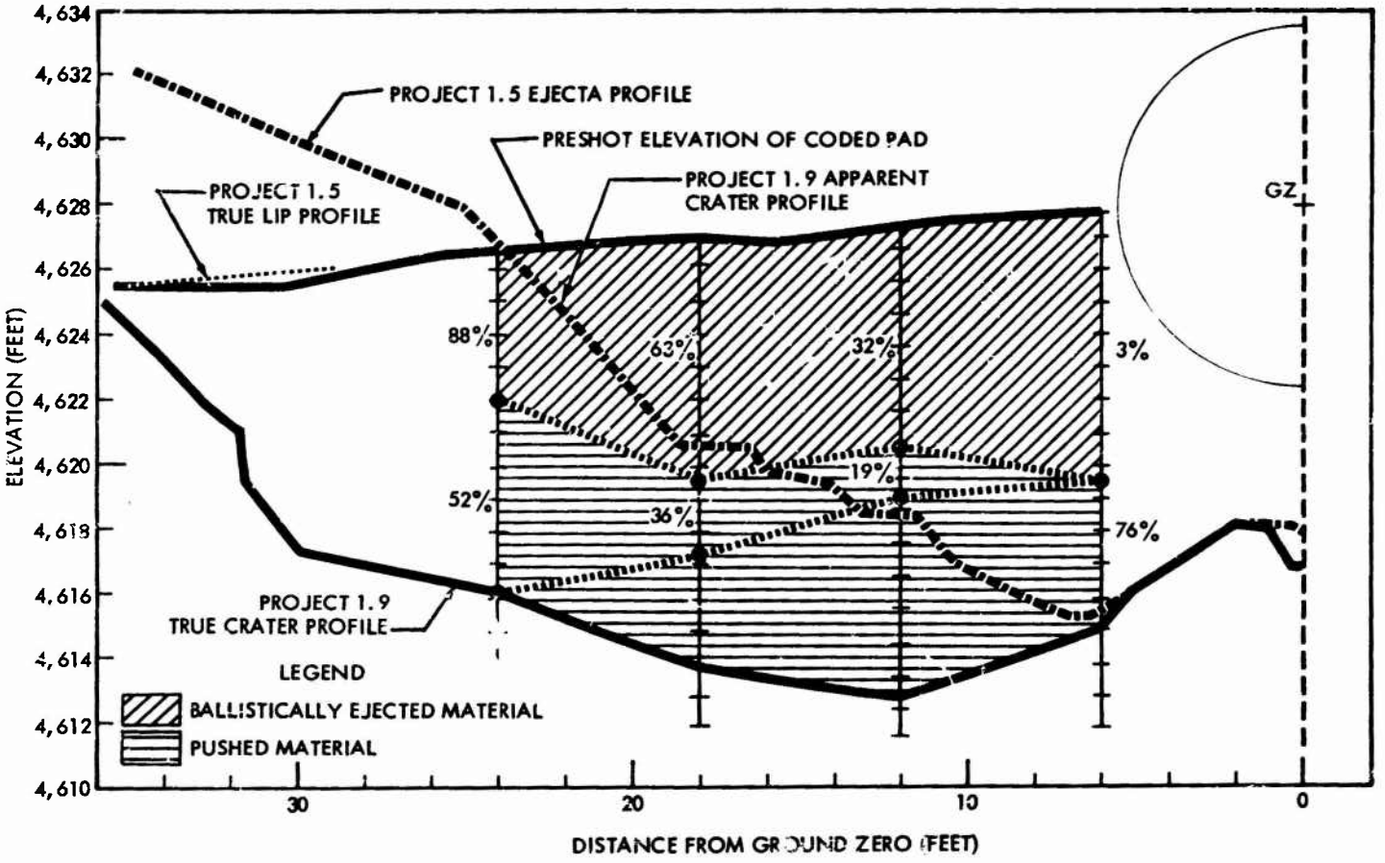

Figure 3.26 Section through crater along S 63° W radial.

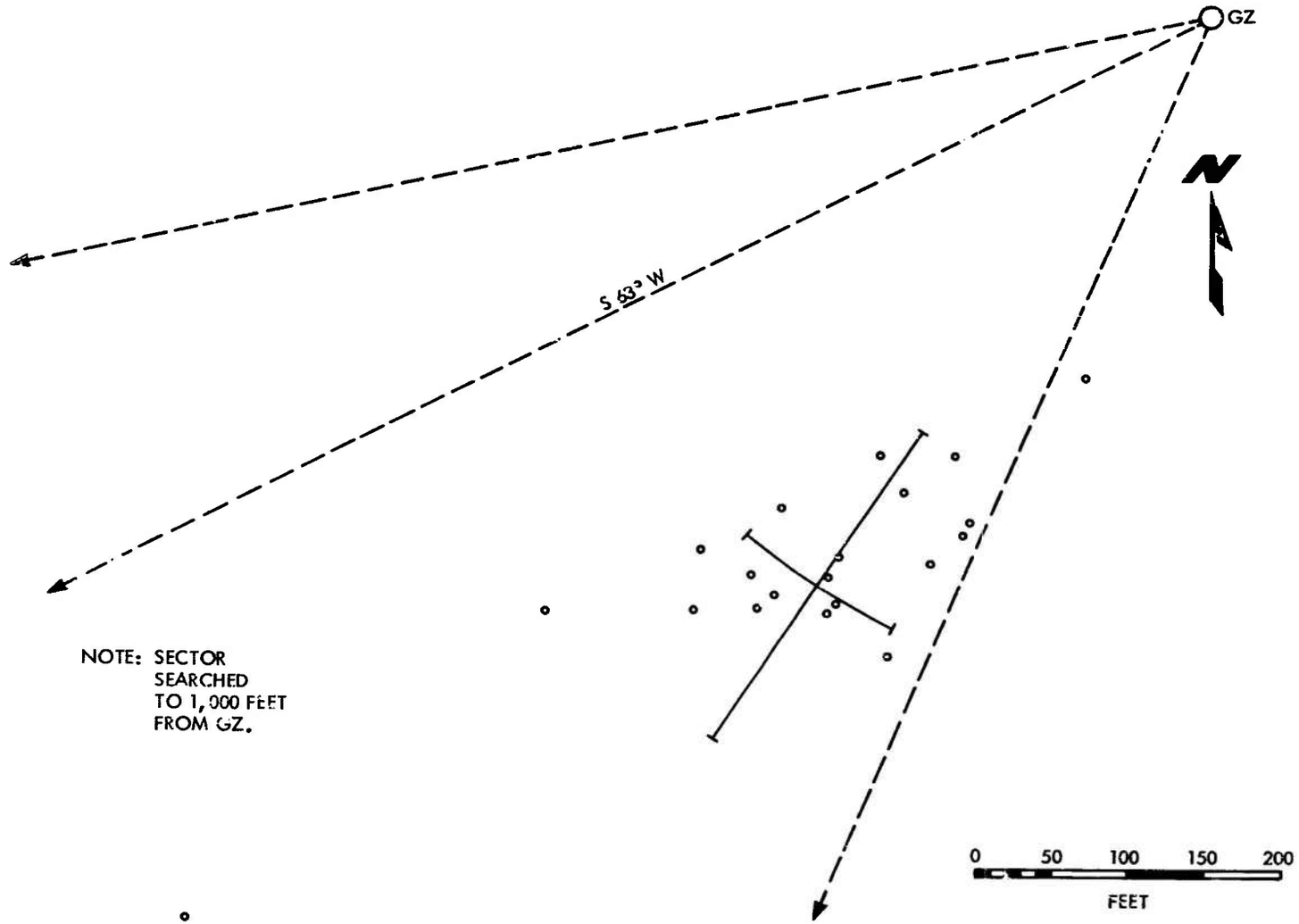

Figure 3.27 Areal distribution of fragments from red cylinder with white bands.

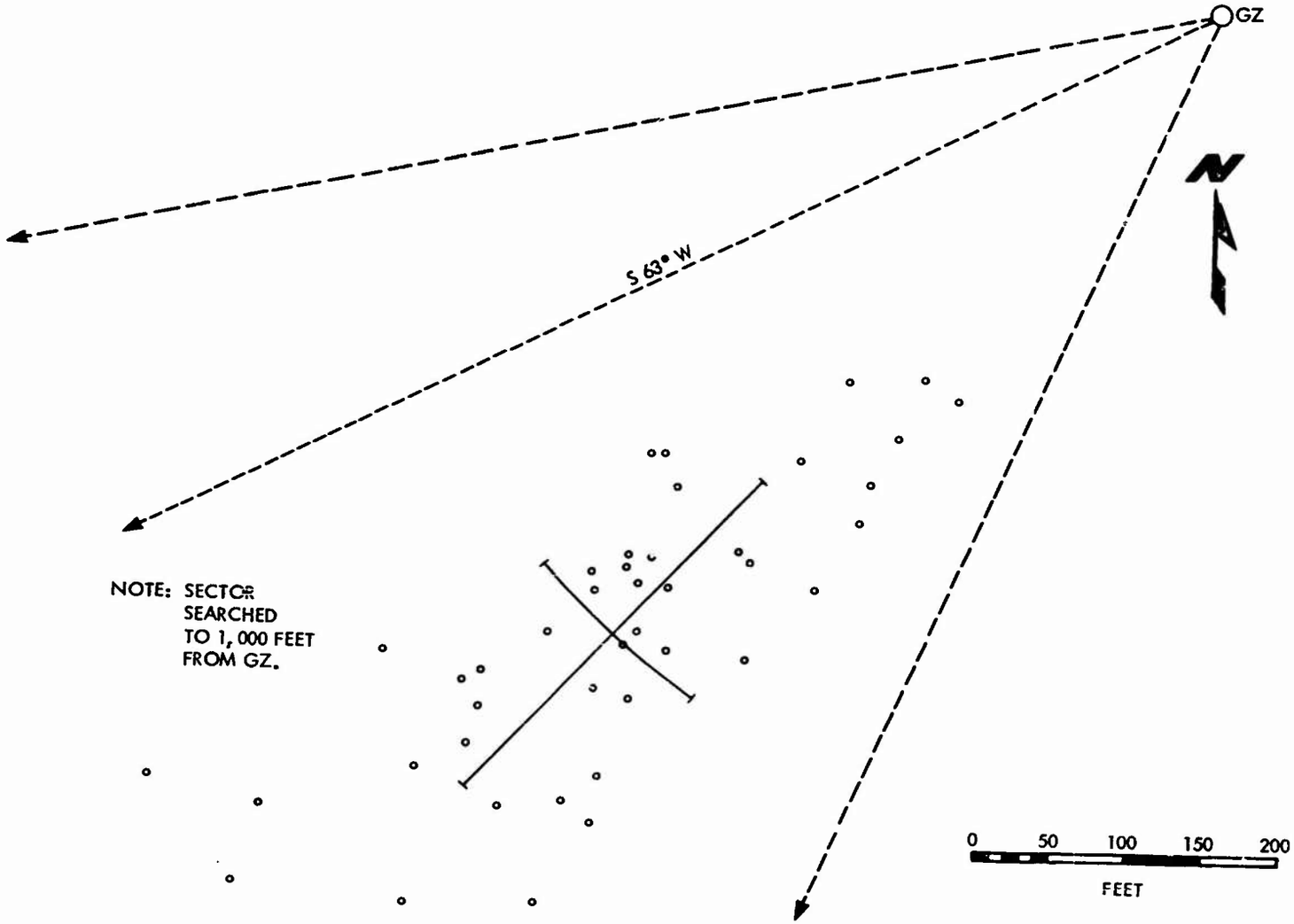

Figure 3.28 Areal distribution of fragments from red cylinder with red beads.

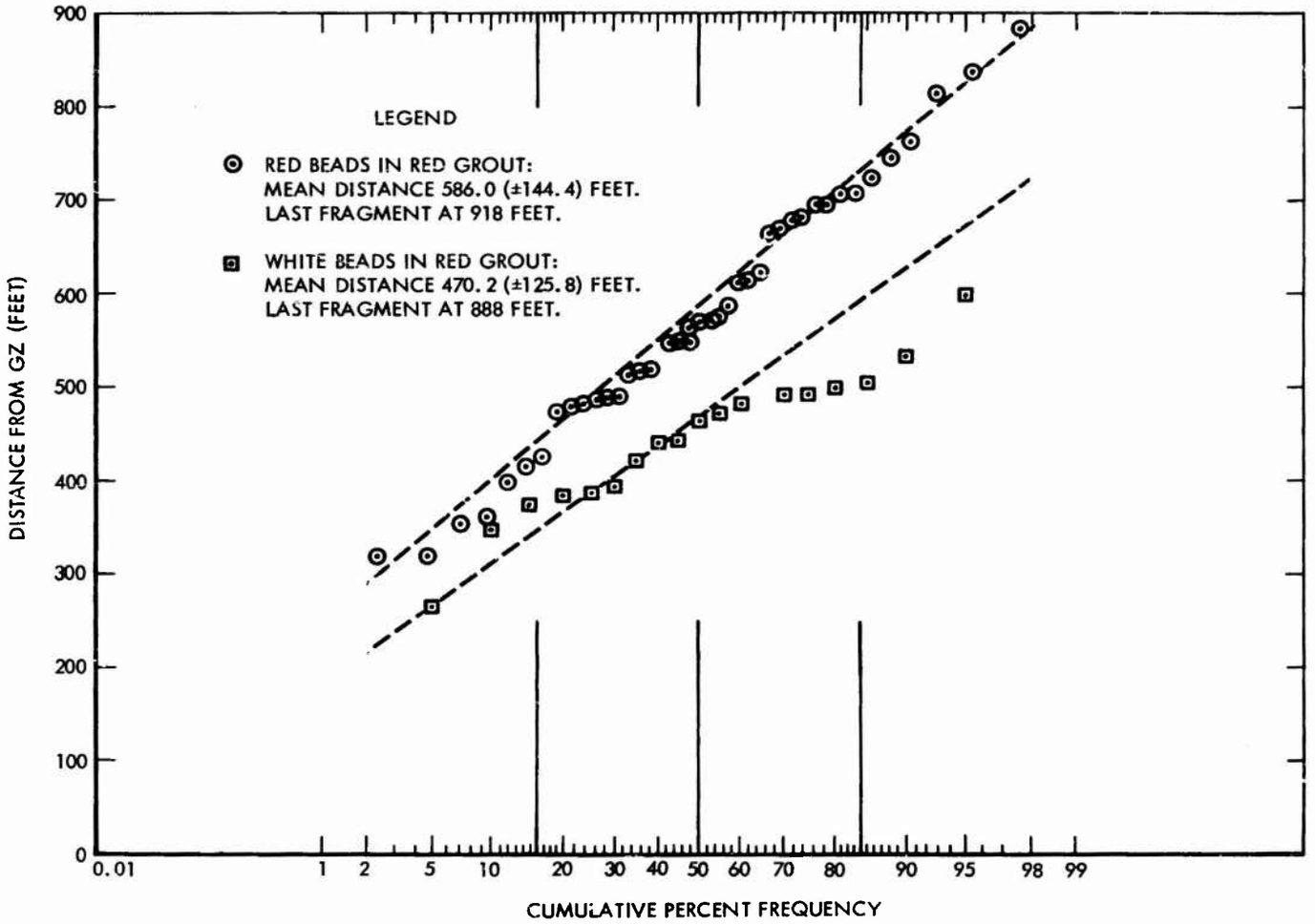

Figure 3.29 Cumulative frequency distribution of coded cylinder fragments.

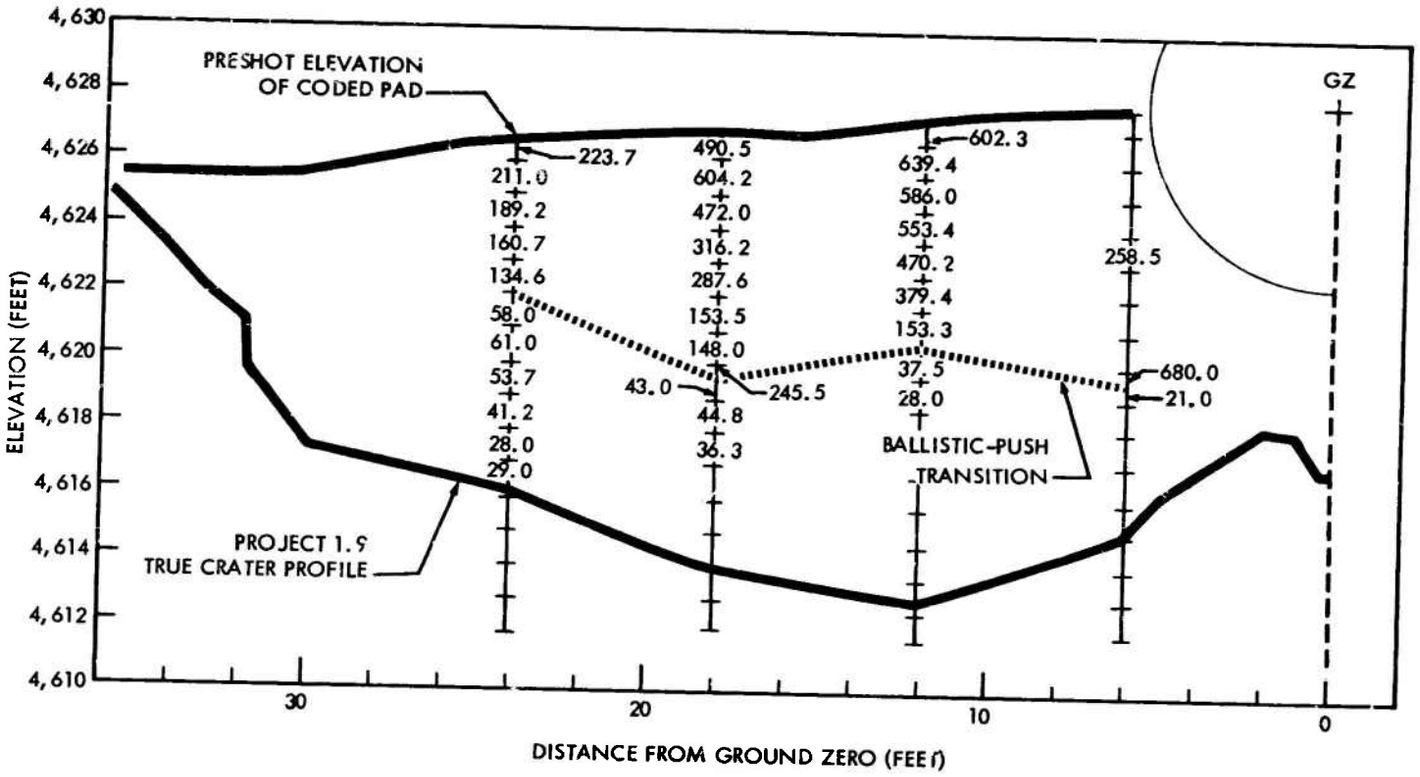

Figure 3.30 Mean distance from ground zero of fragments from individual coded cylinders.

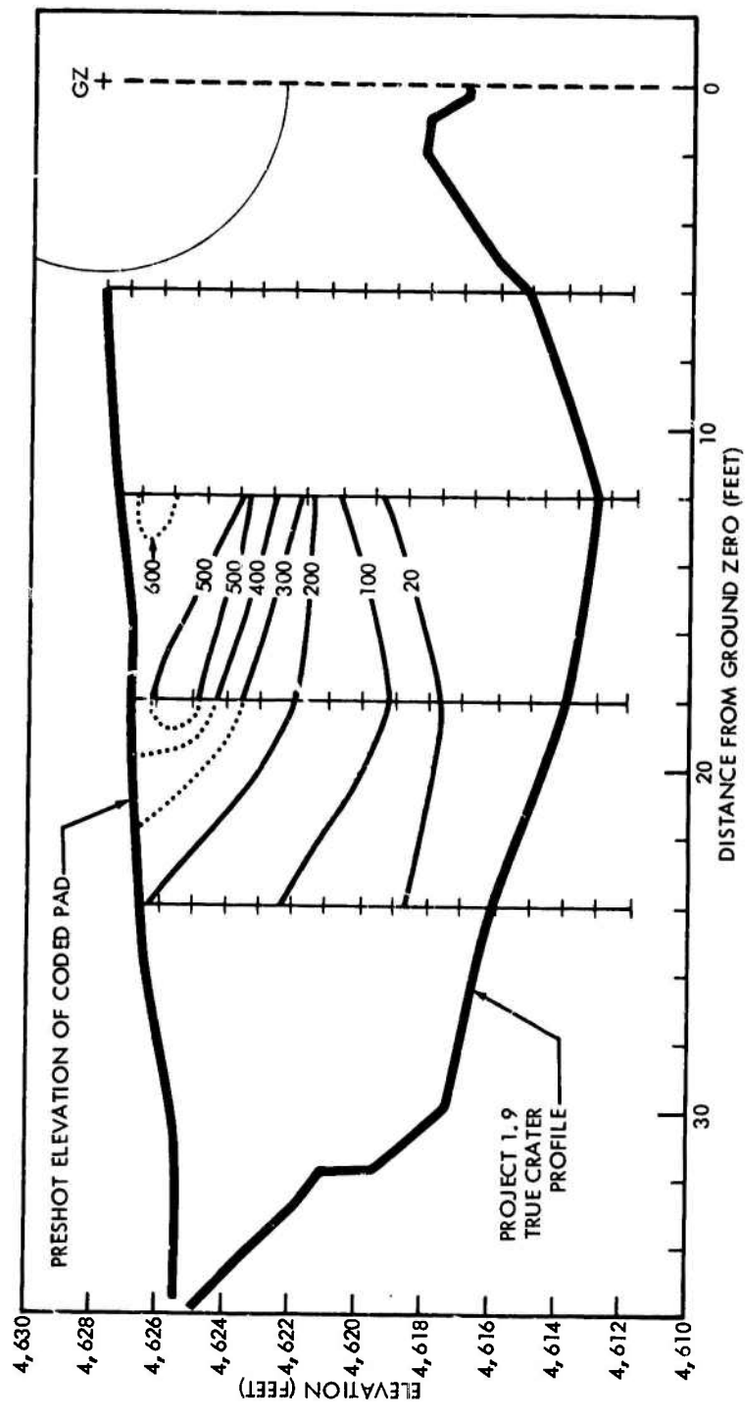

Figure 3.31 Mean horizontal displacement of fragments from individual cylinders.

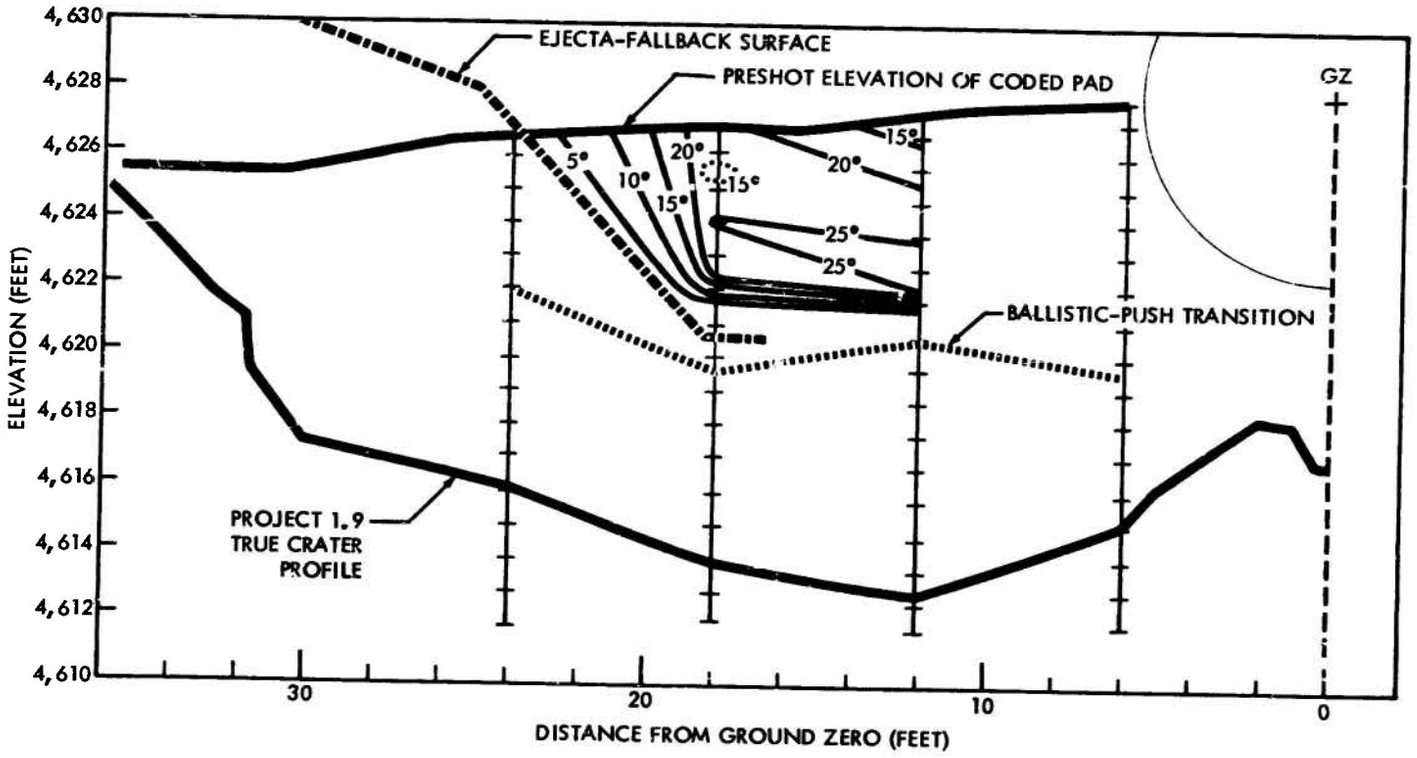

Figure 3.32 Mean angular deflection of fragments from individual cylinders.

Figure 3.33 View from inside crater (looking southeast). (DASA 73-02-NTS-64)

CHAPTER 4

DISCUSSION

4.1 UNEXPECTED ASPECTS OF EJECTA DISTRIBUTION

Two aspects of the Flat Top I ejecta distribution were unexpected. These were the excessive distance of flyrock travel and the large deflection from radial of most ballistically ejected coded fragment trajectories.

It is clear from the results of this study that the statement made in Reference 11, namely, that damage by airblast will extend further than damage by missiles from large shallow underground explosions, is not valid for shots the size of Flat Top I in limestone. Assuming that the predicted flyrock range for Flat Top I was based on data from explosions in brittle rock, the greatly underestimated distance of far-out missiles from this event can be explained, to a first approximation, by the pseudoplastic behavior of carbonate rocks.

The mean dimension of individual particles in Figure 3.15 is between a few ten thousandths and a thousandth of an inch, whereas the mean dimension of the shatter cone fragments was of the order of several inches.

Assuming roughly the same degree of comminution as a function of stress in brittle rocks as in carbonate rocks, but negligible coherence between individual particles of crushed brittle rocks, the mean dimension of fragments ejected from the velocity region comparable to the Flat Top I

pseudoplastic region from an explosion in brittle rock would be at least three orders of magnitude smaller than the mean dimension of Flat Top I shatter cones.

Drag effects on the trajectories of particles having the same initial velocities and exit angles can be compared by their W/AC_D ratios, smaller ratios producing larger drag effects. If the difference between drag coefficients of individual particles and shatter cones is assumed to be negligible, the W/AC_D ratio of ejecta from the velocity region comparable to the Flat Top I pseudoplastic zone surrounding explosions in brittle rock would be about 3 orders of magnitude less than that of the Flat Top I shatter cones.

This large discrepancy in drag effects on ballistic range would cause shatter cones from explosions in carbonate rocks to be deposited farther from the burst point than individual particles from explosions in brittle rock, even though initial trajectory angles and velocities were the same. The reduced effect of drag on shatter cone trajectories is considered to be an ample explanation for the large flyrock travel distances observed from the Flat Top I event.

It was known from the results of previous experiments that the trajectories of material artificially introduced into the medium surrounding cratering explosions are influenced by inhomogeneities of the medium

(References 2, 3, and 12). However, because of the care taken in this experiment to align coded material with known vectors of medium anisotropy, it was expected that the trajectories of coded material would be essentially radial from GZ. Despite the precautions taken, the trajectories of most ballistically ejected fragments were nonradial.

The effect of the wind at shot time was not sufficient to cause the deflections observed. Calculations for various representative particle sizes, assuming maximum travel times and plausible drag coefficients, indicate that only about 1 to 10 percent of the observed mean deflections of coded ejecta from the column emplaced 12 feet from GZ could have been due to the wind.

The major portion of the deflection of ejecta from individual coded cylinders is attributed to shock reflections off a failure surface in the rock beneath GZ. The dip and strike of this shear plane do not correlate with the most likely failure planes in the in situ rock.

It is possible that failure along this shear plane was influenced by the presence of the instrumentation tunnel beneath the crater, since the strike of the shear plane and the direction of the tunnel axis are about the same. Other equally likely explanations, however, such as the presence of an undetected joint plane, etc., could be given.

4.2 LIMITATIONS OF EJECTA SCALING METHODS

Most methods proposed for predicting ejecta distribution from cratering explosions have been based on geometric scaling, either by use of dimensionless ratios or by extrapolation of empirical functions involving some geometric scaling factor. The concept of geometric scaling implies similarity between at least some linear dimensions in the relationship being compared.

It was recognized in References 2 and 3, and confirmed in this study, that the physical processes causing ejecta deposition in the apparent crater lip, the region of ballistically ejected fragments, and the region of wind-transported fine particulate are completely different. Therefore there is no reason based on physical laws to expect geometric similarity between ejecta distributions in these different regions for a given event. Furthermore, there is no reason to expect geometric similarity between ejecta distributions from different events, even in those regions where the same general processes cause deposition, if the physical processes operate in nonsimilar manners for the different events.

An illustration of a process operating in a nonsimilar manner for different events is the trajectories of ballistic ejecta from two events of different yields conducted in the same medium. Even if these events could be scaled so that geometric similarity were preserved for all crater parameters,

ballistic ejecta distributions would not scale with any crater parameter except under highly restrictive conditions.

The horizontal distance from GZ to which a ballistic fragment from one of these events would be thrown is the sum of a distance that scales, representing the fragment's original horizontal distance from GZ, and of the horizontal distance traveled during its ballistic trajectory. A similar ballistic fragment from a similar location of the other event would also be deposited a total horizontal distance from GZ composed of its original horizontal distance from GZ, which scales, and the horizontal portion of its ballistic trajectory.

Neglecting drag effects, the ballistic trajectories of the two fragments would depend only on their exit angles and the square of their initial velocities. Therefore, since crater dimensions are similar, the ratio of horizontal ballistic travel of the two particles would be proportional to the ratio of their exit velocities squared. From this it follows that the ejecta distributions could not be scaled with any crater parameter unless: (1) ballistic displacements of fragments were negligible compared to crater parameters, (2) the ratio of squared exit velocities of all similar ejecta scaled with the craters, (3) drag effects had operated differently on trajectories of similar ejecta from the two craters so that their ballistic ranges scaled. None of these conditions seems likely for cases of practical

interest. The one parameter that has been observed to maintain geometric similarity among explosions of various yields in a given medium is particle velocity. This similarity alone is sufficient to preclude similarity between ejecta distributions because of the close relationship between particle velocities and ejecta exit velocities. Except for variations due to gas-boost and drag effects, the ballistic range of similar particles from explosions of different yields in the same medium would be identical. If, as is often assumed, crater parameters scaled as a function of charge weight, it follows from the above that the distribution of ejecta could not.

Experimental evidence confirms that ejecta distributions do not scale by any law yet proposed. Log-log plots of mean areal density versus range from GZ for most large shots show abrupt changes of slope, probably due mostly to transitions from regions of one mode of deposition to another. Figure 3.7 is fairly typical in this respect. Slopes of areal density curves for regions of the same mode of deposition vary from shot to shot. No method has been found to bring these breaks into alignment or to produce uniform slopes for given regions of different shots by introducing scaling parameters.

References 2 and 3 show that the proportions of total ejecta mass and mass of fine particulate decrease, the latter more rapidly, as a function of increasing crater volume for explosions in desert alluvium. Reference 8

includes mass distribution curves for ejecta from shots of the same yield at different depths of burial in playa silt that show that the proportion of total ejecta mass at given crater radii from GZ varies with depth of burial. Other mass distribution curves in this report show that the proportion of total ejecta deposited at given scaled ranges from surface shots varies as a function of yield, the larger shots having ejecta mass distributions relatively closer to the apparent crater edge.

It is possible to select mass distribution curves that give the appearance of geometric scaling for yields varying by a couple of orders of magnitude. However, the preponderance of data from explosions in desert alluvium indicate that total ejecta mass increases less rapidly than apparent crater volume, and that the relative distribution of total ejecta mass, measured in apparent crater radii, is nearer the crater edge as the size of explosion is increased. Both trends are in accord with elementary theoretical expectations.

In Reference 1 mean ejecta areal densities as a function of distance from given shots are approximated by single power law fits, and dimensionless ratios are formed to give an envelope of scaled ejecta curves. These scaled curves are recommended for use in predicting the possible range of mean areal density at given distances from cratering shots.

Using this scaling method to predict ejecta areal density at the

100-psi distance from a 1-megaton surface burst on desert alluvium gives a maximum value of about 1 ton/ft^2 and a minimum value of about 1 lb/ft^2.

The data used to construct these envelopes came from events with a range of yields covering only 4 orders of magnitude. If scaled data from shots less than 20 tons in yield had been included, the maximum value would have been much greater. When further account is taken of the extreme variation of ejecta distribution as a function of azimuth, it is obvious that a prediction method better than geometric scaling is needed.

4.3 THOUGHTS ON DIRECT COMPUTATION OF EJECTA DISTRIBUTIONS FROM SURFACE BURSTS ON ROCK

Quantitative extrapolation of observed trends in ejecta distribution to the case of large surface bursts on rock is not possible at the present state of the art. Most of the data for large events came from buried shots in soil. Available data are not sufficient to analyze all variables one by one, and possible significant interactions between variables cannot be fully specified.

As stated earlier, a trend toward ejecta distributions, measured in crater radii, to be nearer the crater edge is expected as explosive yield is increased for bursts on any given medium.

If the push mode of ejecta lip formation suggested by this study is generally valid for surface bursts, it is to be expected that a greater proportion of the total ejecta from surface bursts will be concentrated in

the lip area than for shallow penetrating bursts. The high angle of repose of broken rock compared to soil will make this effect more pronounced for bursts on rock than on soil.

Direct computation of ejecta distribution for a surface burst on rock requires knowledge of the distribution of particle sizes due to comminution and the initial velocity field of the ejecta. Neither of these initial conditions can be specified at the present state of knowledge. In the following paragraphs suggestions for studies to provide the insight needed to describe particle size distributions and initial velocity fields are given.

Some insight could be gained from a review of laboratory studies of rock strength, shock propagation in rock, and comminution of rock by single blows. Probabilistic theories of brittle failure of rock materials should be examined for their implications as to particle size distributions from single blows on a semi-infinite medium. Relationships between the size of the largest particle, total mass of particulate, and energy of the blow should be further investigated. It appears from Reference 23 that studies of hypervelocity impacts on rock targets provide valuable analogies to the case of surface bursts on rock. Comminution in both cases seems to follow the same general law, and despite the obvious control exerted by natural fracture patterns in rock, maximum particle size seems to correlate strongly with energy of burst.

Comminution studies of the type undertaken for this project should be repeated on future cratering events and their results examined in the light of laboratory studies like those described. Further studies of ejecta particle-size distribution as a function of distance from burst point, combined with studies of ejecta areal density versus distance, will also provide the basis for predictions of the bulking of ejecta and the size of the largest or median fragments at given distances from cratering explosions.

For surface bursts on carbonate rocks there seems to be some analogy with the case of a sphere indenting a semi-infinite plastic medium. Analysis by plasticity theory of the slip lines represented by shatter cone surfaces might provide useful information on initial trajectory angles of ballistically ejected fragments.

Further studies of coded ejecta distributions using material closely matching the properties of the medium, combined with studies of individual particle trajectories, will provide insight into the initial velocity field of the ejecta. These studies may also provide information on the tail of the areal density-distance curve necessary for closer calculations of total ejecta mass.

The following is a summary outline of an approach to the problem f computing ejecta distribution from surface bursts on rock.

1. A probabilistic relationship between stress and fragment size

should be established for the material being cratered. Tensile as well as compressive modes of fracture should be considered. If nonbrittle behavior and strain-rate effects can be expected to be important in the comminution process, they should be taken into account.

2. The stress field in the medium should be established throughout the region in which the stress history is such that comminution can take place. An approximation based on hydrodynamic theory would not be sufficient. Tensorial restraints imposed on the stress field by the properties of the medium should be taken into account.

3. For the ballistically ejected material, drag effects, interactions between particles in flight, disaggregation of particles in flight and on impact, and initial trajectory angles of individual particles are probably beyond analysis from first principles without resorting to Monte Carlo techniques. These variables, however, cannot be considered to have insignificant effects on ejecta distribution.

It seems possible that their cumulative effect could be simulated by using the simple formula for ballistic trajectory written so that initial particle trajectories are vector quantities composed of vertical and horizontal velocities. Each velocity component could be thought of as a random variable with some model distribution acting over each differential annulus of the forming crater viewed in plan.

Obvious upper and lower bounds of the trajectory velocity components ot a given onnulus are the medium particle velocity ond zero. If the trajectory velocity components are taken to have Gaussian distributions, o Rayleigh distribution of trajectories would be expected.

4. The stress field from 2 combined with the comminution law of 1 would provide o ballistic ejecta mass with o particle-size distribution that could then be given a distribution of initial ballistic trajectories described by 3. The distribution of pushed materiol would have to be treated separately. This problem could be ottacked by the soil mechanics theory of plosticity, using o Coulomb yield criterion. The distribution of fine particulate depends primarily on wind conditions and could not be predicted without meteorologicol considerations. Typically this portion comprises less than 10 percent of the total ejecta and is so widely distributed as to present minor problems other than those associated with radioactivity.

5. The problem of rayed ejecta distributions is related, in part, to inherent variotions in properties of the medium being cratered. Some ottempt should be mode to relote the number ond ozimuthal distribution of ejecta rays to vectors of anisotropy in the medium.

If variotions in physical properties can reasonably be ossumed to be randomly distributed, o probabilistic opproach relating ray-interray ejecta distribution to frequency or severity of medium property variotions might prove feasible.

6. Studies of ejecta distributions from field tests such as those conducted under this project will help provide data for calculations like those described in 4 and 5. If conducted on events for which ejecta distribution predictions have been made, such studies will provide checks on the calculations.

CHAPTER 5

CONCLUSIONS AND RECOMMENDATIONS

5.1 CONCLUSIONS

1. Significant departures from axial symmetry in ejecta size distribution and ejecta areal density were caused by the geology of the site. The configuration of ejecta rays correlates fairly well with anisotropies of the medium due to site geology. Smaller observed deviations from symmetrical ejecta distribution may have been due to topographic features and construction activities at the site.

2. Beyond the ejecta lip, data on mean ejecta areal density as a function of distance is described fairly well by power law fits. Between 100 and 125 feet from GZ, areal density is proportional to $D^{-6.3}$. Between 125 and 520 feet, the curve judged to fit the data best is proportional to $D^{-1.5}$.

Because of inadequate sampling and deposition of ejecta in rays, data scatter is large. The scatter as measured by the ratio of sample range to sample mean at given radial distances increases almost exponentially with distance from GZ. Total ejecta weight through 520 feet from GZ was between 2.5 and 3.0×10^6 pounds.

3. The maximum flyrock travel distance from GZ actually measured was 4,059 feet. On the basis of a helicopter reconnaissance, it is thought likely that this distance was exceeded by fragments deposited to the northwest of GZ in an area where flyrock travel distances were not measured.

4. The size distribution of ejecta fragments varied in a regular manner as a function of distance from GZ. In the 30-degree sector of the ejecta lip where the size distribution was sampled, the median fragment size was 200 millimeters between 29 and 58 feet and 140 millimeters between 58 and 87 feet from GZ. Ejecta from the sampling ring at 100 feet had a median fragment size of 140 millimeters. At the 125-foot sampling ring, the median fragment size was about 50 millimeters.

5. The mass-size distribution of total ejecta through 520 feet is approximately described by an equation of the form

$$m = M_t\left(\frac{e}{b}\right)^a$$

Where: m = cumulative ejecta mass finer than e

M_t = total ejecta mass

e = fragment size of interest

b = maximum fragment size

a = an empirical constant

For the ejecta sampled, the best fit of the data gave a value of 0.58 for a. Using this constant the value of b is calculated to be about 600 millimeters. The measured intermediate dimension of the largest fragment in the sampled sector was 27 inches or 686 millimeters. The median fragment size of all ejecta sampled through 520 feet was about 175 millimeters.

Because of the pseudoplastic behavior of the medium, the value determined for a does not reflect the true extent of comminution due to the explosion.

6. Bulking of the lip ejecta (defined as increase of ejecta volume above the in situ volume of the same mass of material) varied significantly with distance from the crater edge. Between 29 and 58 feet from GZ, bulking averaged 69 percent. Between 58 and 87 feet from GZ, bulking averaged 19 percent.

7. Analysis of ejecta and fallback from coded material indicates two general modes of throwout. One mode, operating in the near-surface region of the true crater, ejected material at relatively high angles and velocities. The other, operating in the lower region of the true crater, pushed broken material down and away from GZ. Part of the pushed material formed the lip ejecta and part of it remained within the true crater boundary, where it was classified as fallback.

8. Ejecta from coded material placed within the crater region a given horizontal distance from GZ, at various depths, was generally deposited farther from GZ with decreasing depth of emplacement. Ejecta from material placed within the crater region at a given depth was generally deposited farther from GZ with decreasing horizontal emplacement distance from GZ. In general, there was an increase in dispersal of these coded ejecta fragments with increased distance of deposition from GZ.

9. Ejecta fragments from coded material placed at the surface along a radial from GZ were deposited farther from GZ and were more dispersed with decreasing distance of emplacement from GZ.

10. A Gaussian distribution of the number of fragments as a function of distance from GZ was observed for coded ejecta fragments from given 1-foot vertical increments within the upper portion of the true crater region.

5.2 RECOMMENDATIONS

It is recommended that studies such as those made under this project be conducted as part of future cratering experiments and that the data be analyzed as suggested in Chapter 4.

Specific recommendations regarding future ejecta sampling experiments are:

1. The sectors chosen for studies of coded ejecta distribution or for size distribution of ejecta should be closed to all traffic.

2. For studies of ejecta size distribution, a scale large enough to weigh truckloads of material should be provided at the site.

3. The size distribution of samples of fallback as well as ejecta should be determined.

4. Flexibility in sampling is necessary if ray and interray areas are to be sampled representatively. Provision should be made to allow

for sampling procedures based on the ejecta distribution found to exist after the event, since rayed ejecta patterns cannot be predicted.

5. For large bursts in rock, large collector surfaces should be used to obtain representative samples.

6. For surface bursts, measures should be taken to keep deposits of fine surface material from being blown onto the sample collectors.

7. Data on areal density at large distances from the burst point should be collected so that the mathematical relationship of decrease in areal density with distance can be well defined. Present limitations on the accuracy of determining total ejecta mass will exist until the mathematical form of the areal density-distance tail is determined.

8. Additional colors of a grout, closely matching the strength properties of the medium, should be provided for future experiments involving coded ejecta. The colors should be as vivid as possible so that fragments of grout may be found easily.

9. Data on the size distribution of the strength-matching coded grout fragments should be obtained.

10. The Project Officer of the ejecta study should be an official photographer, or a photographer should be assigned to the ejecta study on a full-time basis.

Appendix A

POSTSHOT CONDITION OF EJECTA COLLECTION STATIONS

The collection station array is shown in Figure 2.5. The stations are designated by letters A through Q corresponding to the concentric rings and by Arabic numbers 1 through 24 corresponding to the radial lines on the figure.

Collection Station	Condition
A-1	On slight rise; some pileup in front of pad; no damage to pad.
C-1	A few chips in pad from missile impacts.
E-1	No damage.
B-2	No damage.
D-2	On slight rise; no damage.
F-2	On slight rise; one chip from missile.
A-3	Pad cracked; several chips; some pileup in front of pad.
C-3	No damage.
E-3	Station somewhat sheltered by rock ridge between location and GZ. No damage.
G-3	One chip from missile.
B-4	One chip from missile; minor pileup in front of pad.
D-4	One chip from missile.
F-4	Station sheltered by rock ridge between location and GZ.
A-5	Pad badly damaged; major pileup in front of pad; one large leaner.
C-5	Several missile chips; some pileup in front of pad.
E-5	Several missile chips; minor pileup in front of pad.
G-5	One missile chip.
B-6	Several missile chips; major pileup in front of pad.
D-6	Several missile chips; some pileup in front of pad.
F-6	Several missile chips.
A-7	Several missile chips; some pileup in front of pad.
C-7	Pad broken by missile.
E-7	Several missile chips; major pileup in front of pad.
G-7	Several missile chips.

Collection Station	Condition
B-8	Station in slight depression; several missile chips; some pileup in front of pad.
D-8	Several missile chips.
F-8	Several missile chips.
A-9	Several missile chips; some pileup in front of pad.
C-9	Several missile chips.
E-9	Side of pad toward GZ chipped; missile-causing chip piled up in front of pad.
B-10	Minor pileup in front of pad; shatter cone fell on pad.
D-10	One missile chip; minor pileup in front of pad.
F-10	Station behind disturbed alluvium.
H-10	Station behind disturbed alluvium.
J-10	Station behind disturbed alluvium.
L-10	Station behind disturbed alluvium.
N-10	Station behind disturbed alluvium.
P-10	No damage.
A-11	Pad badly cracked; major pileup in front of pad.
C-11	No damage.
E-11	Several missile chips.
G-11	No damage.
I-11	Station beyond dugout for instrument bunker; disturbed alluvium.
K-11	Station behind disturbed alluvium.
M-11	Station behind disturbed alluvium.
O-11	Station behind disturbed alluvium.
Q-11	Station behind disturbed alluvium.
B-12	Pad cracked by missile
D-12	Several missile chips; minor pileup in front of pad.
F-12	Several missile chips.
H-12	Tarpaulin placed on uneven surface beside road.
J-12	No damage.
L-12	Station behind disturbed alluvium.

Collection Station	Condition
N-12	Several missile tears; station behind disturbed alluvium.
P-'2	Several missile tears.
A-13	No damage.
C-13	No damage.
E-13	No damage.
G-13	No damage.
B-14	Pad cracked by missile.
D-14	Minor pileup in front of pad.
F-14	No damage.
A-15	Pad badly cracked; some pileup in front of pad.
C-15	Several missile chips.
E-15	Station partly sheltered by rock ridge; several missile chips.
G-15	One missile chip.
B-16	Pad badly cracked; major pileup in front of pad.
D-16	One missile chip; minor pileup in front of pad.
F-16	One missile chip; some pileup in front of pad. (Pad broken before shot.)
H-16	Front grommets pulled; tear parallel to blast-wave travel.
J-16	No damage.
L-16	Several missile tears.
N-16	One missile tear.
P-16	One missile tear.
A-17	Several missile chips; major pileup in front of pad.
C-17	Several missile chips; some pileup in front of pad.
E-17	Several missile chips; some pileup in front of pad.
G-17	Pad cracked; several missile chips.
I-17	One grommet on front and one on side pulled.
K-17	No damage.
M-17	One missile tear.
O-17	No damage.
Q-17	Very large missile tear caused by direct impact of large missile.

Collection Station	Condition
B-18	Pad cracked; several missile chips.
D-18	Several missile chips; major pileup in front of pad.
F-18	Several missile chips; minor pileup in front of pad.
H-18	Several missile tears.
J-18	Sample lost; all but one grommet pulled; tarpaulin torn along both sides parallel to blast-wave travel.
L-18	One missile tear; two spikes along one edge parallel to blast-wave travel pulled, but grommets held.
N-18	Two missile tears; two spikes along one edge parallel to blast-wave travel pulled, but grommets held.
P-18	Two missile tears.
A-19	Several missile chips; some pileup in front of pad.
C-19	Several missile chips; corner of pad broken; some pileup in front of pad.
E-19	Several missile chips.
G-19	Several missile chips.
B-20	Several missile chips.
D-20	No damage.
F-20	Several missile chips.
A-21	No damage.
C-21	Several missile chips; some pileup in front of pad.
E-21	Corner of pad broken; several missile chips; some pileup in front of pad.
G-21	Several missile chips; partly sheltered by rock ridge; one large rock, which evidently had rolled down a hill, on pad.
B-22	No damage.
D-22	Several missile chips.
F-22	Several missile chips.
A-23	Pad badly damaged; minor pileup in front of pad.
C-23	A couple of missile chips.
E-23	Station in declivity; several missile chips.
B-24	Station in declivity; several missile chips.
D-24	Station on slight rise; one missile chip.

Appendix B

SAMPLE WEIGHTS AND SIZE DISTRIBUTIONS

NOTE: For sized material larger than No. 6 screen, the ejecta were separated from alluvium and organic material by hand and the total ejecta weighed. For material retained on the No. 6 screen, a quartered sample of 50 to 75 grams was separated, the ejecta percentage weight determined, and this percentage used to determine the ejecta weight of the sample.

For material smaller than that retained on the No. 6 screen, the ejecta proportion of a quartered sample of about 20 grams was estimated independently by three different geologists. The mean of these estimates was used to determine ejecta weight of the sample.

Samples were weighed to the nearest 0.1 gram; however, estimated size fractions and total ejecta weights were rounded to the nearest gram before they were reported.

All weights in grams.

Screen Size	Radial No. 1 Ring A	Ring C	Ring E
8-1/2 in.	0	0	0
3 in.	4,103.0	0	0
1 in.	1,176.6	369.8	0
3/8 in.	1,069.5	246.0	93.0
No. 6	697.5	96.9	28.0
No. 16	225	--	--
No. 40	89	--	--
No. 100	35	--	--
No. 200	27	--	--
< No. 200	45	--	--
< No. 6	--	151	10
Total Ejecta	7,459	864	131
Total Sample	10,899.3	921.3	143.9

All weights in grams.

Screen Size	Radial No. 2 Ring		
	B	D	F
8-1/2 in.	0	0	0
3 in.	678.0	0	0
1 in.	257.0	407.9	0
3/8 in.	109.1	58.3	61.8
No. 6	32.1	15.7	8.7
No. 16	15	--	--
No. 40	6	--	--
No. 100	5	--	--
No. 200	5	--	--
< No. 200	10	--	--
< No. 6	--	11	5
Total Ejecta	1,117	493	75
Total Sample	1,389.7	509.0	78.9

All weights in grams.

Screen Size	Radial No. 3 Ring A	C	E	G
8-1/2 in.	0	0	0	0
3 in.	12,438.0	0	0	0
1 in.	2,221.0	0	0	0
3/8 in.	742.0	157.7	43.8	50.0
No. 6	283.3	25.5	12.4	6.0
No. 16	182	--	--	--
No. 40	66	--	--	--
No. 100	37	--	--	--
No. 200	50	--	--	--
< No. 200	65	--	--	--
< No. 6	--	20	6	3
Total Ejecta	16,084	203	62	59
Total Sample	18,587.6	280.3	76.8	151.2

All weights in grams.

Screen Size	Radial No. 4 Ring		
	B	D	F
8-1/2 in.	0	0	0
3 in.	0	0	0
1 in.	325.0	0	0
3/8 in.	65.3	84.3	8.0
No. 6	17.5	15.7	8.8
No. 16	7	--	--
No. 40	2	--	--
No. 100	2	--	--
No. 200	2	--	--
< No. 200	11	--	--
< No. 6	--	7	3
Total Ejecta	433	107	20
Total Sample	538.2	128.5	24.7

All weights in grams.

Screen Size	Radial No. 5 Ring A	C	E	G
8-1/2 in.	29,619.0	5,612.0	0	0
3 in.	9,159.0	4,883.1	0	0
1 in.	1,941.3	688.0	277.3	37.0
3/8 in.	665.5	172.8	37.1	51.0
No. 6	756.2	133.7	32.2	109.8
No. 16	436	--	--	--
No. 40	285	--	--	--
No. 100	212	--	--	--
No. 200	99	--	--	--
< No. 200	562	--	--	--
< No. 6	--	597	22	816
Total Ejecta	43,735	12,087	369	1,014
Total Sample	44,323.8	12,362.3	498.3	1,142.3

All weights in grams.

Screen Size	Radial No. 6 Ring B	Ring D	Ring F
8-1/2 in.	0	0	0
3 in.	1,913.3	0	460.6
1 in.	964.5	72.2	134.5
3/8 in.	331.3	256.9	170.3
No. 6	273.2	146.0	87.1
No. 16	134	--	--
No. 40	64	--	--
No. 100	51	--	--
No. 200	23	--	--
< No. 200	233	--	--
< No. 6	--	116	45
Total Ejecta	3,986	591	898
Total Sample	4,370.3	817.3	975.3

All weights in grams.

Screen Size	Radial No. 7 Ring			
	A	C	E	G
8-1/2 in.	0	0	0	0
3 in.	5,023.0	1,685.6	0	0
1 in.	2,361.0	125.0	0	41.0
3/8 in.	654.6	252.0	87.0	130.2
No. 6	339.8	136.6	59.5	33.3
No. 16	199	--	--	--
No. 40	70	--	--	--
No. 100	66	--	--	--
No. 200	59	--	--	--
< No. 200	58	--	--	--
< No. 6	--	158	70	28
Total Ejecta	8,830	2,357	217	233
Total Sample	9,732.3	2,544.3	344.3	410.3

All weights in grams.

Screen Size	Radial No. 8 Ring B	Ring D	Ring F
8-1/2 in.	0	0	0
3 in.	948.5	0	0
1 in.	595.3	30.6	138.0
3/8 in.	499.5	70.0	87.0
No. 6	305.4	50.3	30.1
No. 16	191	--	--
No. 40	67	--	--
No. 100	41	--	--
No. 200	42	--	--
< No. 200	84	--	--
< No. 6	--	52	24
Total Ejecta	2,774	203	279
Total Sample	3,576.3	258.8	312.3

All weights in grams.

Screen Size	Radial No. 9 Ring A	C	E	G
8-1/2 in.	0	0	0	0
3 in.	1,041.2	0	0	0
1 in.	832.1	19.4	72.0	255.6
3/8 in.	307.0	129.0	94.2	112.8
No. 6	192.9	55.0	35.9	32.7
No. 16	196	--	--	--
No. 40	139	--	--	--
No. 100	86	--	--	--
No. 200	39	--	--	--
< No. 200	120	--	--	--
< No. 6	--	98	45	2
Total Ejecta	2,953	301	247	403
Total Sample	3,394.3	477.3	319.9	462.7

All weights in grams.

Screen Size	Radial No. 10 Ring B	D	F	H	J	L	N	P
8-1/2 in.	0	0	0	0	0	0	0	0
3 in.	0	0	0	0	0	0	0	0
1 in.	845.3	1,322.9	0	46.2	324.9	56.8	0	18.3
3/8 in.	207.6	87.9	61.5	152.3	276.7	160.8	100.3	189.7
No. 6	108.3	45.2	47.6	195.7	181.9	118.9	40.1	44.9
No. 16	112	--	--	--	--	--	--	--
No. 40	94	--	--	--	--	--	--	--
No. 100	37	--	--	--	--	--	--	--
No. 200	25	--	--	--	--	--	--	--
< No. 200	89	--	--	--	--	--	--	--
< No. 6	--	129	64	182	114	61	22	25
Total Ejecta	1,518	1,585	173	576	898	398	162	278
Total Sample	1,898.3	1,921.3	243.0	1,032.3	1,420.3	995.4	315.3	332.4

All weights in grams.

Screen Size	Radial No. 11 Ring								
	A	C	E	G	I	K	M	O	Q
8-1/2 in.	20,228.0	0	0	0	0	0	0	0	0
3 in.	6,957.0	0	0	0	0	0	0	0	0
1 in.	2,407.0	0	328.7	18.8	169.2	78.2	531.3	16.5	34.3
3/8 in.	1,109.5	57.0	102.8	21.2	316.2	286.0	191.5	124.0	92.8
No. 6	443.0	43.4	40.2	13.4	173.8	144.5	58.0	47.4	14.4
No. 16	234	--	--	--	--	--	--	--	--
No. 40	157	--	--	--	--	--	--	--	--
No. 100	73	--	--	--	--	--	--	--	--
No. 200	49	--	--	--	--	--	--	--	--
< No. 200	181	--	--	--	--	--	--	--	--
< No. 6	--	91	68	24	144	69	58	10	4
Total Ejecta	31,838	191	540	77	803	578	839	198	146
Total Sample	32,526.3	327.8	616.3	107.3	1,062.3	849.3	986.3	329.3	288.3

All weights in grams.

Screen Size	Radial No. 12 Ring							
	B	D	F	H	J	L	N	P
8-1/2 in.	0	0	0	0	0	0	0	0
3 in.	1,401.3	0	0	2,290.0	0	0	0	1,681.6
1 in.	1,224.4	109.6	155.2	991.2	1,715.3	1,028.8	1,232.1	702.2
3/8 in.	772.7	171.0	48.3	430.7	614.8	497.4	605.1	277.1
No. 6	395.6	60.5	40.2	191.9	338.9	314.8	250.9	130.7
No. 16	283	--	--	--	--	--	--	--
No. 40	256	--	--	--	--	--	--	--
No. 100	103	--	--	--	--	--	--	--
No. 200	49	--	--	--	--	--	--	--
< No. 200	208	--	--	--	--	--	--	--
< No. 6	--	186	87	176	173	37	46	45
Total Ejecta	4,693	527	331	4,080	2,842	1,378	2,134	2,837
Total Sample	5,259.1	931.3	654.3	4,569.3	3,688.3	2,563.3	3,712.3	3,070.3

All weights in grams.

Screen Size	Radial No. 13 Ring			
	A	C	E	G
8-1/2 in.	0	0	0	0
3 in.	324.0	0	0	0
1 in.	2,623.0	30.4	0	102.4
3/8 in.	1,479.5	136.5	242.5	100.4
No. 6	1,256.8	190.0	120.1	68.4
No. 16	711	--	--	--
No. 40	139	--	--	--
No. 100	49	--	--	--
No. 200	146	--	--	--
< No. 200	123	--	--	--
< No. 6	--	438	252	126
Total Ejecta	6,851	795	615	397
Total Sample	10,612.3	1,370.3	941.3	968.3

All weights in grams.

Screen Size	Radial No. 14 Ring		
	B	D	F
8-1/2 in.	0	0	0
3 in.	0	0	0
1 in.	553.3	20.2	85.9
3/8 in.	328.6	149.9	71.5
No. 6	438.7	210.6	151.8
No. 16	419	--	--
No. 40	237	--	--
No. 100	80	--	--
No. 200	76	--	--
< No. 200	232	--	--
< No. 6	--	375	454
Total Ejecta	2,364	756	763
Total Sample	3,904.3	1,533.6	1,057.0

All weights in grams.

Screen Size	Radial No. 15 Ring A	C	E	G
8-1/2 in.	0	0	0	0
3 in.	6,663.0	0	0	0
1 in.	1,766.3	53.2	48.9	0
3/8 in.	374.7	138.0	167.6	101.2
No. 6	246.8	252.2	142.2	100.1
No. 16	118	--	--	--
No. 40	81	--	--	--
No. 100	50	--	--	--
No. 200	20	--	--	--
< No. 200	91	--	--	--
< No. 6	--	556	307	196
Total Ejecta	9,411	999	666	397
Total Sample	11,053.3	1,331.3	868.3	558.3

All weights in grams.

Screen Size	Radial No. 16 Ring							
	B	D	F	H	J	L	N	P
8-1/2 in.	0	0	0	0	0	0	0	0
3 in.	9,409.0	855.1	4,713.0	972.5	2,037.9	1,414.7	0	462.8
1 in.	1,638.6	345.3	2,684.0	704.0	455.4	198.6	494.4	1,039.8
3/8 in.	983.1	383.3	595.0	797.8	290.2	323.0	333.0	442.0
No. 6	1,441.9	448.0	241.1	664.0	282.9	307.6	231.3	165.3
No. 16	791	--	--	--	--	--	--	--
No. 40	381	--	--	--	--	--	--	--
No. 100	338	--	--	--	--	--	--	--
No. 200	153	--	--	--	--	--	--	--
< No. 200	448	--	--	--	--	--	--	--
< No. 6	--	1,137	325	581	129	115	72	38
Total Ejecta	15,584	3,169	8,558	3,719	3,195	2,359	1,131	2,148
Total Sample	16,084.3	4,009.3	9,130.3	4,149.3	3,480.3	2,856.3	2,070.3	3,013.3

All weights in grams.

Screen Size	Radial No. 17 Ring A	C	E	G	I	K	M	O	Q
8-1/2 in.	0	2,561.0	16,239.0	0	2,933.0	0	0	0	0
3 in.	11,659.0	851.4	493.8	0	1,483.0	0	2,028.0	0	4,186.0
1 in.	21,459.0	1,498.3	809.8	0	694.7	671.8	356.8	554.6	2,374.0
3/8 in.	13,389.0	1,074.7	464.3	91.1	512.2	431.4	221.0	135.0	934.2
No. 8	9,132.0	1,279.2	414.0	58.0	244.4	194.3	141.7	59.3	274.0
No. 16	2,625.0	430.6	144.5	28.2	58	28	11	4	63
No. 40	2,597.9	281	121	41	37	19	10	4	44
No. 100	2,007.0	157	95	42	9	11	7	4	36
No. 200	562.0	50	24	7	4	1	2	1	6
< No. 200	3,647.1	297	140	34	26	14	4	1	23
Total Ejecta	67,078	8,480	18,946	302	6,001	1,370	2,782	763	7,940
Total Sample	67,078	9,251.1	19,421.9	462.2	7,231.1	1,538.3	3,094.3	935.6	8,222.3

All weights in grams.

Screen Size	Radial No. 18 Ring						
	B	D	F	H	L	N	P
8-1/2 in.	0	0	0	0	0	0	0
3 in.	8,274.0	10,460.0	0	4,610.0	0	0	1,029.3
1 in.	1,287.3	7,339.0	604.0	1,494.5	135.4	724.1	979.3
3/8 in.	1,657.0	2,297.0	155.0	793.3	273.0	151.2	663.2
No. 6	1,979.8	968.5	57.1	212.4	76.0	59.3	74.4
No. 16	668	--	--	--	--	--	--
No. 40	318	--	--	--	--	--	--
No. 100	189	--	--	--	--	--	--
No. 200	166	--	--	--	--	--	--
< No. 200	287	--	--	--	--	--	--
< No. 6	--	791	60	61	34	16	35
Total Ejecta	14,826	21,356	876	7,171	518	951	2,781
Total Sample	17,897.6	24,950.6	1,100.3	7,881.3	1,044.3	1,233.8	3,140.3

All weights in grams.

Screen Size	Radial No. 19 Ring A	C	E	G
8-1/2 in.	25,624.0	11,769.0	0	0
3 in.	5,563.0	0	0	0
1 in.	410.3	286.2	166.7	691.7
3/8 in.	1,181.2	43.5	124.7	111.4
No. 6	602.4	50.6	57.0	63.2
No. 16	472	--	--	--
No. 40	277	--	--	--
No. 100	154	--	--	--
No. 200	76	--	--	--
< No. 200	281	--	--	--
< No. 6	--	162	61	35
Total Ejecta	34,642	12,311	409	901
Total Sample	38,361.6	12,377.3	584.3	986.2

All weights in grams.

Screen Size	Radial No. 20 Ring		
	B	D	F
8-1/2 in.	0	0	0
3 in.	0	0	0
1 in.	179.1	180.0	22.0
3/8 in.	170.8	120.8	45.0
No. 6	177.4	57.4	27.3
No. 16	175	--	--
No. 40	96	--	--
No. 100	46	--	--
No. 200	40	--	--
< No. 200	35	--	--
< No. 6	--	47	18
Total Ejecta	919	405	112
Total Sample	2,224.3	503.3	154.3

All weights in grams.

Screen Size	Radial No. 21 Ring A	C	E	G
8-1/2 in.	0	0	0	16,185.0
3 in.	743.6	0	792.3	0
1 in.	643.9	155.7	147.9	0
3/8 in.	395.0	147.?	229.5	67.2
No. 6	215.0	53.6	145.1	38.2
No. 16	112	--	--	--
No. 40	61	--	--	--
No. 100	42	--	--	--
No. 200	21	--	--	--
< No. 200	111	--	--	--
< No. 6	--	75	146	22
Total Ejecta	2,345	432	1,461	16,312
Total Sample	2,538.3	585.1	2,752.3	16,490.3

All weights in grams.

Screen Size	Radial No. 22 Ring		
	B	D	F
8-1/2 in.	0	0	0
3 in.	0	0	0
1 in.	110.8	153.0	33.5
3/8 in.	345.5	589.3	85.4
No. 6	316.7	140.6	36.5
No. 16	174	--	--
No. 40	110	--	--
No. 100	82	--	--
No. 200	37	--	--
< No. 200	125	--	--
< No. 6	--	513	16
Total Ejecta	1,301	1,396	171
Total Sample	1,687.8	4,673.3	183.3

All weights in grams.

Screen Size	Radial No. 23 Ring A	Ring C	Ring E
8-1/2 in.	0	0	0
3 in.	4,638.0	0	0
1 in.	2,044.0	0	570.6
3/8 in.	1,079.0	189.1	257.8
No. 6	573.0	81.6	110.8
No. 16	191	--	--
No. 40	99	--	--
No. 100	78	--	--
No. 200	46	--	--
< No. 200	143	--	--
< No. 6	--	159	129
Total Ejecta	8,891	430	1,068
Total Sample	10,943.6	659.3	1,269.4

All weights in grams.

Screen Size	Radial No. 24 Ring B	Radial No. 24 Ring D
8-1/2 in.	0	0
3 in.	0	0
1 in.	1,338.1	0
3/8 in.	356.1	176.5
No. 6	195.4	49.3
No. 16	75	--
No. 40	33	--
No. 100	27	--
No. 200	16	--
< No. 200	42	--
< No. 6	--	29
Total Ejecta	2,083	255
Total Sample	2,774.3	492.1

Appendix C

PRE- AND POST-EXCAVATION PROFILES

Distances	Excavation Elevations	
	Before	After
ft	ft	ft
	S 42° W[a]	
0+00 (GZ)	4,617.8	
0+05	4,615.4	
0+10	4,616.0	
0+15	4,620.9	
0+20	4,623.8	
0+25	4,626.7	
0+30	4,629.4	
0+35	4,628.6	
0+40	4,627.9	
0+45	4,625.8	
0+50	4,625.1	
0+55	4,624.0	
0+60	4,623.5	
0+65	4,622.6	
0+70	4,621.3	
0+75	4,620.4	
0+80	4,619.1	
0+85	4,618.2	
0+90	4,617.8	
	S 45° W[b]	
0+00 (GZ)	4,617.8	
0+05	4,616.2	
0+10	4,616.4	

[a]No post-excavation shots taken on S 42° W line.

[b]No post-excavation shots taken on S 45° W line.

Distances	Excavation Elevations	
	Before	After
ft	ft	ft
	S 45° W (Continued)	
0+15	4,621.0	
0+20	4,625.6	
0+25	4,626.9	
0+30	4,629.7	
0+35	4,628.8	
0+40	4,627.7	
0+45	4,626.0	
0+50	4,625.4	
0+55	4,624.5	
0+60	4,624.0	
0+65	4,622.4	
0+70	4,621.4	
0+75	4,620.2	
0+80	4,619.3	
0+85	4,618.7	
0+90	4,618.3	
	S 48° W	
0+00 (GZ)	4,617.8	--
0+05	4,615.5	--
0+10	4,617.0	--
0+15	4,620.7	--
0+20	4,625.4	--
0+25	4,626.8	--
0+30	4,630.3	4,627.4
0+35	4,630.1	4,626.6
0+40	4,628.2	4,626.1
0+45	4,626.8	4,624.7

Distances	Excavation Elevations	
	Before	After
ft	ft	ft
	S 48° W (Continued)	
0+50	4,625.1	4,624.1
0+55	4,623.9	4,623.5
0+60	4,623.3	4,622.9
0+65	4,622.4	4,622.3
0+70	4,621.4	4,621.4
0+75	4,620.2	4,620.3
0+80	4,619.4	4,619.3
0+85	4,618.9	4,619.0
0+90	4,618.7	4,618.9
	S 51° W	
0+00 (GZ)	4,617.8	--
0+05	4,615.6	--
0+10	4,617.1	--
0+15	4,621.0	--
0+20	4,625.2	--
0+25	4,626.6	--
0+30	4,630.3	4,627.6
0+35	4,629.7	4,626.4
0+40	4,628.4	4,626.1
0+45	4,627.0	4,624.7
0+50	4,626.0	4,624.1
0+55	4,624.4	4,623.4
0+60	4,623.1	4,622.9
0+65	4,622.6	4,622.4
0+70	4,621.8	4,621.6

Distances	Excavation Elevations	
	Before	After
ft	ft	ft
	S 51° W (Continued)	
0+75	4,620.5	4,620.4
0+80	4,619.8	4,619.6
0+85	4,619.2	4,619.2
0+90	4,619.4	4,619.1
	S 54° W	
0+00 (GZ)	4,617.8	--
0+05	4,615.7	--
0+10	4,617.3	--
0+15	4,620.2	--
0+20	4,624.3	--
0+25	4,628.7	--
0+30	4,629.5	4,626.3
0+35	4,630.3	4,626.2
0+40	4,628.3	4,626.5
0+45	4,627.6	4,624.8
0+50	4,626.2	4,624.3
0+55	4,624.1	4,623.5
0+60	4,623.4	4,622.8
0+65	4,622.3	4,622.3
0+70	4,621.7	4,621.7
0+75	4,620.7	4,620.7
0+80	4,620.1	4,620.0
0+85	4,619.7	4,619.7
0+90	4,620.0	4,619.6

Distances	Excavation Elevations	
	Before	After
ft	ft	ft
	S 57° W	
0+00 (GZ)	4,617.8	--
0+05	4,615.8	--
0+10	4,617.3	--
0+15	4,619.6	--
0+20	4,624.2	--
0+25	4,629.0	--
0+30	4,630.4	4,626.5
0+35	4,630.6	4,625.5
0+40	4,629.0	4,626.7
0+45	4,628.0	4,625.0
0+50	4,626.9	4,624.3
0+55	4,624.9	4,623.4
0+60	4,623.7	4,622.8
0+65	4,622.4	4,622.2
0+70	4,621.8	4,621.6
0+75	4,621.0	4,621.0
0+80	4,620.6	4,620.5
0+85	4,620.5	4,620.4
0+90	4,620.6	4,620.3
	S 60° W	
0+00 (GZ)	4,617.8	--
0+05	4,615.9	--
0+10	4,617.1	--
0+15	4,620.0	--
0+20	4,623.2	--
0+25	4,626.0	--
0+30	4,629.9	4,626.9
0+35	4,631.6	4,624.8

Distances	Excavation Elevations	
	Before	After
ft	ft	ft
	S 60° W (Continued)	
0+40	4,629.4	4,626.4
0+45	4,628.3	4,625.2
0+50	4,627.5	4,624.4
0+55	4,625.6	4,623.6
0+60	4,624.2	4,622.9
0+65	4,622.9	4,622.4
0+70	4,622.3	4,621.9
0+75	4,621.6	4,621.4
0+80	4,621.2	4,621.1
0+85	4,621.3	4,620.8
0+90	4,621.0	4,620.9
	S 63° W	
0+00 (GZ)	4,617.8	--
0+05	4,615.9	--
0+10	4,618.1	--
0+15	4,620.5	--
0+20	4,622.1	--
0+25	4,628.1	--
0+30	4,629.7	4,625.9
0+35	4,632.1	4,625.5
0+40	4,629.5	4,625.3
0+45	4,629.0	4,625.7
0+50	4,627.9	4,625.3[c]
0+55	4,626.2	4,624.6[c]
0+60	4,624.7	4,624.0[c]
0+65	4,623.6	4,623.3[c]

[c]Concrete pad

Distances	Excavation Elevations	
	Before	After
ft	ft	ft
	S 63° W (Continued)	
0+70	4,623.1	4,622.8[c]
0+75	4,622.5	4,622.4[c]
0+80	4,621.6	4,621.5
0+85	4,621.7	4,621.0
0+90	4,621.3	4,621.2
	S 66° W	
0+00 (GZ)	4,617.8	--
0+05	4,616.0	--
0+10	4,617.3	--
0+15	4,619.9	--
0+20	4,621.5	--
0+25	4,626.0	--
0+30	4,630.1	4,625.9
0+35	4,630.8	4,625.7
0+40	4,629.7	4,625.2
0+45	4,629.6	4,625.3
0+50	4,626.9	4,624.6
0+55	4,625.4	4,623.6
0+60	4,624.4	4,623.0
0+65	4,623.3	4,622.8
0+70	4,623.4	4,622.4
0+75	4,622.3	4,622.0
0+80	4,622.0	4,621.6
0+85	4,621.7	4,621.5
0+90	4,621.7	4,621.5

Distances	Excavation Elevations	
	Before	After
ft	ft	ft
	S 69° W	
0+00 (GZ)	4,617.8	--
0+05	4,616.1	--
0+10	4,617.6	--
0+15	4,619.7	--
0+20	4,621.0	--
0+25	4,625.9	--
0+30	4,629.8	4,625.8
0+35	4,630.4	4,626.0
0+40	4,630.4	4,625.2
0+45	4,629.0	4,625.3
0+50	4,626.8	4,624.8
0+55	4,625.7	4,623.6
0+60	4,624.2	4,623.2
0+65	4,623.4	4,622.9
0+70	4,623.1	4,622.7
0+75	4,622.6	4,622.6
0+80	4,621.9	4,621.8
0+85	4,621.7	4,621.7
0+90	4,622.0	4,621.8
	S 72° W	
0+00 (GZ)	4,617.8	--
0+05	4,616.1	--
0+10	4,617.5	--
0+15	4,620.2	--
0+20	4,620.6	--
0+25	4,625.6	--
0+30	4,628.4	4,626.8
0+35	4,630.1	4,625.8

Distances	Excavation Elevations	
	Before	After
ft	ft	ft
	S 72° W (Continued)	
0+40	4,629.2	4,624.8
0+45	4,627.6	4,625.3
0+50	4,626.2	4,625.0
0+55	4,625.6	4,623.8
0+60	4,624.0	4,623.6
0+65	4,623.3	4,623.0
0+70	4,623.1	4,622.9
0+75	4,623.0	4,622.9
0+80	4,622.1	4,621.9
0+85	4,621.9	4,621.9
0+90	4,622.2	4,621.9
	S 75° W	
0+00 (GZ)	4,617.8	--
0+05	4,616.3	--
0+10	4,617.7	--
0+15	4,619.9	--
0+20	4,620.6	--
0+25	4,624.8	--
0+30	4,627.5	4,626.6
0+35	4,629.1	4,626.4
0+40	4,628.8	4,625.1
0+45	4,627.2	4,625.3
0+50	4,626.2	4,624.5
0+55	4,625.7	4,624.2
0+60	4,624.4	4,624.1
0+65	4,623.8	4,623.6
0+70	4,623.5	4,623.3

Distances	Excavation Elevations	
	Before	After
ft	ft	ft
	S 75° W (Continued)	
0+75	4,623.3	4,623.1
0+80	4,622.5	4,622.6
0+85	4,622.5	4,622.5
0+90	4,622.7	4,622.7
	S 78° W	
0+00 (GZ)	4,617.8	--
0+05	4,616.3	--
0+10	4,617.7	--
0+15	4,619.9	--
0+20	4,620.4	--
0+25	4,623.9	--
0+30	4,627.0	4,626.3
0+35	4,628.2	4,626.5
0+40	4,627.8	4,625.2
0+45	4,626.4	4,625.7
0+50	4,625.6	4,625.2
0+55	4,624.9	4,624.7
0+60	4,624.7	4,624.5
0+65	4,623.9	4,623.9
0+70	4,623.6	4,623.6
0+75	4,623.7	4,623.5
0+80	4,623.2	4,623.1
0+85	4,622.8	4,622.7
0+90	4,623.2	4,623.2

Distances	Excavation Elevations	
	Before	After
ft	ft	ft
	S 81° W[d]	
0+00 (GZ)	4,617.8	
0+05	4,617.3	
0+10	4,617.7	
0+15	4,619.7	
0+20	4,620.2	
0+25	4,623.9	
0+30	4,626.3	
0+35	4,627.3	
0+40	4,627.2	
0+45	4,626.2	
0+50	4,625.4	
0+55	4,625.2	
0+60	4,624.9	
0+65	4,624.3	
0+70	4,624.1	
0+75	4,624.1	
0+80	4,624.2	
0+85	4,623.5	
0+90	4,623.5	
	S 84° W[e]	
0+00 (GZ)	4,617.8	
0+05	4,617.2	
0+10	4,618.4	
0+15	4,619.5	
0+20	4,620.2	

[d]No post-excavation shots taken on S 81° W line.

[e]No post-excavation shots taken on S 84° W line.

Distances	Excavation Elevations	
	Before	After
ft	ft	ft
	S 84° W (Continued)	
0+25	4,623.6	
0+30	4,627.0	
0+35	4,626.9	
0+40	4,626.9	
0+45	4,626.1	
0+50	4,625.3	
0+55	4,625.6	
0+60	4,625.5	
0+65	4,624.8	
0+70	4,624.3	
0+75	4,624.4	
0+80	4,624.1	
0+85	4,624.0	
0+90	4,623.9	

Appendix D

SIZE DISTRIBUTION OF CLOSE-IN EJECTA SAMPLES

TABLE D.1 SIZE DISTRIBUTION OF CLOSE-IN EJECTA SAMPLES

Equivalent Diameter	Interval Weight
inches	pounds
Sample No. 1 (29 to 58 Feet from GZ)	
>24	6,992
8-1/2 to 24	57,336
3 to 8-1/2	57,650
1 to 3	32,020
<1	16,610
Total	170,608
Sample No. 2 (58 to 87 Feet from GZ)	
>24	722
8-1/2 to 24	9,490
3 to 8-1/2	14,150
1 to 3	9,166
<1	6,386
Total	39,914

These interval weights were determined on either the Fairbanks-Morse truck scales in Mercury, which are accurate to the nearest 10 pounds, or on a 2,000-pound-capacity platform scale, set up at the site, which could be read to the nearest 2 pounds.

Material less than 1 inch in size was quartered by again passing it through the Jones riffle. After this it was coned and quartered by hand. Three samples of the quartered material from 29 to 58 feet and three samples from 58 to 87 feet from GZ were taken to NTL, where further screening gave the results shown in Table D.2; weights given are for the material retained on the screen.

TABLE D. 2 SIZE DISTRIBUTION OF CLOSE-IN EJECTA SMALLER THAN 1 INCH

All weights are in grams.

Equivalent Diameter	29 to 58 Feet From Ground Zero			58 to 87 Feet From Ground Zero		
	Samples			Samples		
	1	2	3	1	2	3
3/8 in.	453.0	652.2	418.2	903.9	1,051.0	911.0
No. 6	320.5	427.9	280.9	587.0	508.1	552.6
No. 16	169.8	251.0	144.5	341.1	195.7	215.0
No. 40	126.2	234.5	138.5	237.0	88.8	120.0
No. 100	105.0	198.4	124.0	150.7	49.8	70.9
No. 200	31.0	51.0	32.0	41.7	16.5	20.3
<No. 200	29.8	44.7	28.2	50.7	26.9	24.5
Total	1,235.3	1,859.7	1,166.3	2,312.1	1,936.8	1,914.3

Appendix E

LOCATION OF CODED CYLINDER FRAGMENTS

Distances ond azimuth are given from ground zero.

Fragment Number	Grout	Beod	Distonce	Azimuth
			ft	degrees
1	Brown	Silver	70	248
2	Yellow	Brown	95	243
3	Brown	White	160	241
4	Brown	White	163	241
5A	Brown	White	184	241
5B	Brown	Pink	184	241
6	Brown	Pink	193	240
7	Yellow	White	194	240
8	Brown	Red	207	242
9A	Brown	Red	215	243
9B	Brown	Aqua	215	243
10	Yellow	Turquoise	148	242
11A	Brown	M. Blue	134	241
11B	Brown	M. Blue	134	241
11C	Brown	M. Blue	134	241
12	Yellow	Brown	117	248
13A	Yellow	Brown	43	241
13B	Yellow	Brown	43	241
13C	Yellow	Yellow	43	241
14A	Brown	Brown	50	235
14B	Brown	Brown	50	235
14C	Brown	Yellow	50	235
15A	Green	Gold	10	236
15B	Green	Yellow	10	236
15C	Green	Gold	10	236
15D	Green	Yellow	10	236
16A	Green	Gold	10	236
16B	Green	Black	10	236
17	Green	Black	17	243
18	Green	Yellow	15	236

Fragment Number	Grout	Bead	Distance	Azimuth
			ft	degrees
19A	Green	Brown	18	230
19B	Green	Yellow	18	230
20[a]				
21	Brown	Aqua	276	240
22	Yellow	Lt. Green	595	232
23	Yellow	Aqua	614	229
24A	Brown	Brown	61	238
24B	Brown	Turquoise	61	238
25	Yellow	Gold	43	236
26	Brown	Yellow	48	239
27	Brown	White	162	241
28	Yellow	M. Blue	153	243
29	Brown	M. Blue	121	245
30	Brown	M. Blue	126	241
31	Brown	M. Blue	131	241
32	Brown	M. Blue	136	239
33	Brown	M. Blue	142	241
34	Brown	M. Blue	146	241
35	Brown	Pink	197	243
36	Yellow	Silver	160	243
37	Brown	Pink	187	243
38A	Yellow	Yellow	46	241
38B	Brown	Yellow	46	241
39	Brown	Silver	52	240
40	Red	Turquoise	38	238
41	Brown	Yellow	36	238
42	Brown	Silver	52	240

[a] No. 20 used for steel pipe.

Fragment Number	Grout	Bead	Distance	Azimuth
			ft	degrees
43	Yellow	Yellow	46	239
44	Yellow	Yellow	44	240
45	Red	Turquoise	42	237
46	Yellow	Gold	39	238
47	Red	Turquoise	32	243
48A	Yellow	Gold	27	241
48B	Yellow	Black	27	241
49A	Yellow	Black	23	238
49B	Red	Brown	23	238
49C	Red	Yellow	23	238
50	Brown	Yellow	33	243
51	Red	Silver	140	245
52	Red	Yellow	24	247
53	Brown	M. Blue	140	241
54	Brown	White	143	242
55	Yellow	Silver	140	244
56	Brown	White	157	240
57	Red	Brown	32	243
58	Brown	Aqua	196	243
59	Red	Brown	27	243
60	Yellow	Pearl	25	243
61	Green	Yellow	21	243
62	Yellow	Aqua	474	233
63	Red	M. Blue	587	228
64	Red	Lt. Green	595	230
65A	Red	Pink	918	228
65B	Red	White	918	228
66	Red	Pink	706	227

Fragment Number	Grout	Bead	Distance	Azimuth
			ft	degrees
67	Red	Aqua	598	229
68	Red	Pink	702	226
69	Yellow	Lt. Green	686	229
70	Red	Brown	30	243
71	Yellow	Pearl	28	243
72	Brown	Yellow	34	243
73	Brown	Gold	28	243
74A	Brown	Black	28	243
74B	Brown	Gold	28	243
75	Brown	Black	30	243
76	Red	Gold	22	243
77	Red	Gold	23	243
78	Green	Brown	24	243
79	Yellow	N. Blue	22	243
80	Red	Black	20	243
81	Red	Yellow	22	243
82	Red	Gold	20	243
83	Yellow	N. Blue	22	243
84	Red	Turquoise	38	239
85	Green	Gold	18	243
86	Green	Pearl, N. Blue	6	243
87	Red	Orange	11	243
88	Yellow	Orange, Dk. Green	18	243
89	Brown	Pearl	24	243
90	Red	Lt. Green	b	b

[b] Location not mapped.

Fragment Number	Grout	Bead	Distance	Azimuth
			ft	degrees
c				
100	Brown	Pink	185	241
101	Red	Silver	188	250
102	Green	White	244	248
103	Green	White	222	242
104	Yellow	Pink	615	229
105	Yellow	White	348	231
106	Red	Lt. Green	975	236
107	Red	Aqua	900	232
108	Red	Red	885	233
109A	Red	Lt. Green	866	233
109B	Red	Pink	866	233
110	Red	Red	838	250
111	Red	Aqua	799	229
112	Red	Lt. Green	795	239
113A	Green	Brown	740	233
113B	Red	Aqua	740	233
114	Red	Pink	739	227
115	Red	Lt. Green	713	229
116	Red	Lt. Green	700	230
117	Red	Pink	715	230
118	Red	Red	706	231
119	Yellow	Aqua	703	232
120	Yellow	Pink	702	240
121	Red	Pink	656	229
122	Red	Lt. Green	664	231
123	Red	Lt. Green	642	233

[c] No. 91 through No. 99 not used.

Fragment Number	Grout	Bead	Distance	Azimuth
			ft	degrees
124	Red	Aqua	640	230
125	Yellow	Aqua	632	229
126	Red	Lt. Green	598	233
127	Red	Aqua	582	234
128	Yellow	Lt. Green	581	231
129	Yellow	Aqua	598	228
130A	Red	M. Blue	584	228
130B	Red	Aqua	584	228
131A	Yellow	Lt. Green	553	230
131B	Red	Lt. Green	553	230
131C	Red	Pink	553	230
132A	Green	White	562	236
132B	Red	Pink	562	236
133	Red	Lt. Green	564	238
134A	Red	Lt. Green	542	237
134B	Red	Aqua	542	237
135	Red	Lt. Green	546	230
136A	Yellow	Lt. Green	543	229
136B	Red	M. Blue	543	229
137	Yellow	Lt. Green	514	230
138	Red	Lt. Green	505	235
139	Red	Lt. Green	510	236
140	Red	Lt. Green	498	243
141	Red	Red	483	230
142	Red	Red	475	230
143	Red	Lt. Green	477	230
144	Red	M. Blue	458	230
145	Yellow	Pink	452	232

Fragment Number	Grout	Bead	Distance	Azimuth
			ft	degrees
146	Red	Pink	448	229
147	Yellow	White	299	227
148	Yellow	White	301	229
149	Yellow	White	300	234
150	Yellow	M. Blue	295	230
151	Yellow	White	288	233
152A	Yellow	M. Blue	265	227
152B	Red	M. Blue	265	227
153	Green	White	217	244
154	Green	White	220	232
155	Green	White	214	230
156	Yellow	M. Blue	211	228
157	Green	White	200	227
158	Red	M. Blue	189	225
159A	Yellow	Silver	156	242
159B	Yellow	M. Blue	156	242
160	Yellow	Silver	158	242
161	Brown	White	156	241
162	Brown	M. Blue	136	240
163	Red	Silver	132	247
164	Green	White	198	194
165	Red	M. Blue	230	192
166A	Red	White	264	199
166B	Yellow	Pink	264	199
166C	Red	M. Blue	264	199
167	Yellow	Pink	297	193
168	Yellow	Pink	337	201
169	Red	Pink	372	207
170A	Yellow	Lt. Green	381	207
170B	Yellow	M. Blue	381	207

Fragment Number	Grout	Bead	Distance	Azimuth
			ft	degrees
171A	Red	M. Blue	287	198
171B	Yellow	M. Blue	287	198
172	Red	Pink	293	199
173	Red	White	393	205
174A	Red	White	420	206
174B	Yellow	Pink	420	206
175	Red	M. Blue	409	206
176	Yellow	Pink	453	210
177	Red	White	490	206
178	Green	White	188	223
179	Green	White	217	220
180	Yellow	White	223	214
181	Green	White	234	209
182	Yellow	White	240	213
183	Green	White	231	219
184	Green	White	261	203
185A	Red	M. Blue	255	206
185B	Green	White	255	206
186	Red	M. Blue	266	211
187	Red	M. Blue	259	220
188	Yellow	White	261	220
189	Red	M. Blue	295	209
190A	Yellow	*Aqua or Pink	281	141
190B	Red	M. Blue	281	219
191A	Yellow	*Aqua or Pink	284	225
191B	Yellow	White	284	225
192	Red	Red	318	212
193	Red	Red	319	217
194	Yellow	White	323	217
195	Yellow	M. Blue	322	219

Fragment Number	Grout	Bead	Distance	Azimuth
			ft	degrees
196	Yellow	White	317	223
197	Yellow	White	335	221
198	Red	White	347	209
199	Red	M. Blue	342	206
200A	Red	Red	361	215
200B	Yellow	Pink	361	215
201	Red	M. Blue	359	217
202A	Red	Pink	355	221
202B	Yellow	Pink	355	221
203	Red	Red	353	223
204	Red	Pink	352	224
205	Red	Lt. Green	338	225
206	Red	White	374	216
207	Yellow	Lt. Green	371	215
208	Red	Pink	365	209
209	Yellow	White	d	d
210	Yellow	Pink	377	192
211A	Yellow	Pink	384	205
211B	Red	White	384	205
212	Yellow	Lt. Green	383	213
213	Yellow	White	376	217
214	Red	M. Blue	393	221
215	Red	M. Blue	395	224
216	Red	Lt. Green	417	224
217A	Green	White	414	221
217B	Red	Red	414	221
218	Yellow	Lt. Green	422	219
219	Yellow	Lt. Green	414	214
220A	Yellow	White	438	204
220B	Red	Pink	438	204

[d] Location not mapped.

Fragment Number	Grout	Bead	Distance	Azimuth
			ft	degrees
221	Red	White	447	214
222	Yellow	Pink	443	215
223	Red	Pink	432	218
224	Yellow	Lt. Green	425	219
225	Yellow	Pink	431	220
226	Red	White	442	220
227	Red	Pink	450	225
228	Yellow	Pink	442	226
229	Yellow	Pink	466	224
230	Red	Pink	470	217
231A	Yellow	Lt. Green	462	214
231B	Red	White	462	214
232A	Red	Pink	463	215
232B	Red	Lt. Green	463	215
233	Yellow	Pink	460	203
234A	Red	White	482	212
234B	Yellow	Pink	482	212
235	Red	Aqua	500	212
236	Red	White	492	216
237A	Red	Red	490	218
237B	Red	White	490	218
237C	Red	Pink	490	218
238	Red	Red	489	220
239	Red	White	499	223
240	Red	Red	485	227
241	Red	Pink	492	227
242A	Red	Pink	500	226
242B	Yellow	Pink	500	226
243	Red	Pink	512	218
244	Red	White	506	217

Fragment Number	Grout	Bead	Distance	Azimuth
			ft	degrees
245	Red	Pink	508	215
246	Red	Red	425	213
247A	Red	Red	398	214
247B	Yellow	Lt. Green	398	214
248	Red	M. Blue	379	215
249	Red	White	386	212
250	Red	White	475	212
251	Yellow	M. Blue	518	207
252	Yellow	Pink	530	211
253	Yellow	White	532	213
254	Red	Red	545	214
255	Yellow	Pink	530	219
256	Red	White	532	220
257	Red	Aqua	544	221
258	Red	Red	538	222
259A	Yellow	Lt. Green	534	223
259B	Yellow	Pink	534	223
260	Red	Red	530	224
261A	Red	Red	540	225
261B	Red	Pink	540	225
262	Red	Red	565	226
263	Red	Red	546	225
264	Red	Red	549	223
265	Red	Red	572	225
266	Yellow	Pink	567	223
267	Red	Lt. Green	557	223
268	Yellow	Pink	566	219
269	Red	Red	570	219
270	Yellow	Pink	551	217
271	Red	Lt. Green	560	212

Fragment Number	Grout	Bead	Distance	Azimuth
			ft	degrees
272	Red	Red	479	213
273	Yellow	Pink	581	207
274A	Red	Red	574	221
274B	Red	Pink	574	221
275	Red	Red	586	221
276	Yellow	Lt. Green	586	222
277	Red	M. Blue	580	228
278	Red	White	601	227
279	Red	Red	615	225
280A	Red	Red	623	221
280B	Red	Aqua	623	221
281A	Red	Red	610	219
281B	Green	Brown	610	219
282	Red	Aqua	628	217
283	Red	Aqua	627	227
284	Red	Red	666	226
285	Red	Pink	660	222
286A	Red	Aqua	644	219
286B	Yellow	Pink	644	219
287	Red	Red	668	217
288	Red	M. Blue	666	214
289	Red	Red	695	216
290A	Red	Red	696	218
290B	Red	Pink	696	218
291	Red	Red	683	225
292	Red	Red	679	227
293	Red	*Aqua or Pink	709	208
294	Red	Red	708	224
295	Red	Red	744	225
296	Red	Red	726	220

Fragment Number	Grout	Bead	Distance	Azimuth
			ft	degrees
297	Red	*Aqua or Pink	724	219
298	Red	Red	763	215
299	Red	Lt. Green	775	224
300	Red	Pink	776	224
301	Red	Red	816	220
302	Red	Red	888	227
303	Red	*Aqua or Pink	897	227
304	Red	*Aqua or Pink	889	224
305	Red	*Aqua or Pink	908	227
306	Red	M. Blue	440	198

* Bead color was not determined.

Appendix F

LOCATION OF FAR-OUT MISSILES

Missiles are rock fragments from the Flat Top I crater. They were numbered consecutively as found.

Missile Number	Bearing	Distance from GZ
		ft
1	S 36° 59' E	4,059
2	S 46° 13' E	3,312
3	S 46° 34' E	3,349
4	S 47° 05' E	3,381
5	S 49° 55' E	3,545
6	S 51° 59' E	3,378
7	S 55° 00' E	3,439
8	S 55° 32' E	3,483
9	S 57° 24' E	2,905
10	S 58° 38' E	3,538
11	S 58° 45' E	3,422
12	S 62° 22' E	3,402
13	S 63° 10' E	3,426
14	S 56° 24' E	3,051
15	S 58° 55' E	3,226
16	S 60° 07' E	3,304
17	S 53° 07' E	3,199
18	S 54° 02' E	3,037
19	S 53° 02' E	3,001
20	S 53° 03' E	2,918
21	S 53° 02' E	2,817
22	S 53° 37' E	2,844
23	S 56° 34' E	2,817
24	S 59° 51' E	2,996
25	S 59° 28' E	2,870
26	S 61° 32' E	2,783
27	S 55° 38' E	2,718

Missile Number	Bearing	Distance from GZ
		ft
28	S 54° 10' E	2,660
29	S 46° 50' E	2,563
30	S 46° 22' E	2,767
31	S 47° 57' E	2,822
32	S 48° 53' E	2,837
33	S 46° 39' E	2,856
34	S 46° 17' E	2,847
35	S 54° 57' E	3,472
36	S 65° 20' E	3,007
37	S 64° 25' E	2,999
38	S 64° 00' E	2,986
39	S 65° 01' E	2,822
40	S 68° 33' E	2,729
41	S 51° 05' E	2,266
42	S 51° 55' E	2,287
43	S 58° 03' E	2,528
44	S 58° 54' E	2,633
45	S 60° 19' E	2,601
46	S 62° 34' E	2,543
47	S 65° 46' E	2,556
48	S 67° 45' E	2,635
49	S 68° 33' E	2,613
50	S 69° 18' E	2,620
51	S 69° 39' E	2,515
52	S 70° 11' E	2,971
53	S 67° 54' E	3,040
54	S 67° 15' E	3,047
55	S 71° 36' E	3,147

Missile Number	Bearing	Distance from GZ
		ft
56	S 65° 36' E	3,160
57	S 66° 26' E	3,273
58	S 70° 14' E	3,332
59	S 71° 47' E	3,437
60	S 67° 41' E	3,544
61	S 67° 19' E	3,532
62	S 39° 41' E	2,528
63	S 41° 40' E	2,670
64	S 43° 47' E	3,078
65	S 43° 59' E	3,175
66	S 40° 33' E	3,295
67	S 38° 38' E	3,036
68	S 38° 32' E	2,832
69	S 37° 33' E	2,845
70	S 35° 45' E	2,937
71	S 31° 52' E	3,130
72	S 33° 03' E	2,980
73	S 31° 08' E	2,759
74	S 26° 33' E	2,600
75	S 26° 20' E	2,85[illegible]
76	S 27° 15' E	2,885
77	S 23° 14' E	2,879
78	S 23° 11' E	3,037
79	S 23° 54' E	3,114
80	S 19° 11' E	3,412
81	S 17° 45' E	3,558
82	S 16° 26' E	3,614
83	S 11° 29' E	3,279
84	S 12° 50' E	3,060
85	S 11° 14' E	2,957

Missile Number	Bearing	Distance from GZ
		ft
86	S 11° 12' E	2,798
87	S 11° 57' E	2,812
88	S 13° 39' E	2,686
89	S 18° 31' E	2,608
90	S 24° 08' E	2,492
91	S 30° 36' E	2,584
92	S 32° 35' E	2,643
93	S 38° 36' E	2,760
94	S 37° 31' E	2,497
95	S 29° 59' E	2,490
96	S 15° 21' E	2,577
97	S 16° 10' E	2,598
98	S 14° 01' E	2,551
99	S 10° 14' E	2,604
100	S 10° 36' E	2,656
101	S 09° 34' E	2,690
102	S 09° 21' E	2,598

Appendix G

EMPLACEMENT ELEVATIONS OF TOPS OF CODED GROUT CYLINDERS

Elevation of charge center is 4,627.9 feet.

Cords	Grout			
	Green	Red	Yellow	Brown
	ft	ft	ft	ft
Horizontal Distance from GZ	6	12	18	24
Light green	4,627.7	4,627.3	4,627.0	--
Aqua	4,627.0	4,626.6	4,626.1	4,626.6
Red	4,626.0	4,625.6	--	4,626.0
Pink	4,625.0	4,624.6	4,625.0	4,625.0
White	4,624.0	4,623.6	4,624.0	4,624.0
Medium blue	4,623.0	4,622.6	4,623.0	4,623.0
Silver	4,622.0	4,621.6	4,622.0	4,622.0
Turquoise	4,620.9	4,620.5	4,620.9	4,621.0
Brown	4,619.9	4,619.5	4,619.9	4,619.9
Yellow	4,618.9	4,618.5	4,618.9	4,618.9
Gold	4,617.9	4,617.5	4,617.9	4,617.9
Black	4,616.9	4,616.5	4,616.9	4,616.9
Pearl	4,615.8	4,615.5	4,615.8	4,615.8
Navy blue	4,614.8	4,614.4	4,614.8	4,614.8
Orange	4,613.8	4,613.4	4,613.8	4,613.8
Dark green	4,612.8	4,612.4	4,612.8	4,612.8
Bottom of dark green	4,611.8	4,611.6	4,611.9	4,611.8

REFERENCES

1. A. D. Rooke, Jr., and L. K. Davis; "Mass Distribution Measurements of Crater Ejecta and Dust; Final Report"; Project 1.6, Operation Danny Boy, DASA POR-1815, February 1964; U. S. Army Corps of Engineers, Waterways Experiment Station, Vicksburg, Mississippi; Unclassified.

2. A. J. Chabai and others; "20-Ton HE Cratering Experiments in Desert Alluvium; Final Report"; Project Stagecoach, SC-4596(RR), May 1962; Chapters 4 and 5; Sandia Corporation, Albuquerque, New Mexico; Unclassified.

3. A. J. Chabai and others; "Project Scooter; Final Report"; SC-4602(RR), October 1963; Chapter 3; Sandia Corporation, Albuquerque, New Mexico; Unclassified.

4. V. N. Sakharov and others; "Local Distribution of Earth Thrown Up by Underground Explosions"; Doklady Akad. Nauk SSSR, 124, January 1959, No. 2, Pages 314-317 (Transiated in Physics Express, April 1959); Unclassified.

5. R. H. Carlson and W. A. Roberts; "Mass Distribution and Throwout Studies; Final Report"; Project Sedan, PNE-217F, August 1963; The Boeing Company, Seattle, Washington; Unclassified.

7. F. Salaegui; Private Communication; 1964; Reynolds Electrical and Engineering Company; Unclassified.

8. R. H. Carlson and G. D. Jones; "Ejecta Distribution Studies"; Project Air Vent (to be published by Sandia Corporation), June 1964; The Boeing Company, Seattle, Washington; Unclassified.

10. R. B. Vaile, Jr.; "Behavior of Missiles in Underground Explosions"; Technical Report No. 5, November 1951; Stanford Research Institute, Stanford, California; Unclassified.

11. R. B. Vaile and V. Salmon; "Evaluation of Missile Hazard, Underground Shot"; Project 4.5, Operation Jangle, WT-338, May 1952; Stanford Research Institute, Stanford, California; Unclassified.

13. C. Diehl; Private Communication; 1964; Suffield Experimental Station; Unclassified.

14. E. B. Ahlers; Private Communication; 1964; Illinois Institute of Technology; Unclassified.

15. "Ejecta and Mass Distribution Studies"; Technical Proposal, Flat Top I, D2-90504; The Boeing Company, Seattle, Washington; Unclassified.

16. D. Cummings and others; "Results of Exploratory Drilling and Geologic Studies at the Proposed Ferris Wheel A. 3 Site, South End of Banded Mountain, Area 9, Nevada Test Site"; USGS Technical Letter NTS-77, 1964; United States Geological Survey, Mercury, Nevada; Unclassified.

17. A. D. Rooke, Jr.; Private Communication; 1964; Waterways Experiment Station; Unclassified.

18. E. C. Robertson; "Experimental Study of the Strength of Rocks"; Bulletin of Geological Society of America, 1955, Vol 66, Pages 1275-1314; Unclassified.

19. R. C. Bass; Private Communication; 1964; Sandia Corporation; Unclassified.

20. E. C. Robertson; "Viscoelasticity of Rocks"; Rand Memorandum RM-3583, 1963; Chapter 3; The Rand Corporation, Santa Monica, California; Unclassified.

21. H. C. Heard; "Transition From Brittle Fracture to Ductile Flow in Solenhofen Limestone as a Function of Temperature, Confining Pressure, and Interstitial Fluid Pressure"; Geological Society of America, 1960, Memoir 79, Pages 193-226; Unclassified.

22. S. M. Hansen and others; "Recommended Crater Nomenclature"; UCRL-7750, 1964; University of California, Lawrence Radiation Laboratory, Livermore, California; Unclassified.

23. D. E. Gault and others; "Spray Ejected From the Lunar Surface by Meteoroid Impact"; NASA Technical Note D-1767, 1963; National Aeronautics and Space Administration, Washington, D. C.; Unclassified.